

DEVELOPMENT OF TRANSFER FUNCTION LOAD MODELS
AND THEIR USE IN
MODELING THE CSU SOLAR HOUSE I

Michael James Pawelski

MASTER OF SCIENCE
(Mechanical Engineering)

UNIVERSITY OF WISCONSIN-MADISON

1976

DEVELOPMENT OF TRANSFER FUNCTION LOAD MODELS
AND THEIR USE IN
MODELING THE CSU SOLAR HOUSE I

BY

MICHAEL JAMES PAWELSKI

A thesis submitted in partial fulfillment of the
requirements for the degree of

MASTER OF SCIENCE
(Mechanical Engineering)
at the
UNIVERSITY OF WISCONSIN-MADISON

1976

ACKNOWLEDGEMENT

I would like to express my appreciation and gratitude for the guidance and encouragement of my advisors, Professors J.A. Duffie, W.A. Beckman and J.W. Mitchell. I am especially grateful to Professor Mitchell for his tireless efforts to help and assist me. I would also like to thank the staff at the Colorado State University Solar Energy Applications Laboratory, particularly Professors G.O.G. Löf and D.S. Ward and Mr. C.C. Smith. The financial support of the Energy Research and Development Agency (ERDA) grant G - 40457 to Colorado State University and the sub-contract to the University of Wisconsin is appreciated as is ERDA grant E(11-1) - 2588 to the University of Wisconsin Solar Energy Laboratory.

The helpful suggestions of Dr. D.G. Stephenson and Mr. G.P. Mitalas of the National Research Council of Canada were extremely helpful in understanding difficult material. Mr. J.G. Arseneault was also very helpful in assisting me in programming procedures.

I also wish to thank my fellow graduate students at the University of Wisconsin Solar Energy Laboratory for their assistance, ideas and suggestions. Specific thanks go to Sandy Klein, Tom Freeman, Pat Hughes, John Nelson, Tom Olson, Denny Morrison, Howie Grunes and Vern Karman.

Most importantly, I must thank my wonderful parents. To my mother, for her love and unending encouragement and support and also for helping to type the manuscript and to my father, a proud man, who instilled enough pride in me to complete this work. I only hope that this thesis, in some small way, measures up to his image of me and that some day I might approach being half the father and man he was.

TABLE OF CONTENTS

| | <u>Page</u> |
|--|-------------|
| LIST OF FIGURES | v |
| LIST OF TABLES | viii |
| NOMENCLATURE | x |
| SUMMARY | xiv |
| 1.0 INTRODUCTION | 1 |
| 1.1 Objective | 1 |
| 1.2 Development of Load Models | 1 |
| 1.3 Use of Load Models for CSU Simulations | 3 |
| 1.4 Literature Survey | 4 |
| 2.0 FINITE-DIFFERENCE APPROACH TO NUMERICAL HEAT FLOW SOLUTIONS | 5 |
| 2.1 Introduction | 5 |
| 2.2 Governing Equations for Numerical Solutions | 5 |
| 2.3 Finite-Difference Approximations of Non-Homogeneous Walls | 10 |
| 2.4 Conclusion | 17 |
| 3.0 RESPONSE FACTOR AND TRANSFER FUNCTION HEAT FLOW CALCULATIONS | 19 |
| 3.1 Introduction | 19 |
| 3.2 Laplace Transforms of Heat Conduction in Homogeneous Slabs | 20 |
| 3.3 Response Factor Load Calculations | 21 |
| 3.4 Transfer Function Load Calculations | 28 |
| 3.5 Calculation of Heat Conduction Transfer Functions | 33 |
| 3.6 Conclusion | 40 |
| 4.0 VERIFICATION OF TRANSFER FUNCTION METHOD OF LOAD CALCULATION | 41 |
| 4.1 Introduction | 41 |

| | <u>Page</u> |
|--|-------------|
| 7.2 Building Components and Mechanical Equipment | 106 |
| 7.2.1 Collector | 106 |
| 7.2.2 Main Storage Tank | 106 |
| 7.2.3 Domestic Hot Water Tanks | 107 |
| 7.2.4 Heat Exchanger and Air Heater Coils | 107 |
| 7.2.5 Auxiliary Hot Water Boiler | 108 |
| 7.2.6 Pumps and Forced Air Blower | 108 |
| 7.2.7 Air Conditioner | 110 |
| 7.3 System Operation | 110 |
| 7.3.1 Collection | 110 |
| 7.3.2 Heating | 113 |
| 7.3.3 Air Conditioning | 117 |
| 7.3.4 Domestic (Service) Hot Water Operation | 117 |
| 8.0 COMPUTER MODELING OF CSU SYSTEM | 121 |
| 8.1 Introduction | 121 |
| 8.2 Standard TRNSYS Components | 121 |
| 8.2.1 Collector Model | 121 |
| 8.2.2 Storage Tank Model | 123 |
| 8.2.3 Domestic Hot Water Tanks Models | 124 |
| 8.2.4 Controller Models | 125 |
| 8.2.5 Heat Exchanger Model | 127 |
| 8.2.6 Pump Model | 127 |
| 8.2.7 Tee Piece Mixing Valve Model | 127 |
| 8.3 Additional Components Used with TRNSYS | 128 |
| 8.3.1 Radiation Processor | 128 |
| 8.3.2 Transfer Function Wall Model | 132 |

| <u>Figure</u> | | <u>Page</u> |
|---------------|--|-------------|
| 5.2.1 | Cross-Sections of 6" Frame Wall with 6" and 2" of Insulation | 65 |
| 5.4.1 | Flow Chart of Verification Test | 73 |
| 5.5.1 | Cross-Section of CSU Walls | 76 |
| 5.5.2 | SS Surface in b-d Plane | 77 |
| 5.5.3 | Residual Sum of Squares Surface | 77 |
| 5.6.1 | Fluxes for CSU Wall with and without Studs | 81 |
| 5.7.1 | Heat Fluxes for Different Models of CSU Wall | 83 |
| 6.2.1 | Thermal Network of Pitched Roof and Attic - Oonk (10) | 90 |
| 6.2.2 | Thermal Network of Attic and Roof | 91 |
| 6.2.3 | Equivalent Solar-Air Network | 93 |
| 7.1.1 | Colorado State University Solar House I (3) | 103 |
| 7.1.2 | North and South Elevations of CSU Solar House I | 104 |
| 7.1.3 | East and West Elevations of CSU Solar House I | 105 |
| 7.2.1 | CSU Mechanical System | 109 |
| 7.3.1 | Isometric Representation of CSU Mechanical System | 111 |
| 7.3.2 | Mode 1 Energy Collection | 112 |
| 7.3.3 | Mode 1 (Solar) Heating | 114 |
| 7.3.4 | Mode 2 (Auxiliary) Heating | 115 |
| 7.3.5 | Alternate Mode (Solar & Auxiliary) Heating | 116 |
| 7.3.6 | Mode 1 (Solar) Air Conditioning | 118 |
| 7.3.7 | Mode 2 (Auxiliary) Air Conditioning | 119 |
| 7.3.8 | Domestic Hot Water System | 120 |
| 8.1.1 | Overall Schematic of CSU TRNSYS Model | 122 |
| 8.2.1 | Schematic of Main Storage Tank | 123 |
| 8.2.2 | CSU Service Hot Water System Model | 126 |
| 8.2.3 | CSU Air Heating Coils | 129 |

| <u>Figure</u> | | <u>Page</u> |
|---------------|---|-------------|
| 8.3.1 | Sources of Radiation Incident on the Collector | 130 |
| 8.3.2 | Flow Chart for Radiation Processor | 133 |
| 8.3.3 | Transfer Function Wall Flow Chart | 135 |
| 8.3.4 | CSU House I as Modeled | 137 |
| 8.3.5 | Instantaneous and Distributed Solar Heat Gains | 139 |
| 8.3.6 | Instantaneous and Distributed Wall Gains | 139 |
| 8.3.7 | Distribution of Room Potential | 141 |
| 8.3.8 | TRNSYS Thermostat Model | 142 |
| 8.3.9 | Information Flow Diagram for Room System | 144 |
| 8.3.10 | Flow Chart for Room Model in Mode 1 or 2 Heating | 146 |
| 9.2.1 | Storage Tank Temperature versus Time for Simulation I | 156 |
| 9.3.1 | Storage Tank Temperature versus Time for Simulation II | 164 |
| 9.4.1 | Storage Tank Temperature versus Time for Simulation III | 171 |
| 9.5.1 | Energy Exchanges for House | 172 |

| <u>Table</u> | | <u>Page</u> |
|--------------|---|-------------|
| 7.2.1 | Pump Specifications (4) | 108 |
| 8.2.1 | Main Storage Tank Parameters | 124 |
| 8.2.2 | Domestic Hot Water Tanks Parameters | 126 |
| 8.3.1 | Wall and Window Areas for CSU Walls | 136 |
| 9.2.1 | Measured Energy Quantities and Temperatures 11-22-13 hrs to 12-3-19 hrs | 152 |
| 9.2.2 | Simulated Energy Quantities (MJ) 11-22-13 hrs to 12-3-19 hrs | 153 |
| 9.2.3 | Daily Values of Q_u , Q_{ah} and $Q_{T,hw}$ for Simulation I | 155 |
| 9.3.1 | Measured Energy Quantities and Temperatures 12-20-16 hrs to 12-30-10 hrs | 160 |
| 9.3.2 | Simulated Energy Quantities (MJ) 12-20-16 hrs to 12-30-10 hrs | 161 |
| 9.3.3 | Daily Values of Q_u , Q_{ah} and $Q_{T,hw}$ for Simulation II | 162 |
| 9.4.1 | Measured Energy Quantities and Temperatures 1-1-1 hrs to 1-7-23 hrs | 167 |
| 9.4.2 | Simulated Energy Quantities (MJ) 1-1-1 hrs to 1-7-23 hrs | 168 |
| 9.4.3 | Daily Values of Q_u , Q_{ah} and $Q_{T,hw}$ for Simulation III | 170 |
| 9.5.1 | Results of January Simulation of CSU House in Madison | 174 |
| 9.5.2 | Comparison of Detailed Load and Complex Load Operations | 175 |

| | |
|--------------|--|
| P | perimeter |
| q | heat |
| Q_u | useful energy gain from collector |
| R_b | ratio of beam radiation incident on a tilted surface to that on a horizontal surface |
| $R_{i,j}$ | thermal resistance between i and j |
| ΔR | difference in radiation exchange |
| S | Laplace parameter, slope |
| S_c | solar constant |
| SOL | absorbed solar radiation for a surface |
| S_x | standard deviation |
| t, T | temperature |
| T_i | temperature in |
| T_o | temperature out |
| ΔT_x | $T_x - T(0)$ |
| U | overall heat transfer coefficient |
| UA | overall heat transfer coefficient times effective area |
| U_L | overall loss coefficient |
| V | volumetric flow rate |
| x | distance, average |
| x^* | dimensionless distance |

Greek Letters

| | |
|------------|------------------------------|
| α | absorptivity |
| ϵ | emissivity, effectiveness |
| γ | control function (on or off) |

| | |
|-----|-----------------|
| s | storage |
| sa | solar air |
| shg | solar heat gain |
| t,T | total |
| w | wall |
| wdw | window |
| xs | excess |

In addition, all Laplace or z-transforms are indicated by a superscript or line above the symbol (e.g. the transform of the heat flux, q'' , is \bar{q}'').

1.0 INTRODUCTION

1.1 Objective

It is the purpose of this thesis to develop, test and verify an accurate load model and use it with a computer to economically predict hourly thermal response of a building subject to variable ambient and indoor conditions. Computer simulations can be a very helpful design tool when properly used. In the past, however, a major drawback has been the great expense required to run an extensive series of simulations with accurate projections of the required loads. The first part of this thesis covers the development of new and inexpensive, yet accurate, wall and pitched roof models which combine to form the boundary between a thermal room system and the environment. The second part seeks to "fine-tune" and verify this model by comparing the measured thermal performance data of the Colorado State University Solar House I with the corresponding predicted performance of the computer model. The contents of each of these parts of the thesis are outlined, respectively, in the next two sections of this chapter and a literature survey of related studies follows.

1.2 Development of Load Models

In recent years some attention has been directed to the study of time of day energy requirements of buildings. One reason for this is the acknowledged heat storage capabilities of walls and ceilings. The thermal capacitance of these members time delays the effect of ambient conditions, thereby creating peak demands at hours other than those

model a roof and attic. The two models are tested in a simulation to compare accuracy and computing costs.

The load models and procedures developed in Chapters 2-6 are then used to model the CSU house for simulations of the 1974-75 heating season as outlined in the next section of this chapter.

1.3 Use of Load Models for CSU Simulations

The thermal performance of the CSU house is simulated for three different periods of the 1974-75 heating season. The house is modeled by using transfer function representations for the walls and the roof and weather data as measured at the house is used to drive the program.

Chapter 7 is a description of the CSU building components and mechanical equipment. Various modes of operation are presented for energy collection, heating and air conditioning.

Chapter 8 details the computer modeling needed to represent the CSU system. Program TRNSYS (1,2)¹ contains most of the models needed in these simulations. Components that are not modeled by TRNSYS or ones that had to be modified are also explained in this chapter.

Simulations for periods of November, December and January of the 1974-75 winter are explained in Chapter 9. These simulations were done to verify the CSU house model by comparing predicted and actual, measured performances. Another simulation was performed to determine a UA for the house that could be used for heating calculations.

Chapter 10 presents the conclusions obtained from this project and recommendations for future work in this area.

¹

Numbers in brackets refer to the references listed in the Bibliography.

2.0 FINITE-DIFFERENCE APPROACH TO NUMERICAL HEAT FLOW SOLUTIONS

2.1 Introduction

Numerical solutions to transient heat flow problems have become common place due to the availability of hand calculators and computers. The finite-difference approximation to the classical differential equations representing the heat flow and storage in a body seeks to sub-divide the object into smaller sections, each one represented by an electrical circuit of nodes, resistances and capacitances analogous to the thermal properties of the body. In this manner the total flux is the sum of the individual currents in the electrical network.

The finite-difference approximation is used here to represent the thermal network of a wall. Different subdivisions produce somewhat different results, indicating a need for proper placement and number of nodes. Therefore, although the governing equations are presented and derived, an equal effort of this chapter centers on accurately and economically representing walls as a system of finite sub-layers.

2.2 Governing Equations for Numerical Solutions

In most instances, walls can be treated as one-dimensional systems with little vertical transfer of heat and fairly uniform flow horizontally. Exceptions would be constructions employing metal framing and support where the metal acts as a "short" in drawing the heat flow through its area of the cross-section. Since this construction is not common, a one-dimensional analysis is presented.

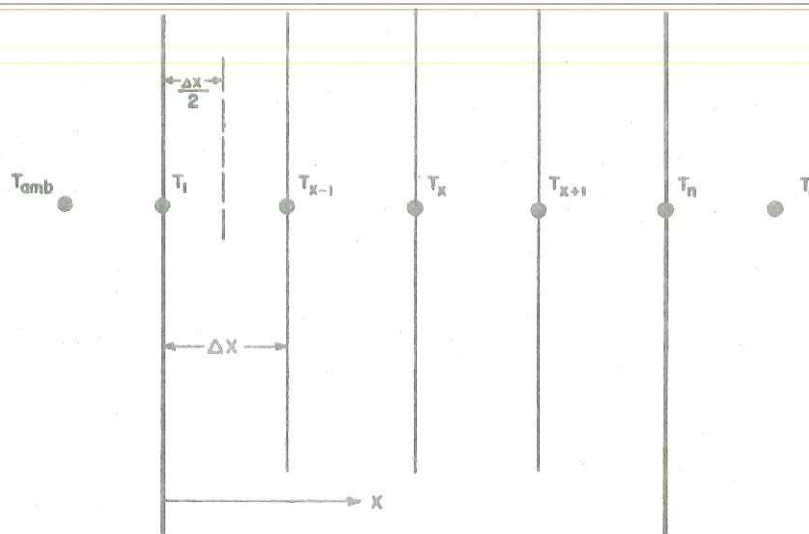


FIGURE 2.2.1. Homogeneous Wall of Δx Layers

temperature plus the average of the two adjacent nodal temperatures.

$$T_x^+ = \frac{\alpha \Delta \tau}{(\Delta x)^2} (T_{x+1}^- + T_{x-1}^-) + \left(1 - 2 \frac{\alpha \Delta \tau}{(\Delta x)^2}\right) T_x^- \quad (2.2.5)$$

An energy balance on the surface node must consider convection and radiation with ambient conditions.

$$h (T_{\infty} - T_0) + k \frac{\partial T}{\partial x} \Big|_{\text{wall}} = \rho c \frac{\partial T}{\partial \tau} \quad (2.2.6)$$

Equation 2.2.6 can be represented by the finite-difference approximation

$$k \frac{(T_{x+1}^- - T_x^-)}{\Delta x} + h (T_{\infty} - T_x^-) = \rho c \frac{\Delta x}{2} \frac{(T_x^+ - T_x^-)}{\Delta \tau} \quad (2.2.7)$$

Similarly, Equation 2.2.8 can be rewritten

$$T_{1,x} = \left(h_o T_{amb} + \text{SOL} + \frac{C_{1,x-1} T_{x-1}}{1} \right) \frac{\Delta T}{1} + \left(1 - \frac{h_o \Delta T}{C_{1,x-1}} \right) T_{x-1} - \frac{\Delta T}{1} \frac{C_{1,x-1} T_{x-1}}{1} \quad (2.2.12)$$

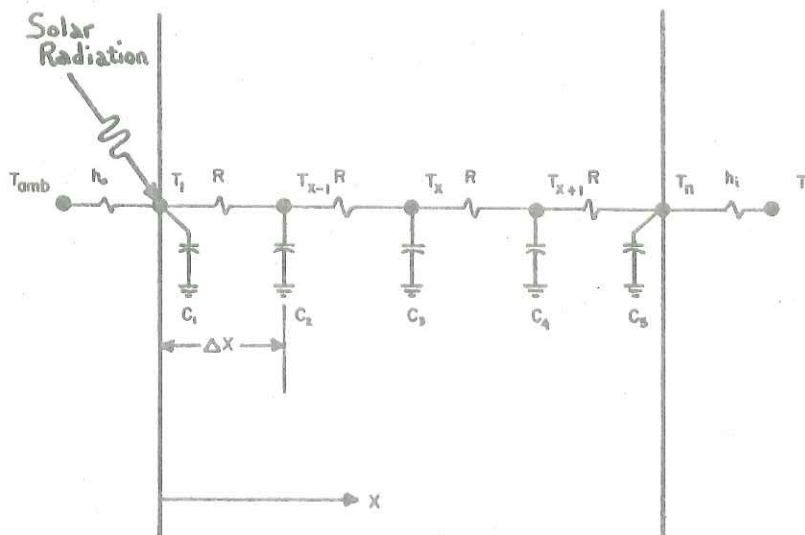


FIGURE 2.2.2

Electrical Network for Homogeneous Wall

For a homogeneous wall of equal Δx increments these equations can be expressed in much simpler form because k , ρ , c and Δx are all constant. However the case of the homogeneous wall is not generally found in the building construction. Instead walls are composed of series or series-parallel combinations of building materials. Calculation of conductance and capacitance values is not as simple for a non-homogeneous wall and a simple relationship between $\Delta \tau$ and Δx does not exist as in Equation 2.2.10. The relationship between these two parameters is not obvious as will be shown in the next section where finite-difference approximations of non homogeneous walls are studied.

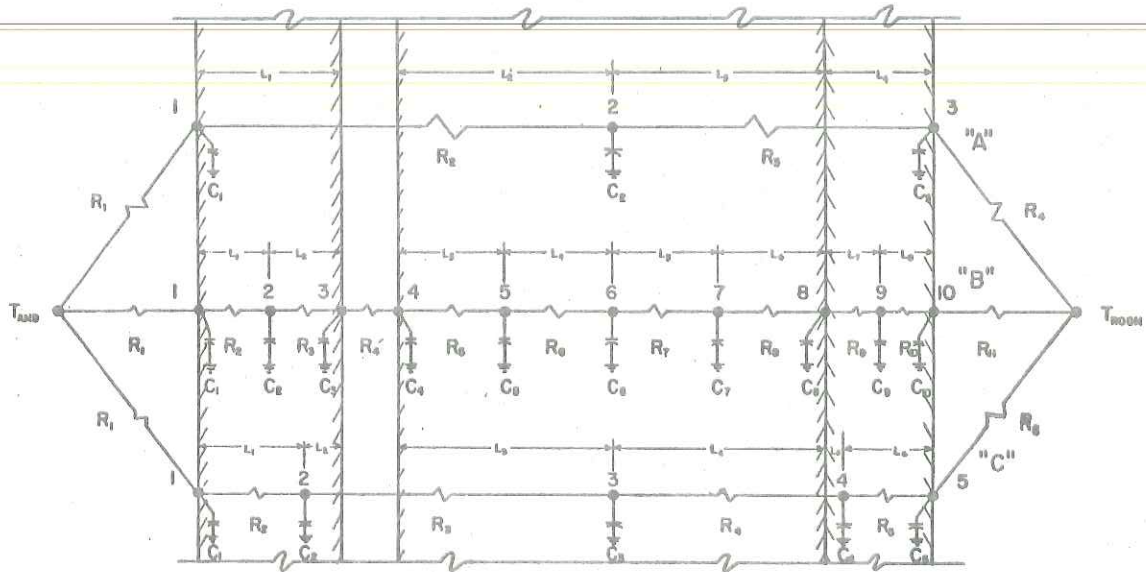


FIGURE 2.3.2. Alternate Networks for Frame Wall.

Models A and B were chosen by locating the nodes according to the physical dimensions of the slab. Conductances were calculated by inverting the sum of the resistances between nodes. The capacitances were found by distributing the thermal mass of the layer between the various nodes. Table 2.3.1 lists the layer properties required to calculate the conductances and capacitances. Values in Table 2.3.1 come from the ASHRAE Handbook of Fundamentals (12). Following this table are example calculations to demonstrate how one obtains the conductance and capacitance values.

TABLE 2.3.1
Thermal Properties of Frame Wall

| LAYER | MATERIAL | t (ft) | k ($\frac{\text{btu}}{\text{hr ft F}}$) | ρ ($\frac{\text{lb}}{\text{ft}^3}$) | c_p ($\frac{\text{btu}}{\text{lb F}}$) | C ($\frac{\text{btu}}{\text{ft}^2 \text{ F}}$) | NOTES |
|-------|------------|----------|---|--|--|--|--|
| 1 | Stucco | 0.0833 | 0.40 | 116 | 0.20 | 1.933 | |
| 2 | Air Space | — | — | — | — | — | $R=0.91 \frac{\text{hr ft}^2}{\text{btu}}$ |
| 3 | Insulation | 0.250 | 0.025 | 2.0 | 0.20 | 0.100 | |
| 4 | Plaster | 0.0625 | 0.42 | 100 | 0.20 | 1.250 | |

The maximum time step allowable for model A would be the minimum time constant,

$$\tau = \frac{C_n}{C_{n-1,n} + C_{n+1,n}} \quad (2.3.1)$$

of the individual three nodes.

$$\begin{aligned} \tau_1 &= 1.80 / (3.0 + 0.163) = 0.569 \text{ hour} \\ \tau_2 &= 0.48 / (0.163 + 0.19) = 1.35 \text{ " } \\ \tau_3 &= 1.00 / (0.19 + 1.46) = 0.605 \text{ " } \end{aligned}$$

A time step of 0.5 hour would be acceptable for model A.

The same procedure was used for model B, the 10 node representation. Table 2.3.2 lists values for resistances, conductances, capacitances and time constants.

Model C was modeled in a slightly different manner. If the cross-section in Figure 2.3.2 were drawn with layer dimensions proportional to capacitance rather than thickness, it would appear as in Figure 2.3.3. The stucco and plaster layers now dominate the cross-section with the insulation markedly smaller. The location of the nodes for this wall were placed so as to approximate equal time constants for each node. Values for model C also appear in Table 2.3.2.

The three systems of Figure 2.3.2 are simulated using TRNSYS and are subjected to an ambient temperature forcing function as shown in Figure 2.3.4. Each system was simulated with room temperature constant. The resultant heat fluxes were recorded and are plotted in Figure 2.3.5. Values past 36 hours are identical to their values at 24 hours previous

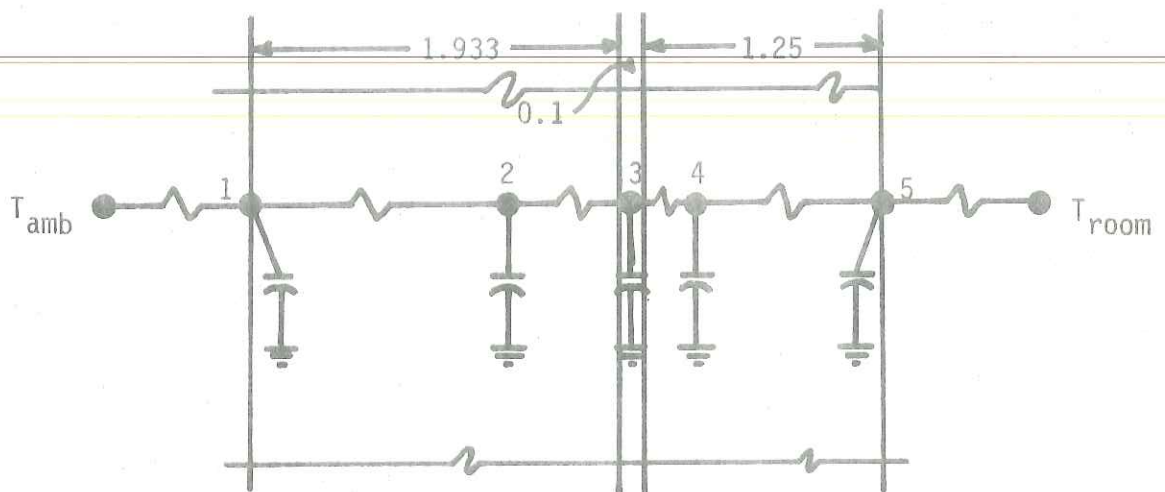


FIGURE 2.3.3. Cross-Section of Frame Wall with Layer Thickness Scaled to Layer Capacitance.

due to the periodicity of the input. The response to ambient change of the three node model is slower than that of the five or ten node system. This is due to the lumping of a large capacitance at the surface node in model A. Models B and C have capacitances that are more distributed over the cross-section and while their sums are equal, the individual capacitances are less and do not take as long to charge.

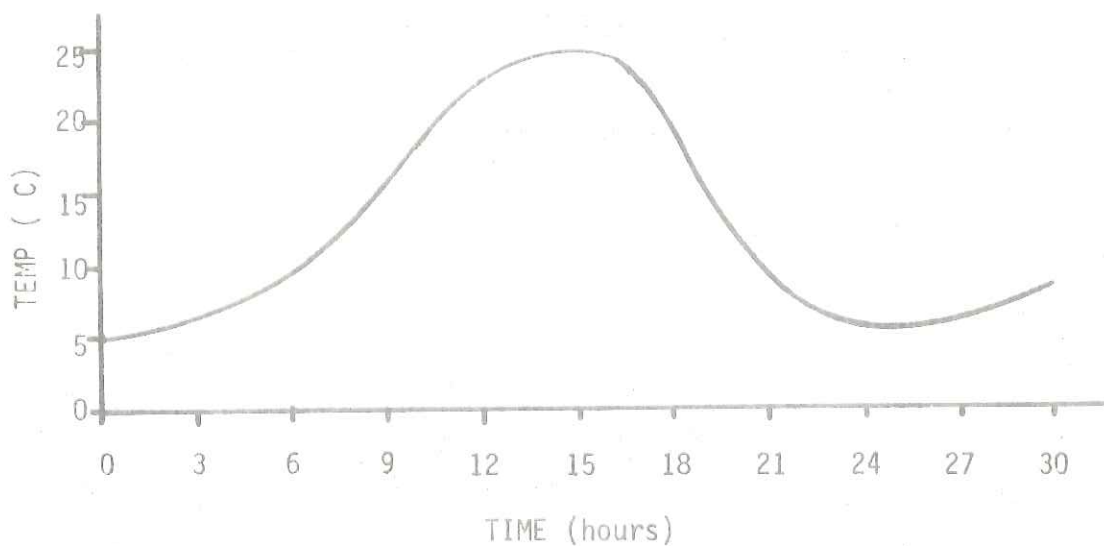


FIGURE 2.3.4. Periodic Forcing Function for Ambient Temperature.

It would be natural to assume that the ten node model would be the most accurate representation of the wall. Yet its response, while extremely close to that of the five node model, actually falls between those of the three and five node models. However the differences between models B and C are so small that when the accuracy of the integrator used in the simulation is considered the plots for practical purposes coincide.

The values of total integrated flux for a four day simulation along with the computer charges are listed in Table 2.3.3. The values for computer costs are only for central processing unit (cpu) time so the charges would be proportional for longer simulations.

TABLE 2.3.3
Flux and Cost Totals for Frame Wall Models

| | q''_{total} (KJ/m ²) | Cost (\$) | q''_{daily} (KJ/m ²) |
|--------------------|---------------------------------------|--------------|---------------------------------------|
| Model A - 3 Nodes | -930.64 | 0.34 | -242.63 |
| Model B - 10 Nodes | -931.50 | 2.12 | -242.60 |
| Model C - 5 Nodes | -930.74 | 0.63 | -242.58 |

2.4 Conclusions

The near identical hourly response coupled with cost savings of 70% indicate that the wall with nodes of nearly equal time constants located by viewing cross-sections with dimensions expressed in capacitance terms is more than an adequate representation when compared to a model of twice as many nodes. If the hourly response were not critical, the lesser node (network A) model would suffice.

3.0 RESPONSE FACTOR AND TRANSFER FUNCTION HEAT FLOW CALCULATIONS

3.1 Introduction

It was found in Chapter 2 that transient heat conduction through walls can be calculated by the finite-difference approximation to the heat conduction equation. The computer allows us to use this approximation for detailed load analysis over long simulations. The complexity of the preparation (calculating resistances and capacitances, placing nodes) and the high computer costs, however, have indicated a need for a different, simpler and more economic means of calculation.

D.G. Stephenson, G.P. Mitalas and J.G. Arseneault of the National Research Council of Canada have developed methods of calculating heat flows without employing the lumped resistance and capacitance concept. They instead use Laplace transforms of the heat conduction equation.

This approach was used to develop the "X-Y-Z response factor" equations which compute multi-layer heat flows in a manner that is totally algebraic and significantly less expensive to use for load calculations.

A time series is a set of observations at specified intervals of time which relate a dependent quantity (in our case heat flux) to the independent observations (outdoor and indoor temperatures in our case). Response factors are three sets of numbers expressed as X_i , Y_i , and Z_i and are coefficients of indoor and outdoor temperatures at time i in a time series which relates current heat flux to temperature histories.

Experience gained from using the response factors led to the development of the transfer function approach to heat flow calculations.

Equation 2.2.1 is transformed using the following Laplace transforms

$$\mathcal{L}\left(\frac{\partial^2 T}{\partial x^2}\right) = \frac{d^2}{dx^2} \mathcal{L}(T) = \frac{d^2 \bar{T}}{dx^2} \quad (3.2.1)$$

$$\mathcal{L}\left(\frac{\partial T}{\partial \tau}\right) = s\bar{T} - t(0) \quad (3.2.2)$$

to get

$$\frac{d^2 \bar{T}}{dx^2} - \frac{s}{\alpha} \bar{T} = -\frac{1}{\alpha} t(0) \quad (3.2.3)$$

For a zero initial condition ($T(0)=0$), Equation 3.2.3 can be expressed in the following non-dimensional coordinates

$$\frac{d^2 \bar{T}}{dx^{*2}} - s\bar{T} = 0 \quad (3.2.4)$$

Initial and boundary conditions of the slab, for $T=T(x,t)$, are

$$T(x,0) = T(0)$$

$$T(0,t) = T_0(t)$$

$$T(L,t) = T_L(t)$$

and the flux at any time t at the outer surface, $q''(0,t)$, is $q_0''(t)$.

Equation 3.2.3 is the basis for much of the work done in later portions of this chapter and is referred to frequently.

3.3 Response Factor Load Calculations

This section presents the development of the response factor heat conduction equations from the Laplace transformation done in the last section. All derivations are from Mitalas and Stephenson (13) unless

$$T(x^*, \tau^*) = a \left(x^* \tau^* + \frac{x^{*3} - x^*}{6} + \frac{2}{\pi^3} \sum_{m=1}^{\infty} \frac{(-1)^{m-1}}{m^3} e^{-m^2 \pi^2 \tau^*} \sin m \pi x^* \right) \quad (3.3.8)$$

Mitalas and Stephenson (13) compute the heat flux to be

$$q''(x^*, \tau^*) = k \frac{\partial(T(x^*, \tau^*))}{\partial x^*} \quad (3.3.9)$$

Calculations are done at finite intervals of time of $\Delta=1$ hour. This gives 24 data points for a daily temperature distribution and data (ambient temperature) is readily available. If smaller intervals are required, interpolation can be used without significant error. Since

$$T(1, \tau^*) = a \tau^* = a \alpha \tau / L^2 \quad (3.3.10)$$

a is chosen such that

$$a = L^2 / \alpha \Delta \quad (3.3.11)$$

which gives a unit surface temperature at $t=\Delta$. Substituting $t=n\Delta$ ($\tau = \alpha n \Delta / L^2$) into Equations 3.3.8 and 3.3.9 gives

$$q''(x^*, n\Delta) = \frac{k}{L} \frac{L^2}{\alpha \Delta} \left(\frac{\alpha n \Delta}{L^2} + \frac{3x^{*2} - 1}{6} + \frac{2}{\pi^2} \sum_{m=1}^{\infty} \frac{(-1)^{m-1}}{m^2} e^{(-m^2 \pi^2 \alpha \Delta / L^2) n} \right) \quad (3.3.12)$$

Fluxes at the respective outer and inner surfaces are found to be

$$q''(0, n\Delta) = \frac{kL}{\alpha \Delta} \left(\frac{\alpha n \Delta}{L^2} - \frac{1}{6} + \frac{2}{\pi^2} \sum_{m=1}^{\infty} \frac{(-1)^{m-1}}{m^2} \gamma^n \right) \quad (3.3.13)$$

$$Y_1 = -\frac{k L^2}{L \alpha \Delta} \left(-\frac{1}{6} + \frac{2}{\pi^2} \sum_{m=1}^{\infty} \frac{(-1)^m (\gamma_m^2 - 2\gamma_m)}{m^2} \right) \quad (3.3.20)$$

$$X_n = -\frac{k L^2}{L \alpha \Delta} \frac{2}{\pi^2} \sum_{m=1}^{\infty} \frac{\gamma_m^{n+1} - 2\gamma_m^n + \gamma_m^{n-1}}{m^2} \quad (3.3.21)$$

$$Y_n = -\frac{k L^2}{L \alpha \Delta} \frac{2}{\pi^2} \sum_{m=1}^{\infty} \frac{(-1)^m (\gamma_m^{n+1} - 2\gamma_m^n + \gamma_m^{n-1})}{m^2} \quad (3.3.22)$$

Equations 3.3.21 and 3.3.22 are for all $n > 2$.

Mitalas and Stephenson (13) show that due to symmetry of the homogeneous slab, values of X and Z are the same. They also show that the response factor method is easily extended to multi-layer walls. Figure 3.3.1 is a cross-section of a two layer wall.

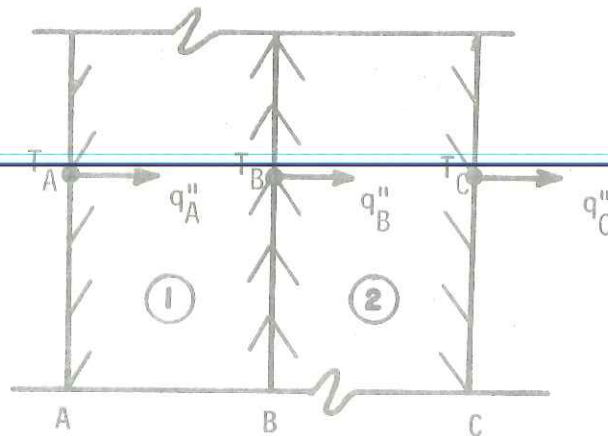


FIGURE 3.3.1. Cross-Section of Two Layer Wall.

The fluxes at the respective three surfaces are represented as

$$q''_A = \sum_{j=0}^{\infty} T_A X_{j1} - \sum_{j=0}^{\infty} T_B Y_{j1} \quad (3.3.23)$$

$$q''_B = \sum_{j=0}^{\infty} T_A Y_{j1} - \sum_{j=0}^{\infty} T_B Z_{j1} \quad (3.3.24)$$

Stephenson observed that the number of terms required in the response factor method could be reduced significantly by observing past records of heat flux as well as temperature. It was this observation plus the inherent storage requirement difficulties of the response factor calculations that led Stephenson and Mitalas to evolve Equation 3.2.3 in a slightly different direction. This resulted in the transfer function method for heat flow calculations that is described in the next section.

Despite the computer storage limitations, the response factor technique has been used by a number of people and is included in ASHRAE (12). Stephenson and Mitalas (16) and Mitalas and Stephenson (13) have used this approach for determining room thermal response factors that calculate a comfort range for cooling load design. Mitalas (17) used response factors to study transient heat flows through walls and roofs. Kusuda (18) has extended the approach to include cylindrical and spherical heat transfer problems. NASA (19) and NBS (20) utilize response factors to calculate building loads in their design programs (NECAP and NBSLD, respectively).

The response factor approach is a major improvement over finite-difference methods and has been used widely as mentioned above. However, the transfer function method described in the next section is easier to use and for this reason was used in the research described in later chapters.

The Laplace transform of heat flux, \bar{q}'' , is found from

$$\bar{q}'' = \mathcal{L}(q'') = \mathcal{L}\left(-k \frac{\partial \Delta T}{\partial x}\right) = -k \frac{\partial \Delta \bar{T}}{\partial x} \quad (3.4.7)$$

$$\bar{q}'' = -kA\lambda \sinh \lambda x - kB\lambda \cosh \lambda x \quad (3.4.8)$$

The following conditions are used to solve for A and B

$$T(0,t) = T_0(t), \quad \bar{T}(0) = \bar{T}_0 \quad (3.4.9)$$

$$q''(0,t) = q_0(t), \quad \bar{q}''(0) = \bar{q}_0 \quad (3.4.10)$$

Solving for A and B in Equations 3.4.6 and 3.4.8 yields

$$\Delta \bar{T}_x = \Delta \bar{T}_0 \cosh \lambda x - \bar{q}_0'' / \lambda k \sinh \lambda x \quad (3.4.11)$$

$$\bar{q}_x'' = -k\lambda \Delta \bar{T}_0 \sinh \lambda x + \bar{q}_0'' \cosh \lambda x \quad (3.4.12)$$

where

$$A = \Delta \bar{T}_0 \quad (3.4.13)$$

$$B = -\bar{q}_0'' / k\lambda \quad (3.4.14)$$

It is convenient to represent Equations 3.4.11 and 3.4.12 together in the following matrix form

$$\begin{vmatrix} \bar{q}_x'' \\ \Delta \bar{T}_x \end{vmatrix} = \begin{vmatrix} A & B \\ C & D \end{vmatrix} \cdot \begin{vmatrix} \bar{q}_0'' \\ \Delta \bar{T}_0 \end{vmatrix} \quad (3.4.15)$$

where the subscript x denotes any location x in the slab. The A,B,C and D terms are constants (A and B different than Equations 3.4.13 and 3.4.14) for the hyperbolic sine and cosine terms from Equations 3.4.11 and 3.4.12 with

$$\begin{vmatrix} \bar{q}''_{x2} \\ \Delta\bar{T}_{x2} \end{vmatrix} = \begin{vmatrix} A_3 & B_3 \\ C_3 & D_3 \end{vmatrix} \cdot \begin{vmatrix} \bar{q}''_{x0} \\ \Delta\bar{T}_{x0} \end{vmatrix} \quad (3.4.18)$$

The constant matrix in the above equation is the matrix product of the initial constant matrices.

Figure 3.4.2 illustrates an extension of the combination idea to include convection exchanges over a pure resistance to ambient or room air temperature.

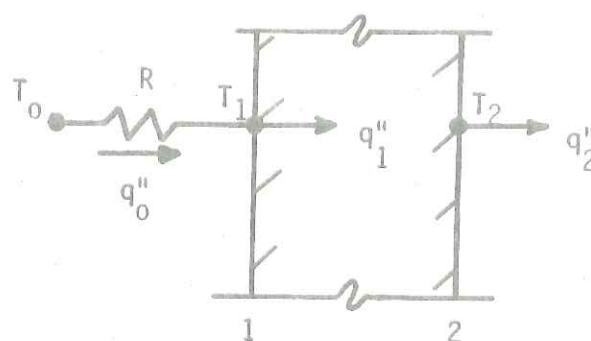


FIGURE 3.4.2. Heat Flows for Convection-Conduction.

$$\bar{q}''_{x1} = \bar{q}''_0 + 0 \cdot \Delta\bar{T}_{x0} \quad (3.4.19)$$

$$\Delta\bar{T}_{x1} = -\bar{q}''_0/R + \Delta\bar{T}_{x0} \quad (3.4.20)$$

The matrix equation for the system of Figure 3.4.2 is

$$\begin{vmatrix} \bar{q}''_{x2} \\ \Delta\bar{T}_{x2} \end{vmatrix} = \begin{vmatrix} A & B \\ C & D \end{vmatrix} \cdot \begin{vmatrix} 1 & 0 \\ -R & 1 \end{vmatrix} \cdot \begin{vmatrix} \bar{q}''_0 \\ \Delta\bar{T}_0 \end{vmatrix} \quad (3.4.21)$$

A similar procedure can be used to relate temperature and flux transforms between a pure resistance, a slab and a second pure resistance as would exist in the case of a wall.

If boundary conditions are such that $\Delta\bar{T}_0$ and $\Delta\bar{T}_x$ are known and

function, $1/B$, times the difference of the transforms of the outer and room air temperatures. After inverse transformation Equation 3.4.29 relates q''_{room} not only to the temperature-time distribution as the X-Y-Z method did but also to the heat flux-time distribution. This is illustrated in the next section.

It should be recognized that Equation 3.4.26 could be used for cases where room temperature is not constant. However, this would be more difficult due to the presence of a second transfer function, A/B . The calculation of these transfer functions is explained in the next section.

3.5 Calculation of Heat Conduction Transfer Functions

It was found in section 3.4 that the Laplace transfer function, $1/B$, relates the transform of the heat flux to or from a room to the transforms of the boundary temperatures. The transfer function, $1/B$, is of a rather complex nature due to the presence of many $\cosh\lambda x$ and $\sinh\lambda x$ terms. The inverse transform of this function would be difficult to find for this reason. It is therefore convenient to represent the transfer function as the ratio of two polynomials in s ,

$$\frac{1}{B(s)} = \frac{N(s)}{D(s)} = \frac{a_0 s^0 + a_1 s^1 + a_2 s^2 + \dots + a_i s^i}{b_0 s^0 + b_1 s^1 + b_2 s^2 + \dots + b_n s^n} \quad (3.5.1)$$

The denominator, $D(s)$, is factored to yield

$$\frac{N(s)}{D(s)} = \frac{N(s)}{(s+\beta_n)(s+\beta_n)\dots(s+\beta_n)} \quad (3.5.2)$$

where $s = -\beta_n$ are roots of $D(s)=0$.

The coefficients of Equation 3.5.6 are the observed outputs, $f(n\Delta)$.

The z-transform of the function $f(t)$ can be obtained by substituting z for $e^{s\Delta}$.

$$F(z) = f(0)z^0 + f(\Delta)z^{-1} + f(2\Delta)z^{-2} + \dots \quad (3.5.7)$$

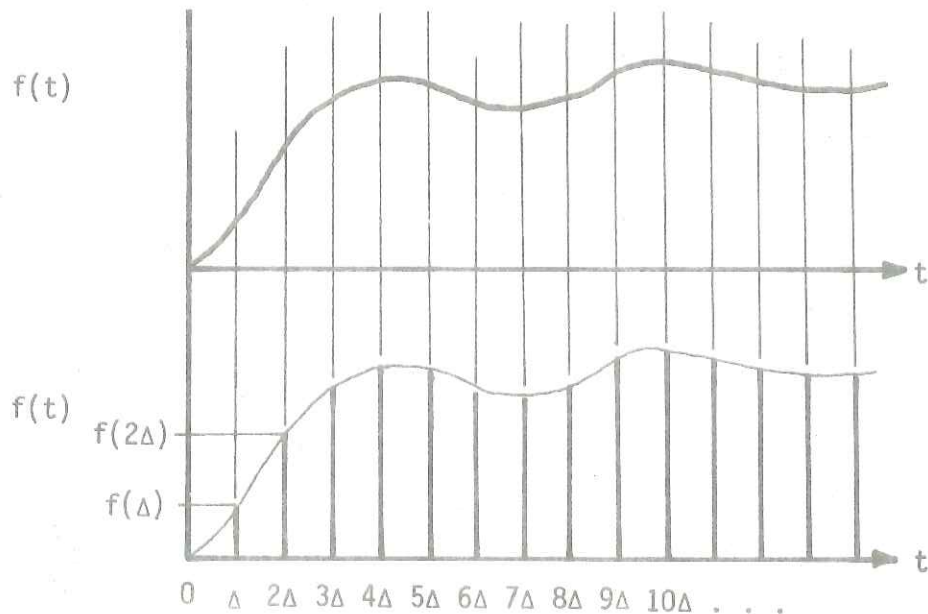


FIGURE 3.5.1. $f(t)$ represented by observations at $n\Delta$.

The daily outdoor temperature distribution is approximated by recorded values measured at hourly time intervals. The heat flux through a wall could be treated in a similar manner. If these observed values are expressed in terms of their z-transforms, with temperature as input and flux as output, the ratio of output/input is a z-transfer function for the system of the wall. If the input and output can be expressed as polynomials in z^{-1} (their z-transforms), this transfer function, $K(z)$, is

$$K(z) = \frac{1}{B(z)} = \frac{N(z)}{D(z)} = \frac{a_0 + a_1 z^{-1} + \dots + a_j z^{-j}}{b_0 + b_1 z^{-1} + \dots + b_p z^{-p}} \quad (3.5.8)$$

before heat flow calculations can be done. The z -transfer function is obtained by changing the Laplace transform of the output ($q''(s)$) partial expansion in Equation 3.5.5 to an equivalent transform in z .

$$\bar{q}''(z) = \frac{C_0 \Delta}{z(1-z^{-1})^2} + \frac{C_1}{1-z^{-1}} + \sum_{n=1}^{\infty} \frac{d_n}{1-e^{-\beta n \Delta} z^{-1}} \quad (3.5.13)$$

A short table of equivalent transforms used by Stephenson and Mitalas (21) is given in Table 3.5.1.

TABLE 3.5.1

Short Table of Equivalent Transforms

| $f(t)$ | $F(s)$ | $F(z)$ |
|-----------|-----------------|-----------------------------------|
| 1 | $1/s$ | $\frac{1}{1-z^{-1}}$ |
| t | $1/s^2$ | $\frac{\Delta}{z(1-z^{-1})^2}$ |
| e^{-at} | $\frac{1}{s+a}$ | $\frac{1}{1-e^{-a\Delta} z^{-1}}$ |

If the terms of Equation 3.5.13 are added together, the common denominator of the sum representing $q''(z)$ is

$$z(1-z^{-1})^2 \sum_{n=1}^{\infty} (1-e^{-\beta n \Delta} z^{-1}) \quad (3.5.14)$$

The denominator of the transfer function $O(z)/I(z)$ is found by dividing Equation 3.5.14 by the z -transform of the input, giving

$$D(z) = \sum_{n=1}^{\infty} (1-e^{-\beta n \Delta} z^{-1}) \quad (3.5.15)$$

point is reached beyond which additional β_n have negligible effect.

The same procedure can be used to find the a coefficients once an expression for $N(z)$ is found. By definition

$$N(z) = \frac{O(z)}{I(z)} D(z) \quad (3.5.19)$$

Recall that

$$I(z) = \frac{\Delta}{z(1-z^{-1})^2} \quad (3.5.20)$$

$$D(z) = \sum_{n=1}^{\infty} (1-e^{-\beta_n \Delta} z^{-1}) \quad (3.5.15)$$

Therefore

$$N(z) = \frac{z(1-z^{-1})^2}{\Delta} \sum_{n=1}^{\infty} (1-e^{-\beta_n \Delta} z^{-1}) \cdot O(z) \quad (3.5.21)$$

where $O(z)$ is $\bar{q}''(z)$ from Equation 3.5.13. The a coefficients are now obtained by equating like terms of Equation 3.5.21 as was done for the b coefficients. The calculations become quite difficult due to the large number of terms and the values of the a coefficients are not calculated here. For these calculations see Stephenson and Mitalas (21). They show that

$$a_0 = \frac{1}{\Delta} (C_0 \Delta + C_1 + \sum_{n=1}^{\infty} d_n e^{-\beta_n \Delta}) \quad (3.5.22)$$

As with the b coefficients, there is a "cut-off" point beyond which additional a coefficients have little effect.

It is obvious that calculation of the transfer function coefficients

4.0 VERIFICATION OF TRANSFER FUNCTION METHOD OF LOAD CALCULATION

4.1 Introduction

The finite-difference approximation for heat transfer calculations is an established method included in most heat transfer texts. Experimental verification of finite-difference predictions has greatly aided its acceptance. The transfer function method is still in its infancy by comparison, having been introduced by Stephenson and Mitalas (16) in 1972. It is the purpose of this chapter to verify the transfer function method by simulating finite-difference and transfer function models for the same weather data. These models are compared over week long periods for various wall constructions and different convection heat transfer coefficients.

The concept of solar-air temperature is also introduced. It is a convenient way to combine the solar and ambient temperature inputs into a single heat source (or sink).

4.2 Derivation of the Solar-Air Temperature

The equations derived in Chapter 3 for transfer function load calculations are in terms of an outer air or outside surface temperature, t_o . The outside surface temperature is not frequently known for it is a function of solar radiation, wind, ambient temperature and the internal properties of the wall. For this reason an outer air temperature is most often used. However it is necessary to include the effect of solar radiation in load calculations and the ambient temperature by itself does not do this. For this reason the concept of solar-air

This results in

$$q'' = I_t \alpha + (h_w + \sigma \epsilon_w F_{w\text{-sky}} (T_o + T_w)(T_o^2 + T_w^2) + \sigma \epsilon_w F_{w\text{-surr}} (T_o + T_w)(T_o^2 + T_w^2)) (T_o - T_w) + \sigma \epsilon_w F_{w\text{-sky}} (T_{\text{sky}}^4 - T_w^4 - T_o^4 + T_w^4) + \sigma \epsilon_w F_{w\text{-surr}} (T_{\text{surr}}^4 - T_w^4 - T_o^4 + T_w^4) \quad (4.2.4)$$

Equation 4.2.4 can be simplified by letting

$$\sigma \epsilon_w (T_o + T_w)(T_o^2 + T_w^2) \approx 4\sigma \epsilon \bar{T}^3 = h_r \quad (4.2.5)$$

where

$$\bar{T} = \frac{1}{2}(T_o + T_w)$$

This changes Equation 4.2.4 to

$$q'' = I_t \alpha + h_o (T_o - T_w) + \epsilon_w \Delta R \quad (4.2.6a)$$

where

$$h_o = h_w + h_r \quad (4.2.6b)$$

$$\Delta R \equiv \sigma (F_{w\text{-sky}} (T_{\text{sky}}^4 - T_o^4) + F_{w\text{-surr}} (T_{\text{surr}}^4 - T_o^4)) \quad (4.2.7)$$

ASHRAE (12) defines ΔR as

the difference between the longwave radiation incident on the surface from the sky and surroundings and the radiation emitted by a black body at outdoor air temperature.

It is now necessary to incorporate the concept of solar-air temperature into Equation 4.2.6. ASHRAE (12) defines solar-air temperature as

that temperature of outdoor air which, in the absence of all radiation exchanges, would give the same rate of heat entry into the surface as would exist with the actual combination of incident solar radiation, radiant exchange with the sky and other outdoor surroundings, and convective heat exchange with the outdoor air.

With this definition of solar-air temperature in mind, Equation 4.2.6

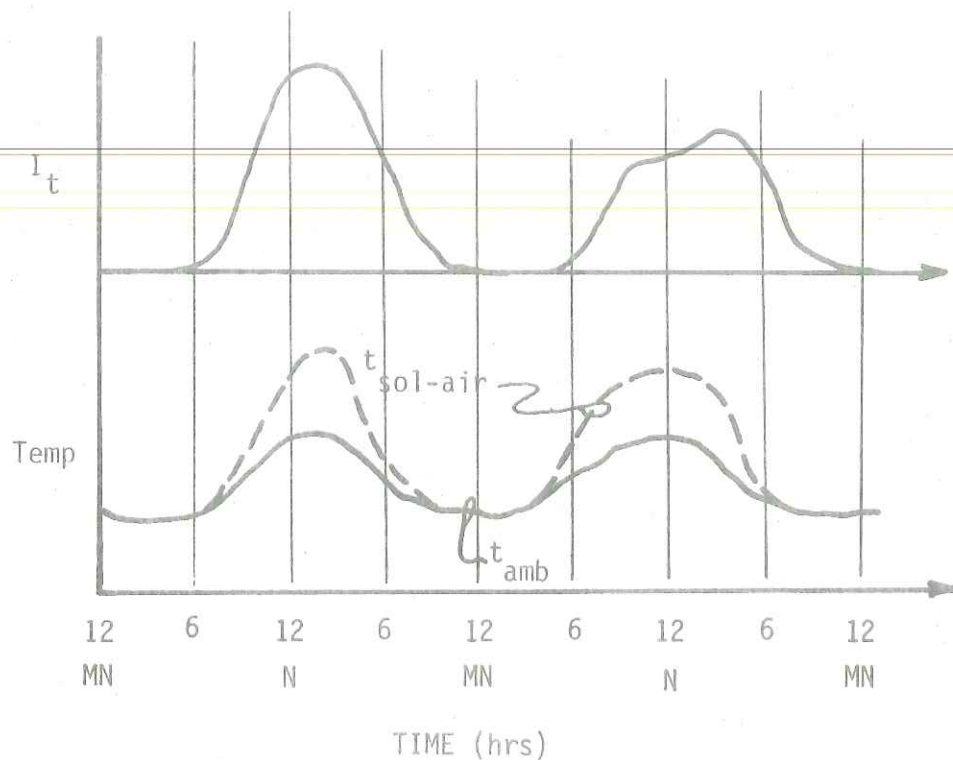


FIGURE 4.2.2. Variations in Sol-Air Temperature.

4.3 ASHRAE Transfer Function Model for Heat Gain (Loss) Calculations

As discussed at length in Chapter 3, ASHRAE (12) has incorporated the transfer function technique into their chapter on calculating cooling loads. They utilize an equation similar to Equation 3.5.12 to calculate heat gain through a wall by

$$q''_{\tau} = \sum_{n=0} b_n (t_{sa, \tau - n\Delta}) - \sum_{n=1} d_n q''_{\tau - n\Delta} - t_{rc} \sum_{n=0} c_n \quad (4.3.1)$$

where b_n are the a coefficients from Chapter 3 and d_n are the b coefficients from Chapter 3. This equation is more conveniently expressed as

$$q''_{\tau} = \sum_{n=0} b_n (t_{sa, \tau - n\Delta} - t_{rc}) - \sum_{n=1} d_n q''_{\tau - n\Delta} \quad (4.3.2)$$

where $\sum b_n = \sum c_n$.

ASHRAE (12) has calculated the transfer function coefficients for

The outside convection heat transfer coefficient, h_w , is found by Jennings (24) to be

$$h_w = 1.6 + 0.3W \quad (4.3.5)$$

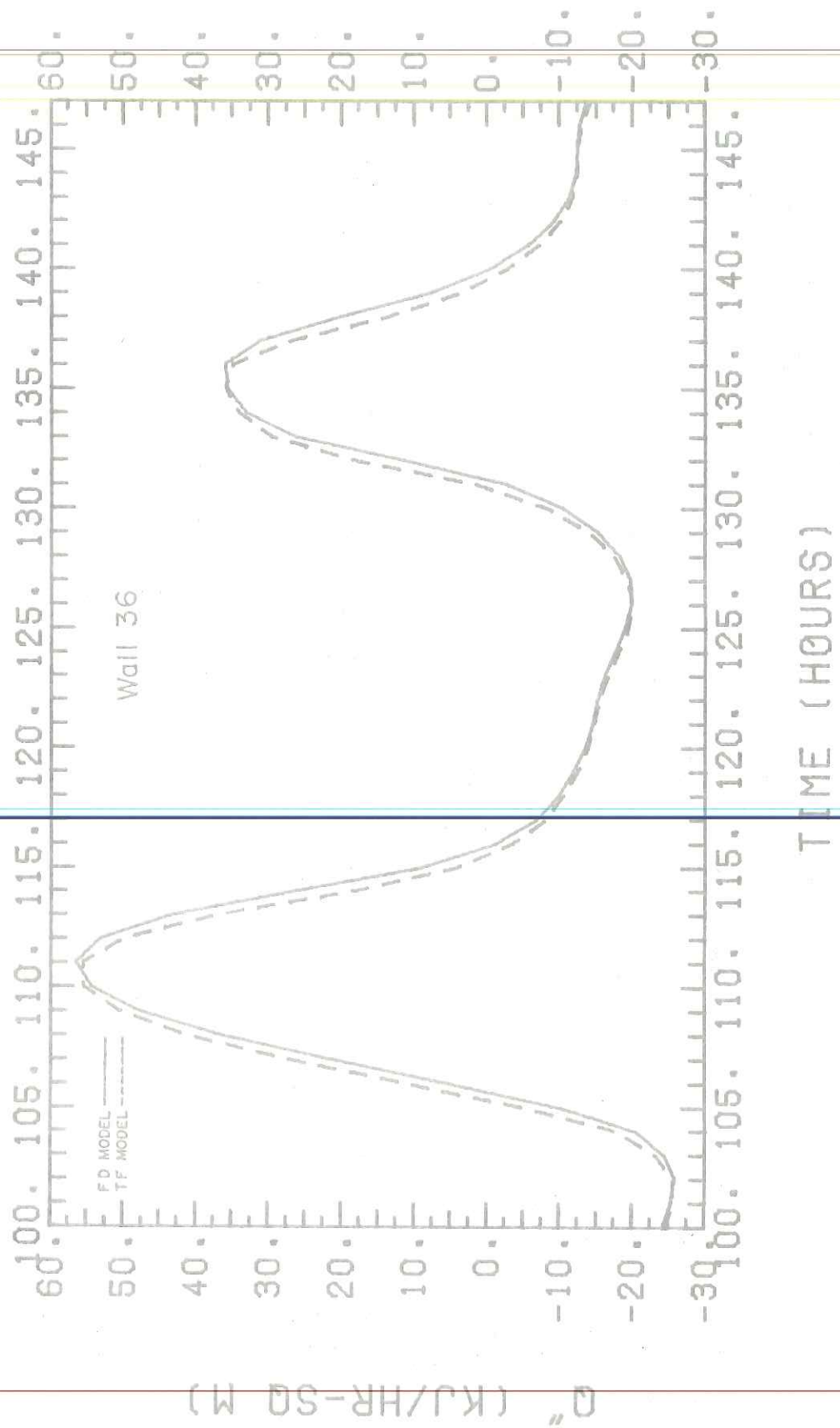
where W is wind speed in miles per hour. This produces values of h_o ranging from 2.6 Btu/hr-ft²-F for no wind to 6.2 Btu/hr-ft²-F for what ASHRAE (12) calls heavy wind climates of 12 mph.

The very nature of the transfer function coefficient calculation scheme requires a constant h_o value. Errors would occur if these coefficients were used for variable h_o conditions (according to Equation 4.3.3) because h_o is used in the t_{sa} calculation. There is the possibility, though, that these coefficients (calculated for $h_o=3.0$) can be used for both constant and variable h_o conditions with little appreciable error. Both of these cases (constant h_o and varying h_o) are tested in later sections of this chapter. In each case, the hour by hour response will be observed versus a finite-difference wall of the same construction and for the same h_o conditions. In this manner the validity of the ASHRAE (12) model can be established using an accepted technique as a check.

4.4 Comparisons of F.D. and T.F. Models for Constant and Varying h_o

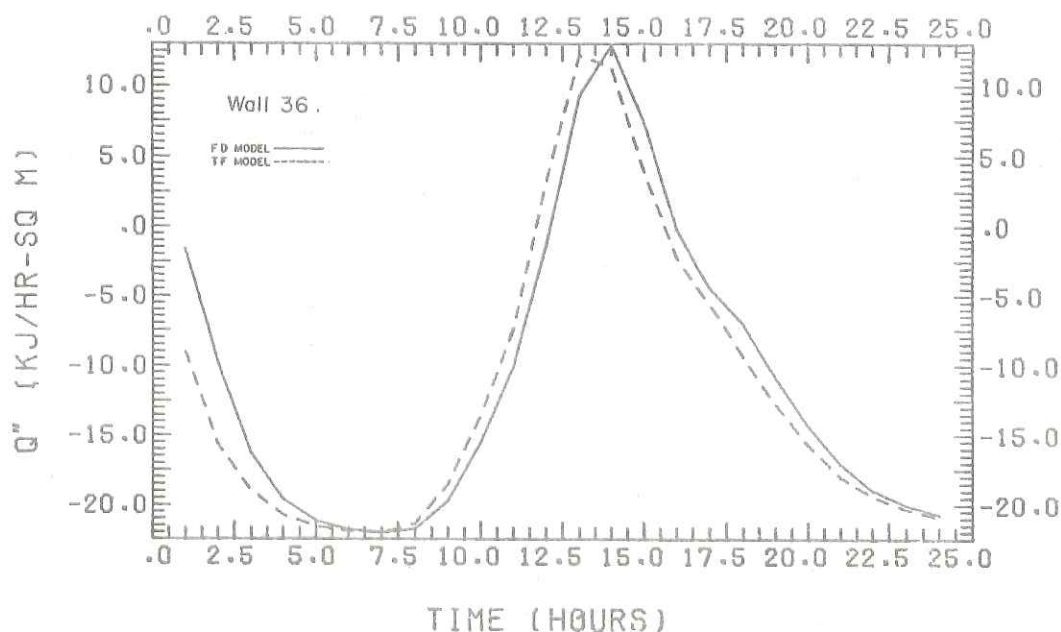
In Chapter 2 a frame wall with 3" of insulation was used in developing a finite-difference model that was accurate but at the same time economic to simulate. This was, in fact, Wall 36 from the ASHRAE (12) table of wall models. The five node finite-difference model is used in a simulation of heat fluxes through a south wall in Madison, Wisconsin for the first week in May. A transfer function model of Wall 36 using

FIGURE 4.4.1
 FLUXES FOR F.D. AND T.F. WALL MODELS FOR CONSTANT H₀



for the wall and that each could just as well predict the true response of the wall as the other.

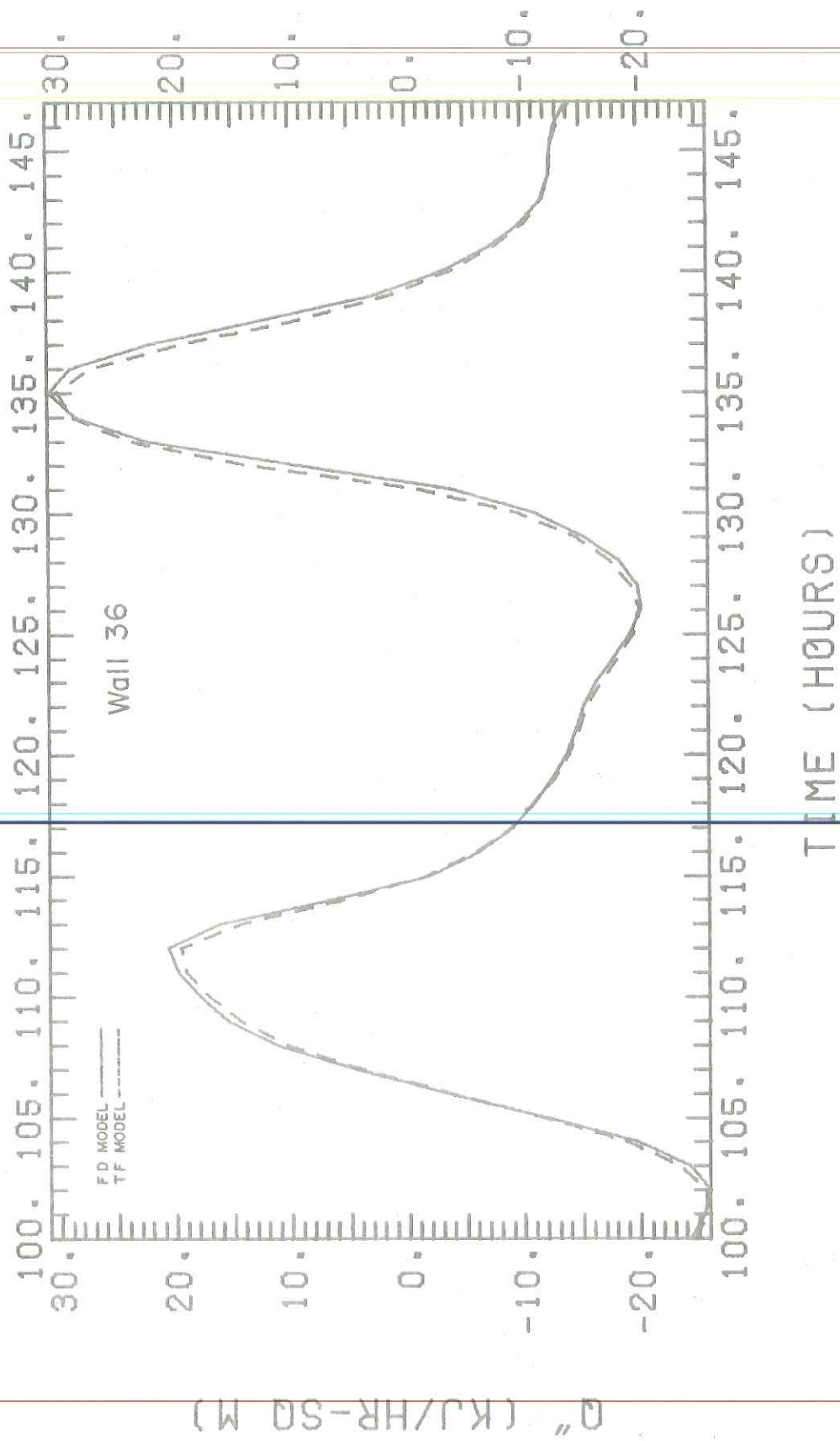
FIGURE 4.4.2
INITIAL FLUXES FOR F.D. AND T.F. WALL MODELS FOR CONSTANT h_0



The second test was run for Wall 36 using a variable h_0 . The outside convection coefficient was calculated by Equation 4.3.3. For the simulation, h_w varied from 33-140 KJ/hr-m²-C for wind speeds varying from 0-8.75 m/sec. The average value was around 110 KJ/hr-m²-C (5.7 m/sec). The radiation coefficient, h_r , was assumed constant and equal to 20.44 KJ/hr-m²-C (1.0 Btu/hr-ft²-F).

Results of this test are given in Table 4.4.3 and Figure 4.4.3. These tend to show that the transfer function wall model will work for variable h_0 . Integrated totals agree and the hourly values are, if anything, in closer agreement. It is important that the model be acceptable for variable values of h_0 for the difference in flux calculations can be

FIGURE 4.4.3
 FLUXES FOR F.D. AND T.F. WALL MODELS FOR VARIABLE H₀



| WALL | LAYER | t (ft) | k ($\frac{\text{Btu}}{\text{hr-ft}^2\text{-F}}$) | ρ ($\frac{\text{lb}_m}{\text{ft}^3}$) | c_p ($\frac{\text{Btu}}{\text{lb}_m\text{-F}}$) | c ($\frac{\text{Btu}}{\text{ft}^2\text{-F}}$) |
|------|-------|--------|--|--|---|---|
| 1 | 1 | 0.333 | 0.770 | 125 | 0.22 | 9.158 |
| | 2 | 0.167 | 0.025 | 2 | 0.20 | 0.067 |
| | 3 | 0.333 | 0.220 | 38 | 0.20 | 2.531 |
| | 4 | 0.063 | 0.420 | 100 | 0.20 | 1.250 |
| 11 | 1 | 0.083 | 0.400 | 116 | 0.20 | 1.933 |
| | 2 | 1.000 | 1.000 | 140 | 0.20 | 28.00 |
| | 3 | 0.063 | 0.420 | 100 | 0.20 | 1.250 |
| 25 | 1 | 0.333 | 0.770 | 125 | 0.22 | 9.158 |
| | 2 | 0.167 | 0.025 | 2 | 0.20 | 0.067 |
| | 3 | 0.042 | 0.240 | 78 | 0.26 | 0.850 |
| 32 | 1 | 0.005 | 26.00 | 480 | 0.10 | 0.240 |
| | 2 | 0.167 | 0.025 | 2 | 0.20 | 0.067 |
| | 3 | 0.333 | 1.000 | 140 | 0.20 | 9.324 |
| | 4 | 0.042 | 0.240 | 78 | 0.26 | 0.850 |

TABLE 4.4.5. Layer Properties of Walls 1, 11, 25 and 32.

transfer function models when h_o is a constant value of 3.0. The percent difference ranges from ± 2.6 -3.6, with Wall 36 the only one below 3.0%.

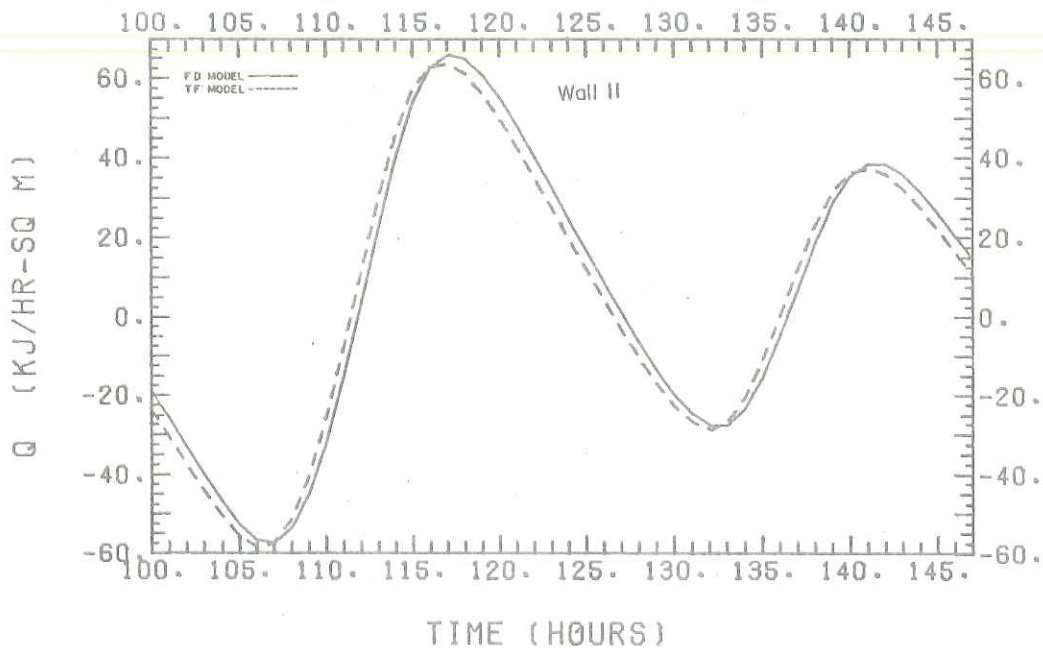
| WALL NO. | h_o | TIME | q_T'' (KJ/m ²) | | % DIFFERENCE |
|----------|-------|-------|------------------------------|------------|--------------|
| | | | F.D. MODEL | T.F. MODEL | |
| 1 | C | 0-168 | -1357 | -1408 | 3.6 |
| | V | " | -2057 | -2120 | 2.9 |
| 11 | C | " | -5771 | -5948 | 3.0 |
| | V | " | -8750 | -8760 | 0.11* |
| 25 | C | " | -1571 | -1620 | 3.0 |
| | V | " | -2416 | -2480 | 2.6 |
| 32 | C | " | -1625 | -1678 | 3.1 |
| | V | " | -2501 | -2529 | 1.1 |
| 36 | C | " | -1058 | -1086 | 2.6 |
| | V | " | -1714 | -1673 | -2.4 |

* If first 36 hours' heat flux totals are neglected
% difference is 3.4%.

TABLE 4.4.6. Total Heat Fluxes for Test Walls.

Variable h_o tests do not correlate as well. The hourly plots show significant differences between finite-difference and transfer function models, especially during peak hours. The integrated totals appear to be in closer agreement but this is due to initial disparities like those in Figure 4.4.2. These differences are more pronounced in the variable h_o models, especially for Wall 11 where the differences

FLUXES FOR F.D. AND T.F. WALL MODELS FOR CONSTANT H_0



FLUXES FOR F.D. AND T.F. WALL MODELS FOR VARIABLE H_0

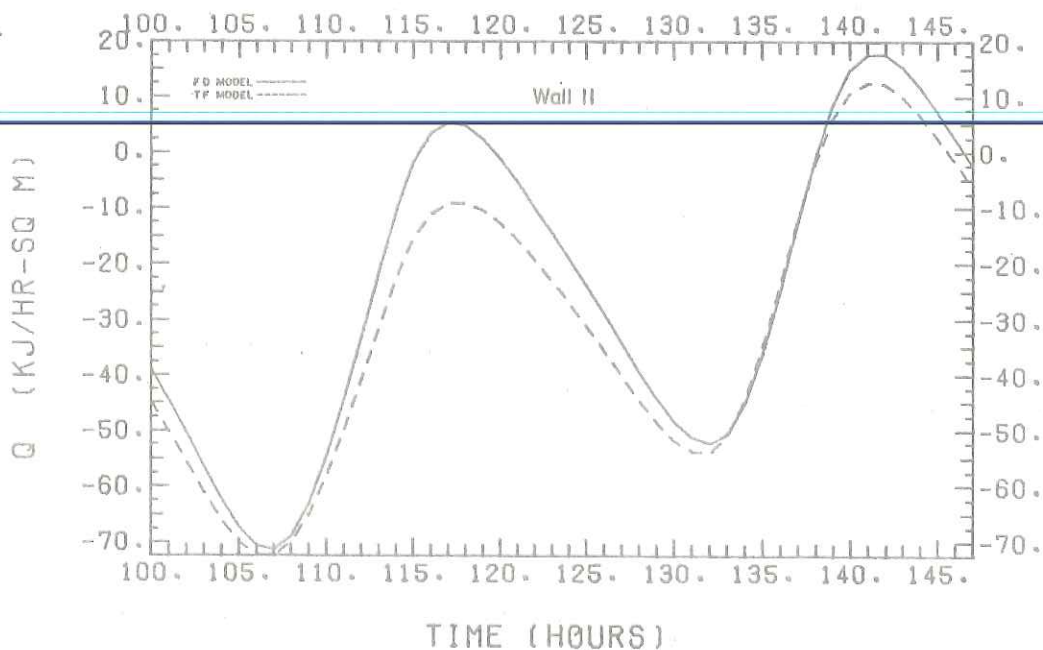
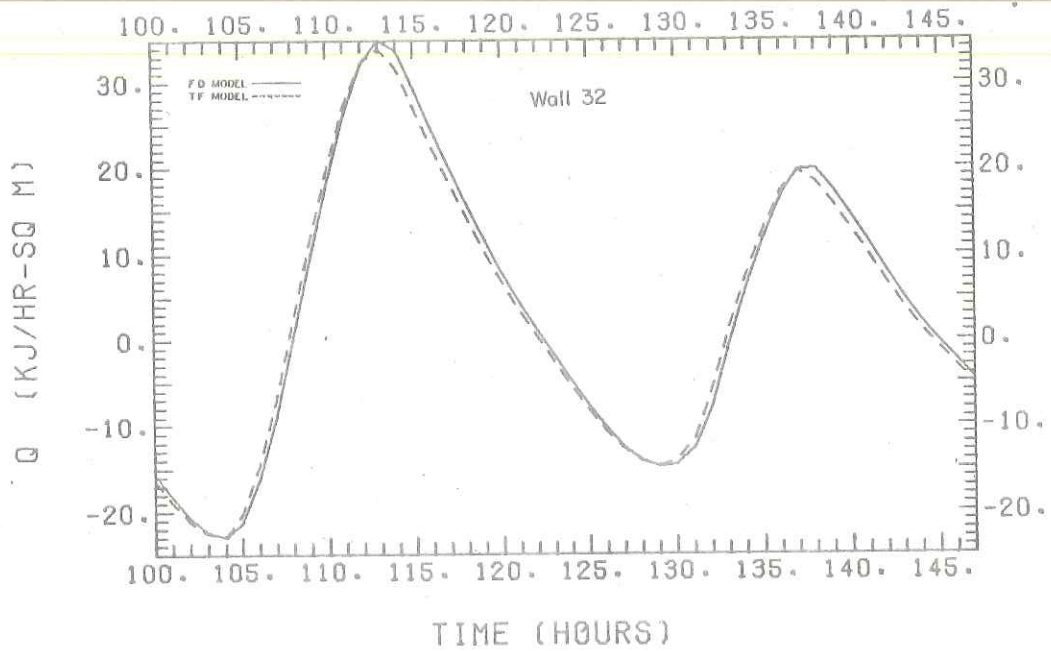


FIGURE 4.4.6. Hourly Heat Fluxes for Wall II.

FLUXES FOR F.D. AND T.F. WALL MODELS FOR CONSTANT H_0



FLUXES FOR F.D. AND T.F. WALL MODELS FOR VARIABLE H_0

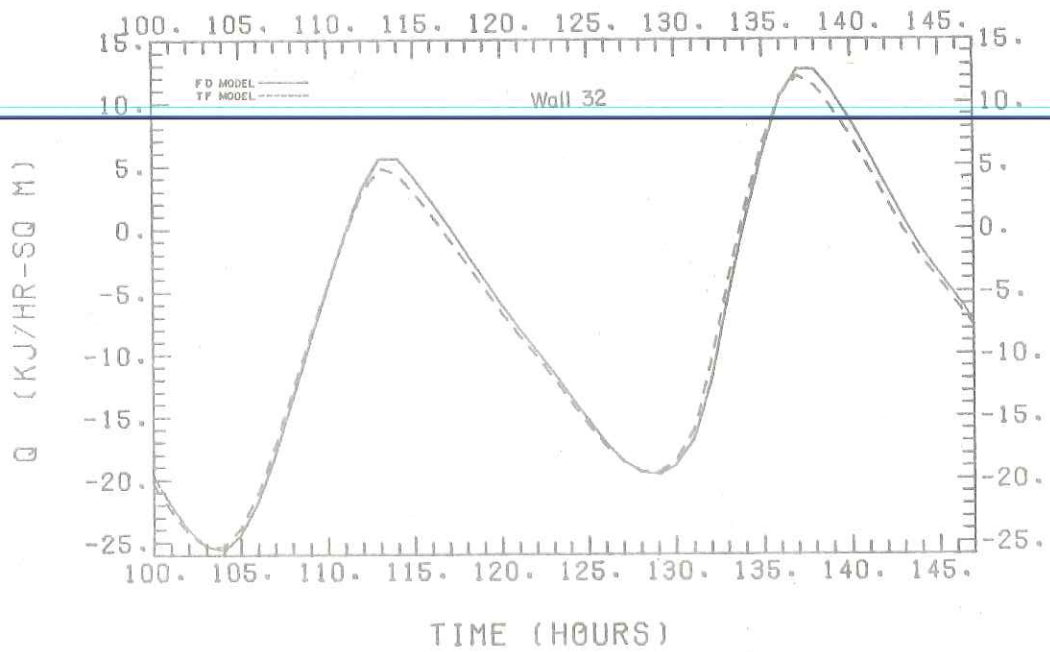


FIGURE 4.4.8. Hourly Heat Fluxes for Wall 32.

wall model for constant and variable outside heat transfer coefficients. Integrated totals vary by around $\pm 3.0\%$ for one week simulations and hourly values are very close although there are some small deviations for low total resistance constructions under variable outside coefficient conditions. These differences (total and hourly) are not significant for one must remember that both methods are approximations and one could just as well be right as the other. It is important to restate one item in the interest of clarity. A variable h_o is used to calculate the solar-air temperature even though the coefficients were derived from a constant value of h_o . This modification did not result in significant error. With this in mind, it is obvious that the transfer function's low cost and simplicity make it the sensible method to use.

Energy Lab's files and is currently available for use.

The program requires as input the constant resistances of outside and inside air (as well as any air spaces within the wall) and the thickness, thermal conductivity, density and specific heat of all other slabs of the wall cross-section. A frame wall using 2x6 studs will be used as an example since it is not available in the ASHRAE (12) tables. Thermal characteristics of the studs are neglected in this example but will be included in later sections of this chapter.

Figure 5.2.1 shows a cross-section of this wall for 6" and 2" of insulation. Table 5.2.1 lists the format required for the input information (6" insulation wall only) and Table 5.2.2 is the output obtained from the transfer function program. Input and output are in English units to conform with other ASHRAE coefficients.

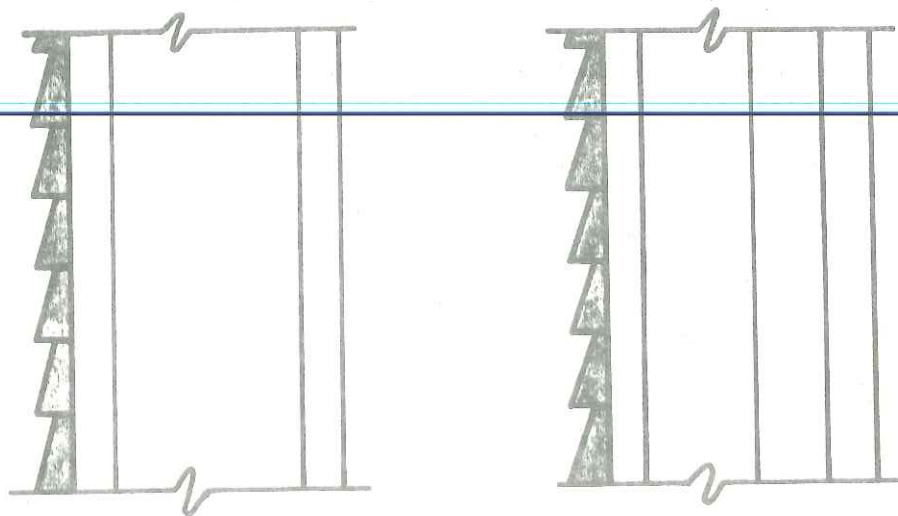


FIGURE 5.2.1. Cross-Sections of 6" Frame Wall with 6" and 2" of Insulation.

The program output lists the numerator and denominator coefficients of the transfer functions. The numerator coefficients (b_n in Equation 4.3.2) are listed for transfer functions D/B , $1/B$ and A/B respectively.

NUMERICAL DATA FOR EXAMPLE PROBLEM.
RUN ONE - WALL WITH 6" OF INSULATION.

| LAYER THICKNESS | CONDUCTIVITY | DENSITY | SP HEAT | RESISTANCE | DESCRIPTION OF LAYER |
|-----------------|--------------|----------|---------|------------|----------------------|
| 1 | .0000 | .0000 | .0000 | .6850 | AIR INSIDE SURFACE |
| 2 | .4200 | 100.0000 | .2000 | .0000 | 3/4" PLASTER |
| 3 | .0250 | 2.0000 | .2000 | .0000 | 6" INSULATION |
| 4 | .0316 | 18.0000 | .3100 | .0000 | 1/2" SHEATHING |
| 5 | .0660 | 32.0000 | .3100 | .0000 | 1" CEDAR SIDING |
| 6 | .0000 | .0000 | .0000 | .3333 | AIR OUTSIDE SURFACE |

THERMAL CONDUCTANCE, U = .042

SAMPLING TIME INTERVAL, DT = 1.000

COEFFICIENTS FOR RAMP INPUT

| J | D1/B | 1/B | A/B | D1/Z |
|---|-----------------------|----------------------|------------------------|-----------------------|
| 0 | .84604274716714+000 | .143378487514050-003 | .69942110803406+000 | 1.00000000000000+001 |
| 1 | -.125805513140274+001 | .53357268117640-002 | -.10336840827858+001 | -.83317343979183+000 |
| 2 | .12579785897154+001 | .50379258110884-002 | .30980161714004+000 | 1.9901034805305+000 |
| 3 | -.2784725816525-001 | .14920958154997-002 | -.42432325878288-001 | 1.1015204333130-003 |
| 4 | .35366738101307-004 | .24687321537971-004 | -.1080483589653886-002 | 1.468278947118-004 |
| 5 | -.2188362578784-007 | .13633088778653-007 | -.703182171940037-006 | -.353477791274570-009 |
| 6 | .44337970232693-012 | .13570778730977-012 | .12208186078783-010 | .868344252913828-017 |
| 7 | .121333172652426-017 | .40486291411004-018 | -.95781450884978-018 | |

NUMERICAL DATA FOR EXAMPLE PROBLEM.
RUN TWO - WALL WITH 8" AIR SPACE AND 2" OF INSULATION.

| LAYER THICKNESS | CONDUCTIVITY | DENSITY | SP HEAT | RESISTANCE | DESCRIPTION OF LAYER |
|-----------------|--------------|----------|---------|------------|----------------------|
| 1 | .0000 | .0000 | .0000 | .6850 | AIR INSIDE SURFACE |
| 2 | .4200 | 100.0000 | .2000 | .0000 | 3/4" PLASTER |
| 3 | .0250 | 2.0000 | .2000 | .0000 | 2" INSULATION |
| 4 | .0000 | .0000 | .0000 | 2.8000 | 8" AIR SPACE |
| 5 | .0316 | 18.0000 | .3100 | .0000 | 1/2" SHEATHING |
| 6 | .0660 | 32.0000 | .3100 | .0000 | 1" CEDAR SIDING |
| 7 | .0000 | .0000 | .0000 | .3333 | AIR OUTSIDE SURFACE |

THERMAL CONDUCTANCE, U = .076

SAMPLING TIME INTERVAL, DT = 1.000

COEFFICIENTS FOR RAMP INPUT

| J | D1/B | 1/B | A/B | D1/Z |
|---|----------------------|----------------------|----------------------|----------------------|
| 0 | .84634340183724+000 | .24972958891159-002 | .69874334058736+000 | 1.00000000000000+001 |
| 1 | -.10274798392314+001 | .210043168114453-001 | -.90579524252123+000 | -.65094245097825+000 |
| 2 | .25587355483949+001 | .10480668411754-001 | .25195229873558+000 | 10.434194761233+000 |
| 3 | -.42573737782848-003 | .3218429814245-003 | -.1059985743258-001 | 1.0702917140209-003 |
| 4 | .1564351121737-004 | .13595808572588-004 | .44314839785338-005 | .31513730091716-009 |
| 5 | -.3792584663396-012 | .13832908154586-012 | -.93911034278895-011 | -.14599732691235-017 |
| 6 | -.34287056301614-017 | .67151549270227-018 | .78835011073247-018 | |

TABLE 5.2.2. Transfer Function Coefficients for 6" Frame Wall.

5.3 Linear Least Squares (LLS) Regression Analysis

The z-transfer function is a very convenient way to obtain coefficients for wall models. In a later section of this chapter a method is presented which allows the program to be used for parallel paths of heat flows (studs and insulation) even though the program was initially limited to cross-sections of series heat flows.

A frame wall was also modeled in an "experimental" manner to include thermal characteristics of the studs. A statistical approach is used to model a transfer function wall from finite-difference wall model data. Equation 5.3.1 is a long hand expression for the transfer function heat flux equation.

$$q_0'' = b_0(t_{sa,0} - t_{rc}) + b_1(t_{sa,1} - t_{rc}) + b_2(t_{sa,2} - t_{rc}) + \dots + b_p(t_{sa,p} - t_{rc}) - d_1 q_1'' - d_2 q_2'' - \dots - d_m q_m'' \quad (5.3.1)$$

A wall could be instrumented and the solar-air temperature and heat flux recorded on an hourly basis. If this data were arranged in a time-series of the form in Equation 5.3.1, the only unknowns would be the b and d coefficients. If there were more observations than unknowns (coefficients) a linear least squares routine could solve for the number of coefficients required and their values.

The coefficients of the time-series have an unique relationship that is best seen by holding the solar-air temperature constant. Then

$$t_{sa,n} - t_{rc} \equiv t_{sa} - t_{rc} \quad (5.3.2)$$

Recall from Chapter 3 that the coefficient (d_0) of the current heat

The value of the mean square, \overline{SS} , is also calculated

$$\overline{SS} = SS/n_{\text{obs}} \quad (5.3.7)$$

and is the average difference between y_{obs} and y_p , squared.

It would be very difficult to monitor and instrument a wall to obtain q'' values precise enough to calculate b and d coefficients to the accuracy needed. Instead, a finite-difference model of a wall could be simulated and its heat flux output recorded along with solar-air temperature to provide the data needed to drive the regression analysis. The number of coefficients is a variable and the b - d combination which produces the minimum residual sum of squares will be the best model of the system. Of course, there is a practical limit beyond which additional coefficients do not produce a significant reduction in SS . This is the "cut-off" point that should be used for the model.

The linear least square regression analysis will be used to model the Colorado State University Solar House I walls. Prior to this, however, in the next section of this chapter, the approach will be verified using an existing wall for which the coefficients are already available.

5.4 Verification of the Regression Analysis Procedure

The procedure outlined in the last section is used here on a wall for which the transfer function coefficients are known. The accuracy of the method can be found by comparing the calculated coefficients to the known values.

ASHRAE Wall 36 will be used as a test case. The tabulated coefficients will be used in a TRNSYS transfer function subroutine for

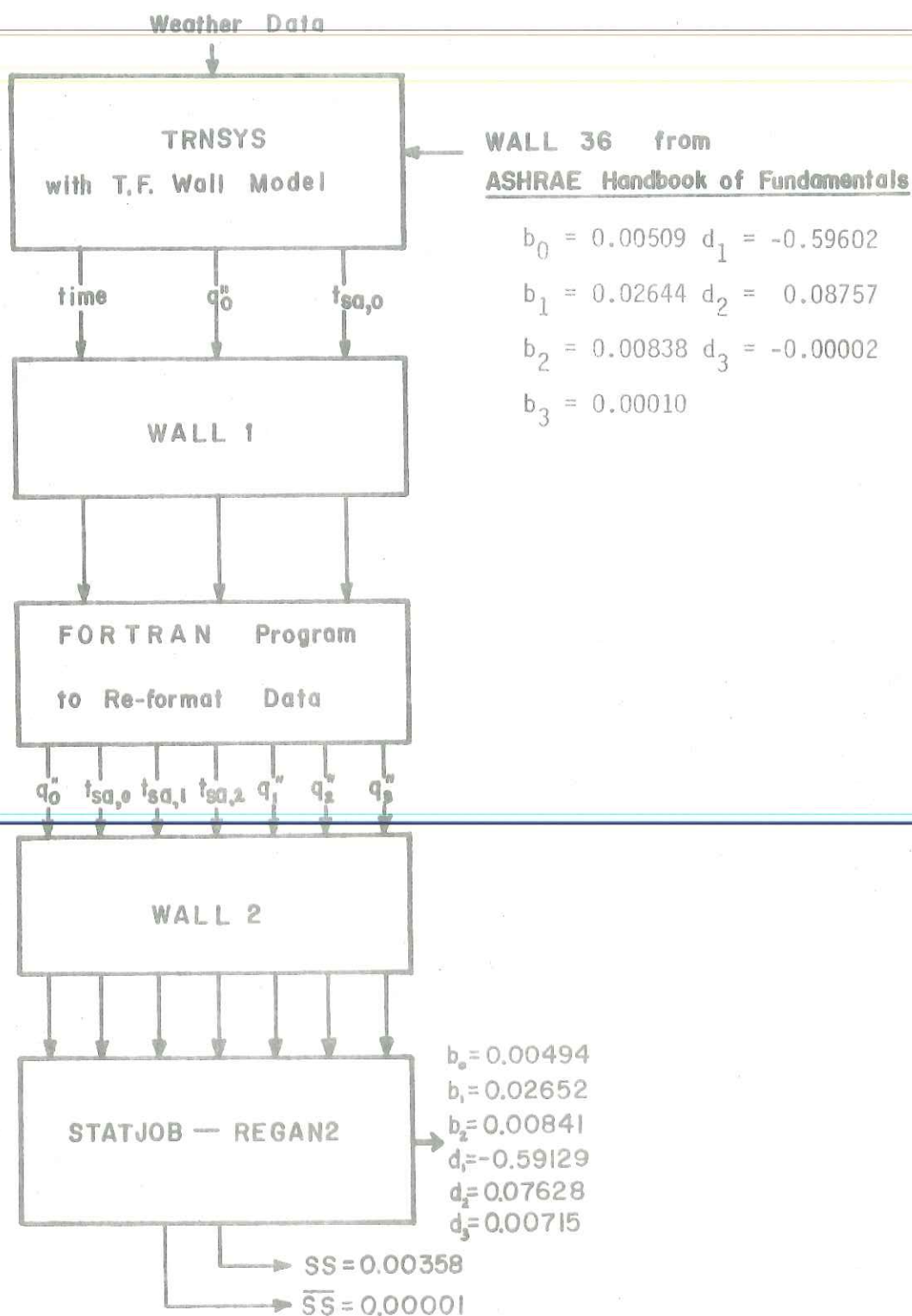


FIGURE 5.4.1. Flow Chart of Verification Test.

| LAYER | MATERIAL | t(ft) | $k\left(\frac{\text{Btu}}{\text{hr-ft}^2\text{-F}}\right)$ | $\rho\left(\frac{\text{lb}}{\text{ft}^3}\right)$ | $c_p\left(\frac{\text{Btu}}{\text{lb}_m\text{-F}}\right)$ | $C\left(\frac{\text{Btu}}{\text{ft}^2\text{-F}}\right)$ |
|-------|--------------|--------|--|--|---|---|
| 1 | Cedar Siding | 0.0883 | 0.055 | 32 | 0.33 | 0.880 |
| 2 | Sheathing | 0.0416 | 0.032 | 18 | 0.31 | 0.233 |
| 3 | Insulation | 0.2922 | 0.025 | 2 | 0.20 | 0.099 |
| 3 | Studs | 0.2922 | 0.063 | 32 | 0.33 | 0.462 |
| 4 | Plaster | 0.0416 | 0.093 | 50 | 0.22 | 0.459 |

TABLE 5.5.1. Thermal Properties of CSU Wall Layers.

| NODE | $R_{i,i+1}\left(\frac{\text{hr-m}^2\text{-C}}{\text{KJ}}\right)$ | $C_{i,i+1}\left(\frac{\text{KJ}}{\text{hr-m}^2\text{-C}}\right)$ | $C_i\left(\frac{\text{KJ}}{\text{m}^2\text{-C}}\right)$ | $\tau(\text{hour})$ |
|------|--|--|---|---------------------|
| 1 | 0.060 | 16.618 | 9.800 | 0.126 |
| 2 | 0.052 | 19.275 | 8.176 | 0.228 |
| 3 | 0.264 | 3.781 | 5.631 | 0.244 |
| 4 | 0.232 | 4.313 | 2.422 | 0.300 |
| 5 | 0.022 | 45.581 | 8.176 | 0.164 |
| 6 | 0.034 | 29.840 | 9.376 | 0.125 |

TABLE 5.5.2. R, Cap, Cond and τ Values for CSU Wall.

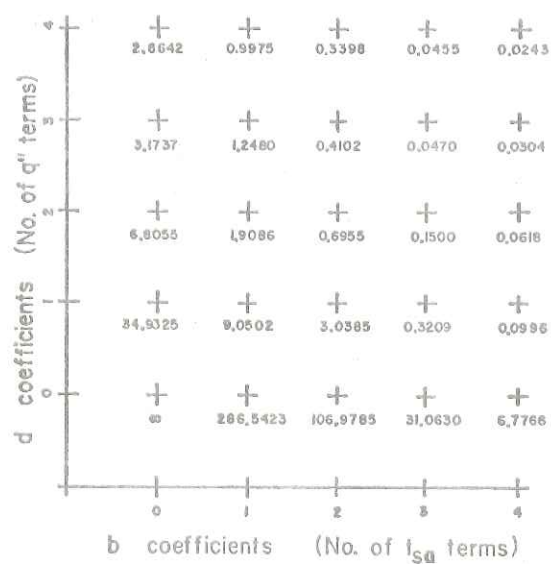


FIGURE 5.5.2. SS Surface in b-d Plane.

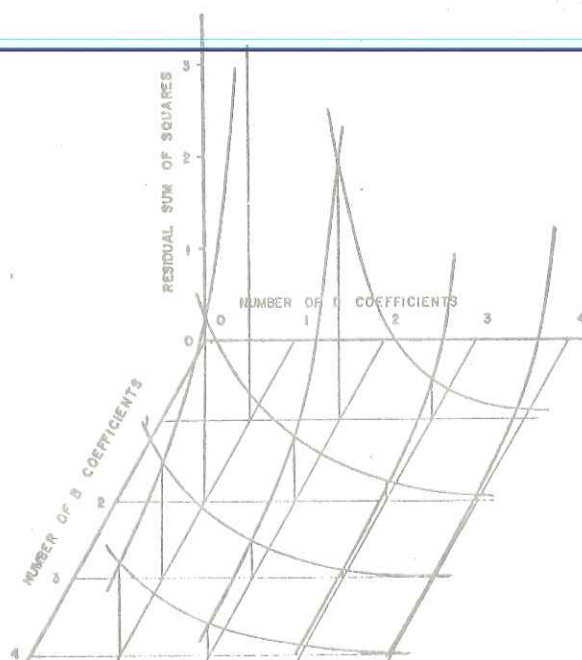


FIGURE 5.5.3. Residual Sum of Squares Surface.

$$\rho_{eq} = (2.0)(0.85) + (32)(0.15) = 6.5 \text{ lb}_m/\text{ft}^3$$

$$c_{p,eq} = (0.2)(0.85) + (0.33)(0.15) = 0.22 \text{ Btu/lb}_m\text{-F}$$

These composite values were then used to represent the composite layer. Table 5.6.2 is the output from the z-transfer function program obtained from this run and one where the frame thermal properties were ignored. The importance of including the frame properties is evidenced by the reduction of the U value from 0.074 to 0.064 Btu/hr-ft²-F when the thermal characteristics are ignored. This is further evidenced by plots shown in Figure 5.6.1, heat fluxes generated by the respective sets of coefficients. The total heat fluxes for the week simulated are listed in Table 5.6.1. The magnitude of the difference clearly indicates the need for a model that includes the thermal characteristics of the studs.

TABLE 5.6.1

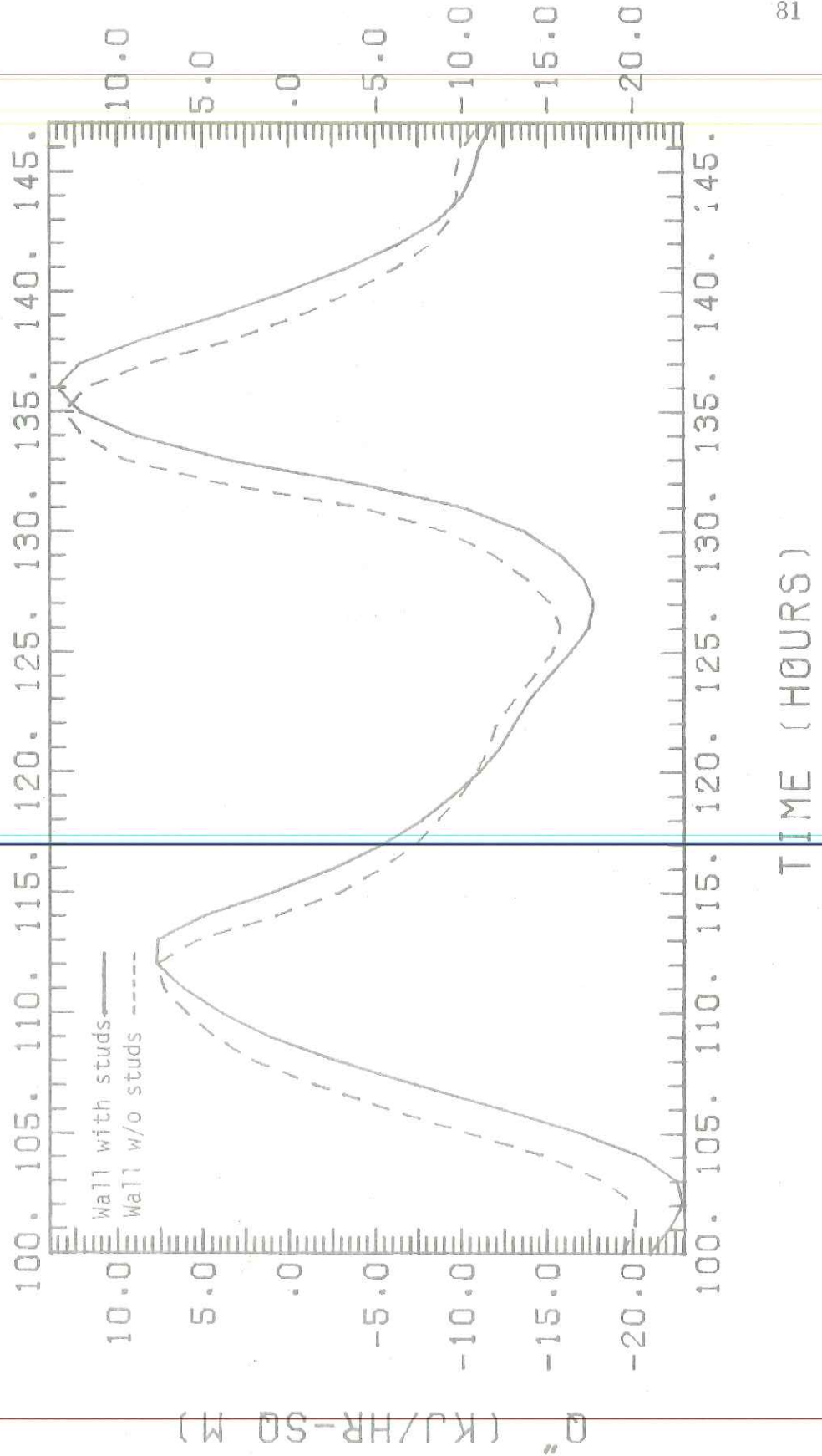
Total Heat Fluxes for CSU Wall Models

| TIME | WALL1(w/studs) | WALL2(w/o studs) | % DIFFERENCE |
|-------|-------------------------|-------------------------|--------------|
| 0-168 | -1899 KJ/m ² | -1629 KJ/m ² | 14.2 |

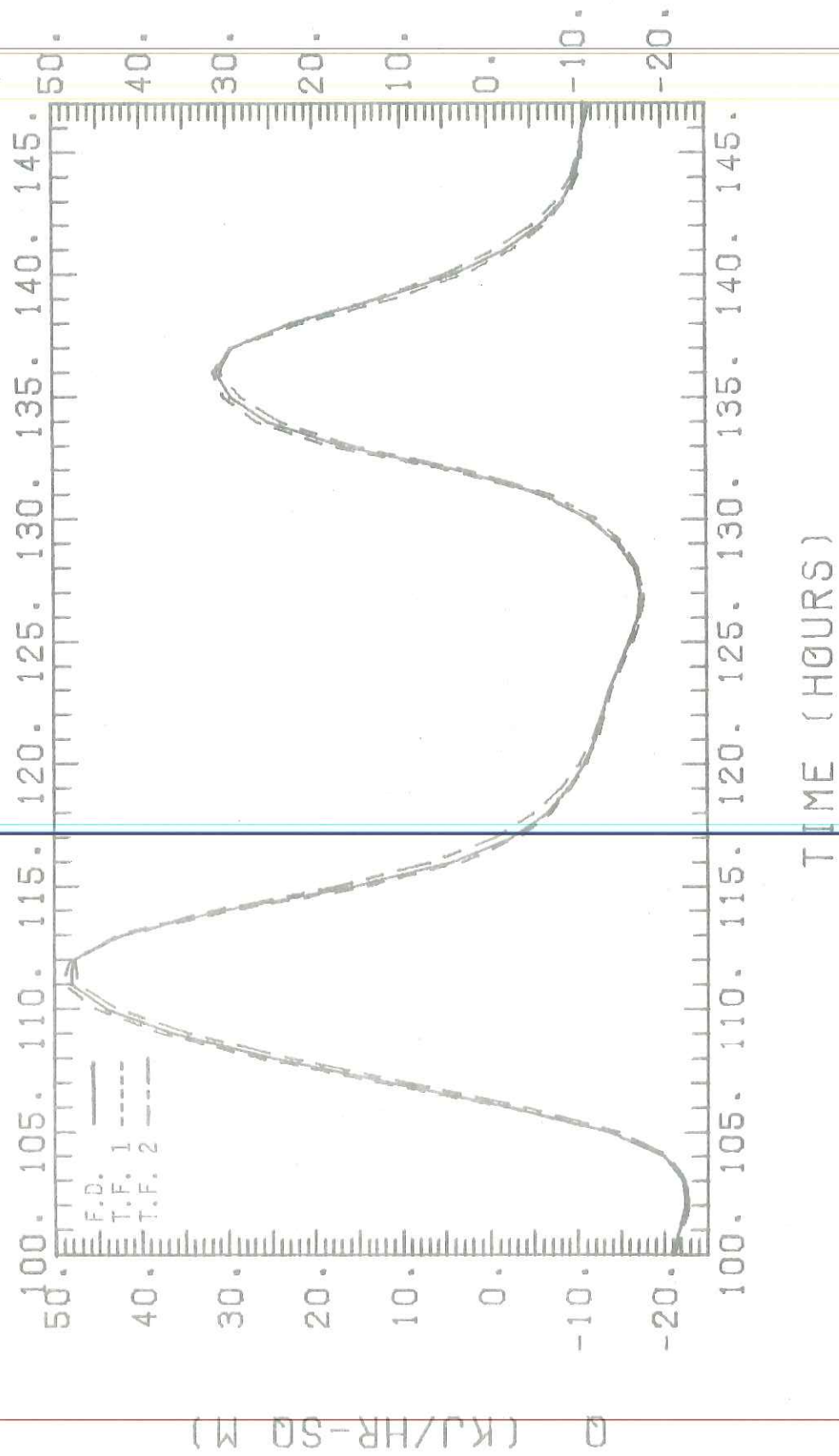
5.7 Comparison of CSU T.F. Models with F.D. Model

Three different models of the CSU walls have been developed, two using transfer functions and the third finite-difference. A one week simulation is run to compare the response of the transfer function models (one obtained from regression analysis, the other using the z-transfer program) to the basic CSU nodal wall.

FIGURE 5.6.1
 FLUXES FOR CSU WALL WITH AND WITHOUT STUDS



HEAT FLUXES FOR DIFFERENT MODELS OF CSU WALL
FIGURE 5.7.1



a function of ambient temperature and incident radiation. Therefore the $t_{sa,0}$ terms in Equation 5.8.4 are not equal unless there is no solar radiation (nighttime or very cloudy days).

A flux that is representative of the total heat gain (or loss) to the room could be expressed by

$$q''_{T,0} = Q_0/A_T \quad (5.8.5)$$

where A_T is the total area of the four walls. If Equations 5.8.4 and 5.8.5 are combined and like terms combined, the total flux is

$$q''_{T,0} = \frac{b_0 (A_s t_{sa,0_s} + A_e t_{sa,0_e} + A_n t_{sa,0_n} + A_w t_{sa,0_w} - (A_w + A_s + A_e + A_n) t_{rc})}{A_T} - \frac{d_1 (A_s q''_{l_s} + A_e q''_{l_e} + A_n q''_{l_n} + A_w q''_{l_w})}{A_T} \quad (5.8.6)$$

Let

$$F_w = A_w/A_T$$

$$F_s = A_s/A_T$$

$$F_e = A_e/A_T$$

$$F_n = A_n/A_T$$

Then the total heat flux is

$$q''_{T,0} = b_0 (F_s t_{sa,0_s} + F_e t_{sa,0_e} + F_n t_{sa,0_n} + F_w t_{sa,0_w} - t_{rc}) - d_1 (F_w q''_{l_w} + F_s q''_{l_s} + F_e q''_{l_e} + F_n q''_{l_n}) \quad (5.8.7)$$

The second bracketed term is the total flux from the previous hour

radiation. ASHRAE (12) presents a detailed procedure for calculating F , the dimensionless ratio of the solar heat gains to the incident solar radiation. The solar heat gain, Q_{shg} , through a window is

$$Q_{shg} = Q_{wdw,R} = A_{wdw} F I_t \quad (5.8.13)$$

The total heat addition effects of the walls can be found from two calculations. Equation 5.8.13 calculates the radiation gain. The total conduction gain is found by adding the respective gains through the walls and windows

$$Q_{wall,C} = A_{T,walls} q''_{T,o} + A_{T,wdws} U_{wdw} (t_{amb} - t_{rc}) \quad (5.8.14)$$

The total heat gain by radiation is found by applying Equation 5.8.13 to all four walls to obtain the following.

$$Q_{shg,T} = A_{T,wdw} F (F I_{t,w} + F I_{t,s} + F I_{t,e} + F I_{t,n}) \quad (5.8.15)$$

The incident solar radiation, I_t , should be reduced by a shading factor if the window is partially shaded.

5.9 Conclusion

Transfer function wall coefficients can be obtained for walls with parallel heat flows. Two methods are available, one using the Mitalas and Arseneault (23) z-transform program with modified input and the other using regression analysis to fit a finite-difference wall model. Both yield essentially the same result as they accurately produce coefficients that model the wall comparably with a finite-difference model. The z-transform program is much easier and faster to use, however, and should be used rather than the regression model. The regression procedure does

6.0 MODELING OF ROOFS AND ATTICS

6.1 Introduction

A means of modeling the heat gain or losses through a roof is necessary before any accurate projection of building loads can be made. Flat roofs are very common in commercial and industrial buildings and in some regions of the country where snow accumulation is not a significant structural concern flat roofs are used in residences as well. Flat roofs are not difficult to model and 36 various constructions are given with transfer function coefficients in ASHRAE (12). Minor modifications of the solar-air temperature calculation allow flat roofs to be treated as walls (section 6.3).

Pitched roofs and attics have not been extensively modeled and little or no work has been done prior to this thesis on developing transfer function models. Stephenson (27) suggested treating the attic as a separate room and calculating attic gains (losses) from the attic-room temperature difference. Conceptually this would work but it would require a second TRNSYS room model. A different approach is taken in this thesis. The roof and attic are regressively modeled by using an effective solar-air temperature that is a function of all roof surface solar-air temperatures and the infiltration effects. This method is an improvement of a finite-difference approach used by Oonk (10), which is also presented in the next section.

In this manner heat gains (losses) through the ceiling can be calculated using roughly the same scheme as was used for the walls, with minor modifications for different solar-air temperatures.

Energy balances on the north roof surface and attic nodes give equations for calculating attic temperature which then drives the finite-difference model just as ambient air temperature did in the wall finite-difference model. These equations become somewhat cumbersome and although they are easy to program, are not easily visualized. See Oonk (10).

Figure 6.2.2 is an electrical network representing a pitched roof and attic. The resistances between solar-air temperatures are totals representing the resistances of outside air and inside (attic) air. The thermal storage effects of the roof layers are small relative to the ceiling and will be ignored. East and west attic walls are included to give a total picture of the attic heat balance. The infiltration resistance is calculated as an amount of air that is heated from ambient to attic temperature each hour. This hourly infiltration rate is found using ASHRAE (12) procedures outlined later in this chapter.

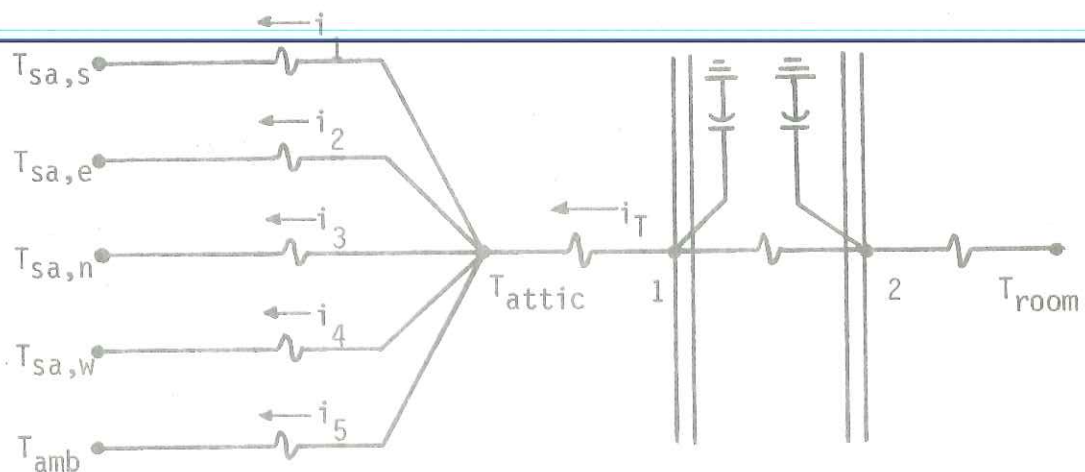


FIGURE 6.2.2. Thermal Network of Attic and Roof.

A current (heat flow) balance on the attic node results in

Combine Equations 6.2.7 and 6.2.8 and rearrange to get

$$t_{sa,eq} - t_{attic} = \frac{C_s t_{sa,s} + C_e t_{sa,e} + C_n t_{sa,n} + C_w t_{sa,w} + C_{inf} t_{amb}}{C_{eq}} - \frac{(C_s + C_e + C_n + C_w + C_{inf}) t_{attic}}{C_{eq}} \quad (6.2.9)$$

But $(C_s + C_e + C_n + C_w + C_{inf}) / C_{eq} = 1$, so Equation 6.2.9 reduces to

$$t_{sa,eq} = \frac{C_s t_{sa,s} + C_e t_{sa,e} + C_n t_{sa,n} + C_w t_{sa,w} + C_{inf} t_{amb}}{C_{eq}} \quad (6.2.10)$$

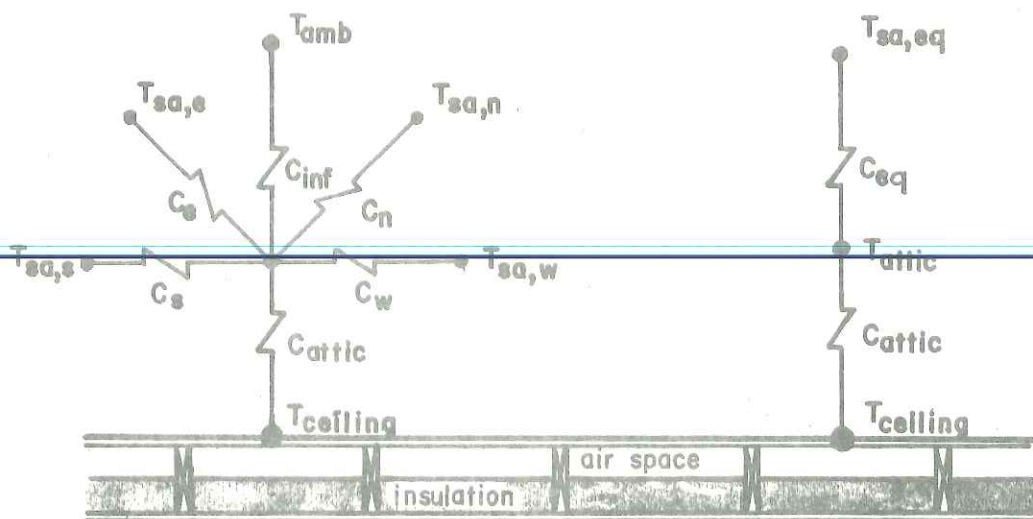


FIGURE 6.2.3. Equivalent Solar-Air Networks.

An equivalent source (sink) temperature has been found which represents the five individual sources (sinks). The southern solar-air temperature can be collector temperature if C_s is the combined back loss and attic heat transfer coefficient. This equivalent temperature

| $Q_{T,ceiling}$ (KJ) | | |
|----------------------|----------|--------|
| V^* | January | July |
| 0 | -479,000 | 81,290 |
| 0.5 | -480,000 | 79,610 |
| 1.0 | -480,900 | 78,000 |
| 1.5 | -481,800 | 76,460 |
| 2.0 | -482,700 | 74,990 |

$V_{attic} = 230 \text{ m}^2$ $V^* = \dot{V} / V_{attic}$

TABLE 6.3.1. Effect of V on Ceiling Heat Flow.

Under winter conditions, changing V^* from 0 to 2 increases the ceiling load by only 0.8%. This indicates that the ceiling heat load is not strongly dependent on attic infiltration and that a value of one (1) air change per hour is reasonable. Summer conditions show a significant difference, for when V^* is changed from 0 to 2 the cooling load is reduced by 7.8%. This is, of course, the reason that many attics are ventilated in the summer in hopes of keeping attic temperatures at ambient levels.

The infiltration conductance, C_{inf} , is

$$C_{inf} = \dot{V} \rho c_p \quad (6.3.2)$$

and it is this quantity that is used in Equation 6.2.6. A value of one air change per hour (244 m^3) was used for the CSU roof and attic.

it is a function of the temperatures of ground, buildings, foliage, etc. However, since most of the radiation exchange from the north roof is to the sky due to its 30° pitch, errors incurred should be small. Table 6.4.1 shows values of various quantities in the ΔR expression when

$$T_{\text{surr}} = T_{\text{amb}} + 10 \quad (6.4.4)$$

where temperatures are again in degrees Kelvin. T_{sky} is from Equation 6.4.3.

| T_{amb} | T_{surr} | T_{sky} | ΔR (KJ/hr-m ²) | $\epsilon \Delta R/h_0$ (K) |
|------------------|-------------------|------------------|------------------------------------|-----------------------------|
| 263 | 273 | 235 | -225.02 | -3.67 |
| 273 | 283 | 249 | -208.18 | -3.39 |
| 283 | 293 | 263 | -179.72 | -2.93 |
| 293 | 303 | 277 | -137.61 | -2.24 |
| 303 | 313 | 291 | -79.75 | -1.30 |

$$F_{\text{surf-sky}} = 0.933, F_{\text{surf-surr}} = 0.067, \epsilon = 1$$

$$h_0 = 61.32 \text{ KJ/hr-m}^2\text{-C}, = 2.041092 \times 10^{-7} \text{ KJ/hr-m}^2\text{-K}$$

TABLE 6.4.1. ΔR Values for North Facing Roof.

The $\Delta R/h_0$ term for most cases is less than 3°C. The view factor to the surroundings is very small (0.067) for a roof with a 30° slope so errors involved with the surroundings temperature assumption in Equation 6.4.4 are relatively small. For this reason, the assumption that surroundings are at 10°C above ambient is used for all solar-air temperature calculations for roof surfaces.

response and it indicates excellent agreement between the two models.

This plot is for the same weather data as was used in the regression analysis but other weather data produces similar results.

This roof model will be used in the CSU simulations that follow in Chapter 9. It is a model that seeks to accurately fit the actual roof and attic. Table 6.5.2 lists respective roof and attic areas used in this model.

TABLE 6.5.2
CSU Roof and Attic Areas

| | |
|-------------------|----------------------|
| west attic | 18.0 m ² |
| east attic | 6.1 m ² |
| south attic | 87.8 m ² |
| north attic | 98.9 m ² |
| north room | 24.9 m ² |
| east room | 11.9 m ² |
| overhang | 31.0 m ² |
| effective ceiling | 129.1 m ² |

6.6 Conclusion

A "black box" transfer function model of a pitched roof and attic is available which is much easier and more economic to use than a finite-difference model. This transfer function model has a single, equivalent solar-air temperature which is derived from the individual roof surface solar-air temperatures. This roof model then becomes an integral part of the house model, combining with the wall model to form the building envelope.

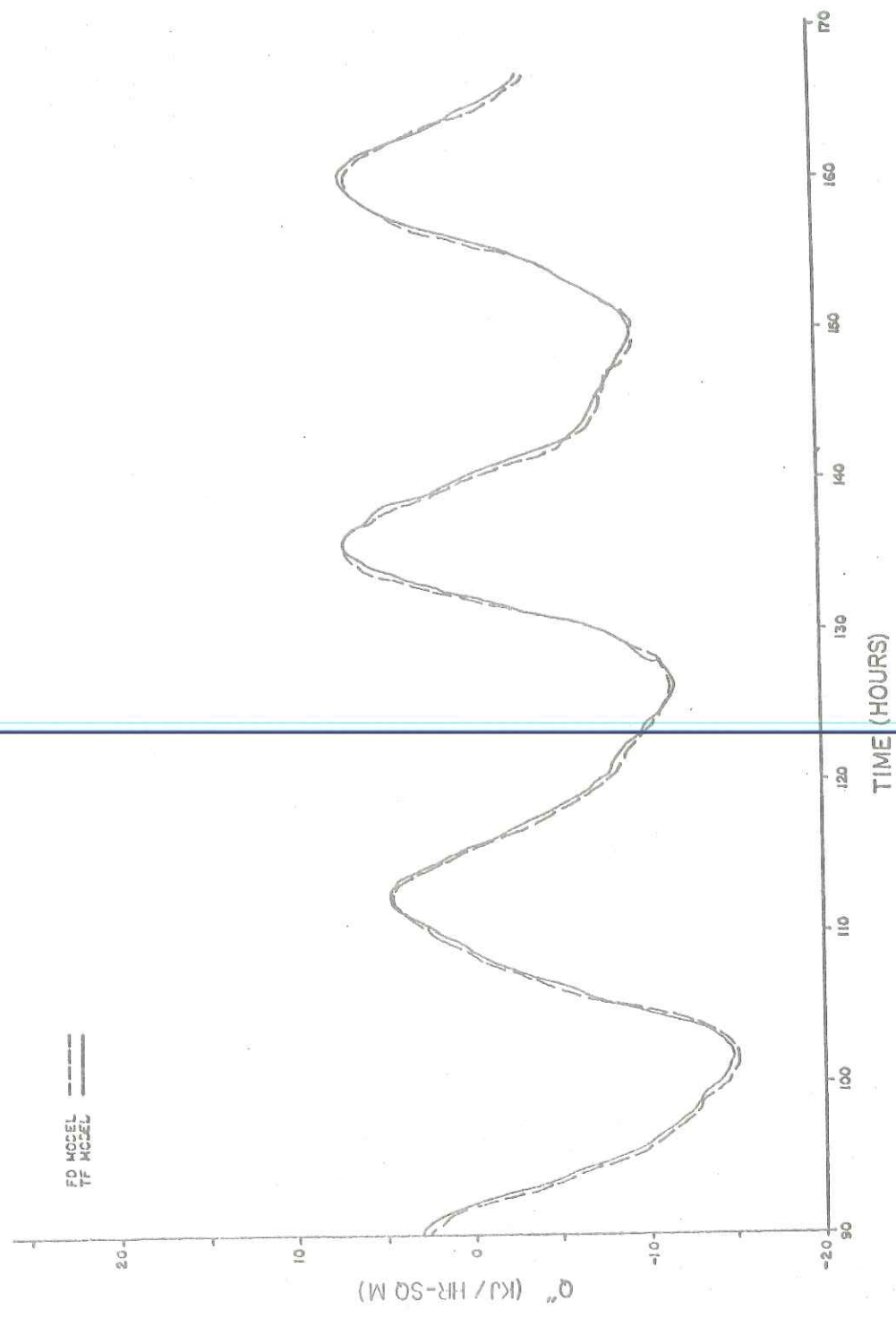


FIGURE 6.5.1 (con'd)

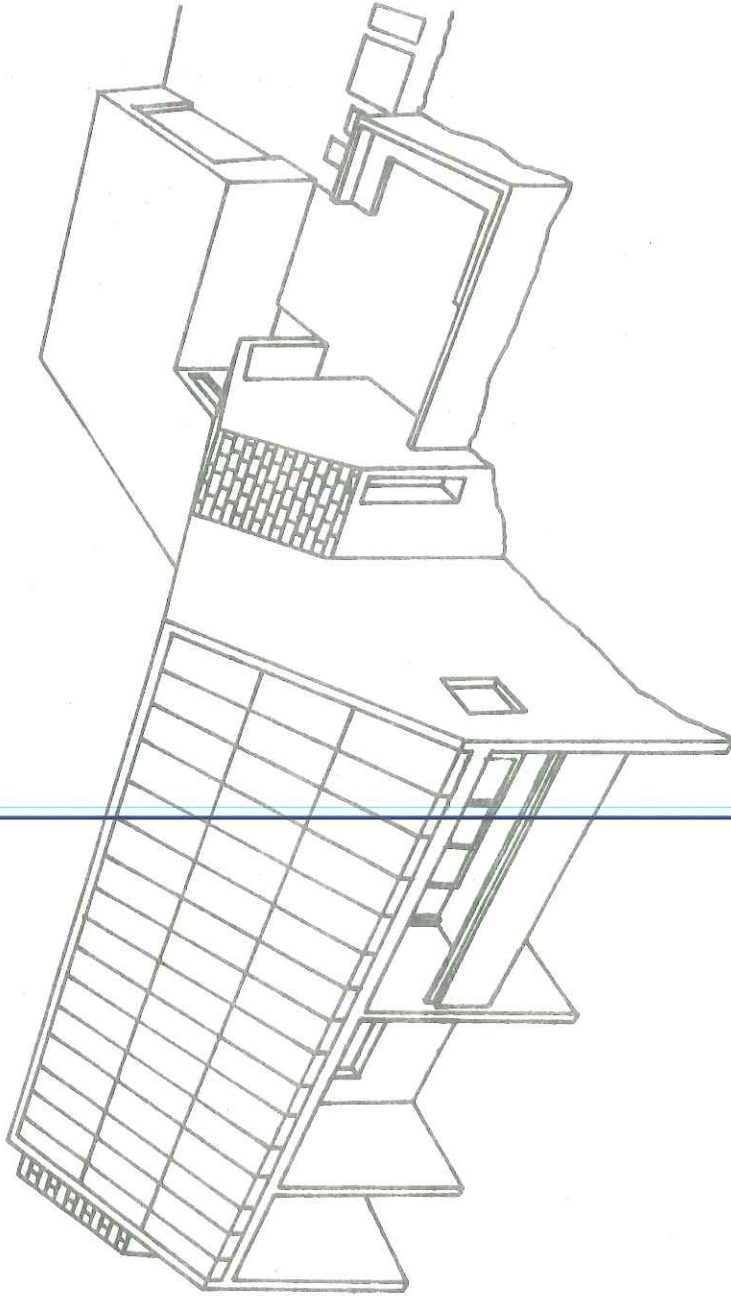
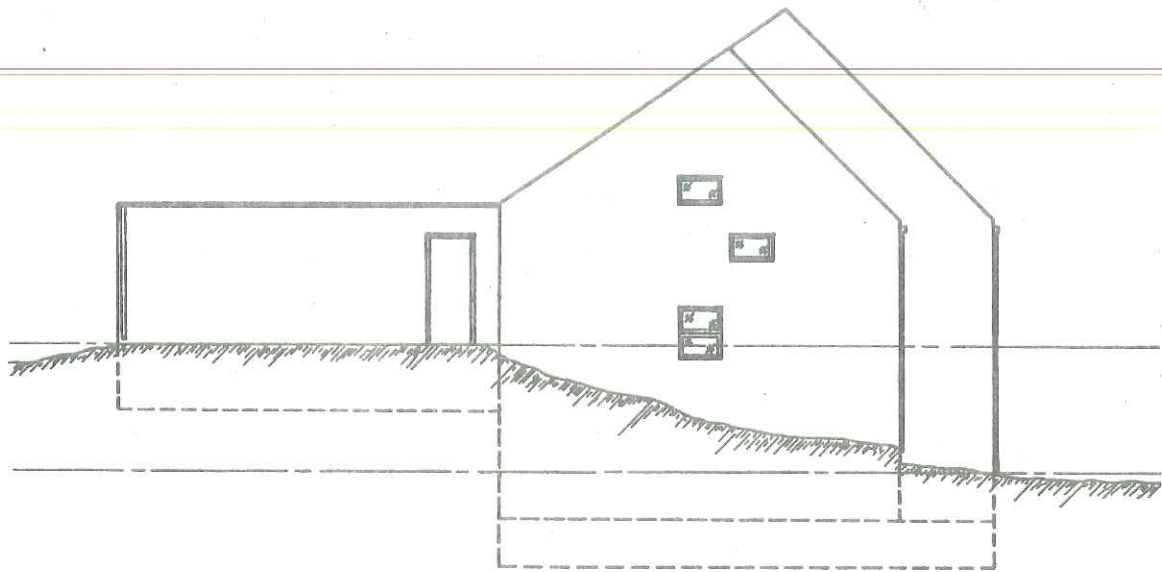
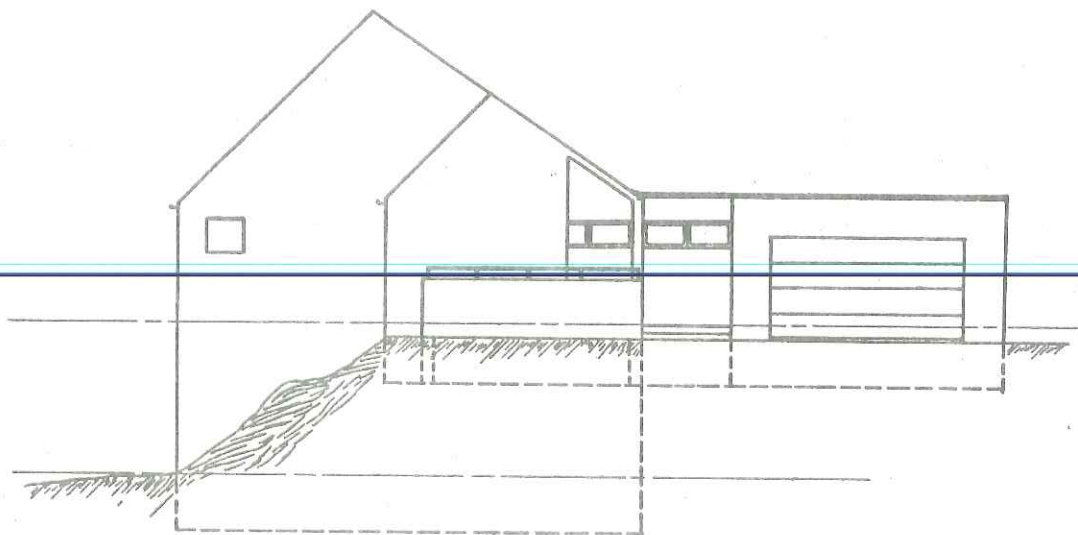


FIGURE 7.1.1. Colorado State University Solar House I (3).



WEST ELEVATION



EAST ELEVATION



FIGURE 7.1.3. West and East Elevations of CSU Solar House I.

cylinder. The 16 gauge (0.152 cm) galvanized sheet steel tank was originally insulated by 15 cm of fiberglass on the sides and 5 cm of fiberglass and 15 cm of concrete block tank supports. Additional insulation was sprayed on the tank in the summer of 1975 when heat losses were found to be excessive and increasing the air-conditioning load.

7.2.3 Domestic Hot Water Tanks

Service hot water is pre-heated in a 302.8 liter hot water heater (heating element and controls disconnected) and transferred on demand to a standard, 151.4 liter, gas-fired hot water heater. Cold water from the mains enters the pre-heat tank and is heated through a heat exchanger by the main tank. Added insulation was also sprayed onto these tanks in the summer of 1975.

7.2.4 Heat Exchanger and Air Heater Coils

Single-pass, counterflow, shell and tube heat exchangers are used to transfer the energy obtained from the collector to the main storage tank and to pre-heat the domestic hot water. The collector heat exchanger is two units in series mounted horizontally in front of the main tank while the single service hot water heat exchanger is positioned vertically between the main storage and pre-heat tanks. The collector heat exchanger is rated at an UA of 23,740 KJ/hr-C while the smaller hot water heat exchanger has a rating of 1900 KJ/hr-C.

Copper tubed, aluminum finned air heating coils are located in 50.8 cm ducting. Two coils are provided, each rated at 3150 KJ/hr-C, to be used for various solar/auxiliary modes as explained in the next section of this chapter.

SOLAR ENERGY HOUSE
Heating — Air Conditioning — Hot Water
Equipment

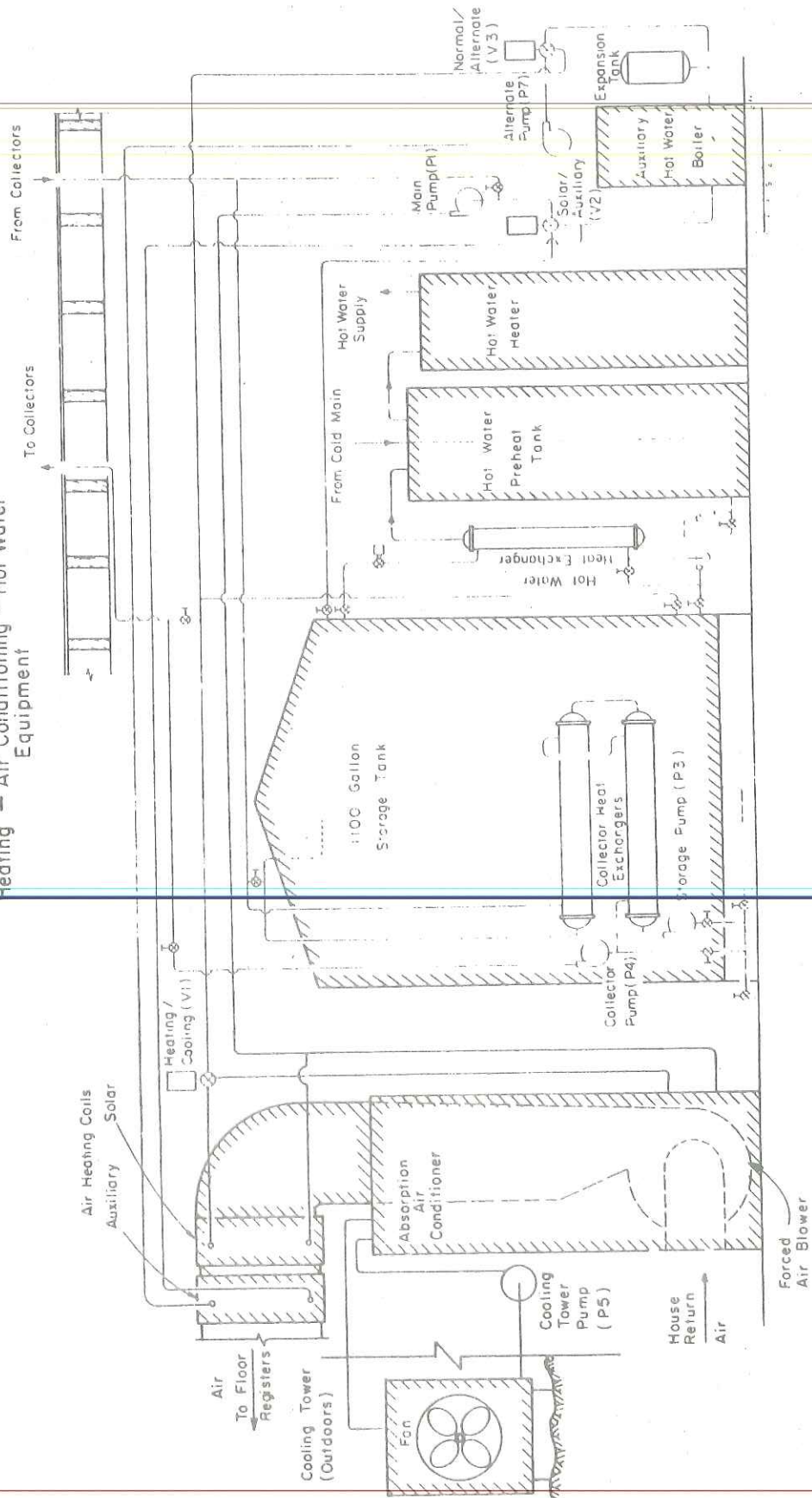
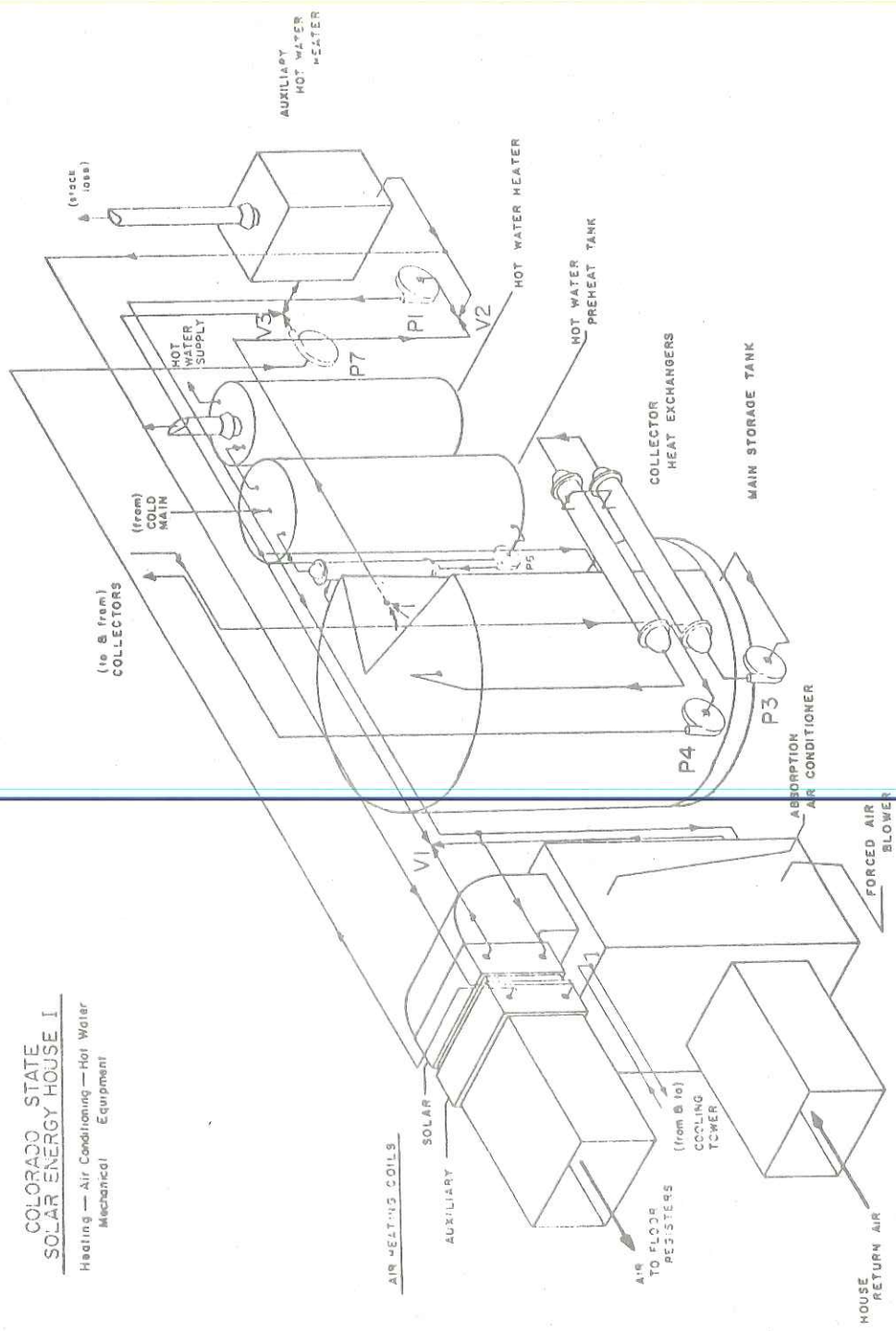


FIGURE 7.2.1. CSU Mechanical Equipment.



COLORADO STATE
SOLAR ENERGY HOUSE I
Heating — Air Conditioning — Hot Water
Mechanical Equipment

FIGURE 7.3.1. Isometric Representation of CSU Mechanical System.

Mode 3 (not shown) air conditions directly from the collectors and would be used to avoid the temperature drop in the heat exchanger which reduces the water temperature used in the air-conditioner generator.

Mode 1 is almost always used for it is much cheaper for heating as a significantly smaller amount of anti-freeze solution is required. Mode 1 collection is used for all simulations in this thesis. For more detailed descriptions of Mode 2 and 3, see (3,4).

7.3.2 Heating

Heating is provided in one of three modes. If room temperature drops 1°C below a desired level, Mode 1 heating is initiated as flow is started from the main storage tank through valve V2 and pump P1 as shown in Figure 7.3.3 and onto the solar heating coil in the ductwork. The forced air blower is started at the same time. Should the room temperature continue to fall (indicating insufficient energy in storage to meet the load) V2 closes and Mode 2 heating is started as shown in Figure 7.3.4. Mode 2 heats solely with auxiliary energy as there is no flow between the storage tank and air heating coils.

Heating as defined by Modes 1 and 2 allows for heating with solar or auxiliary but never both. This can often leave some extractable solar heat untouched for the controls switch from Mode 1 (solar) to Mode 2 (auxiliary) when the tank temperature drops below 37.78°C . An Alternate Heating Mode as shown in Figure 7.3.5 can utilize tank temperatures down to 30°C to pre-heat the air with solar and provide the remaining energy required with an auxiliary boost. This mode makes use of even low temperature solar-collected energy and was used for six weeks during the 1974-75 heating season.

COLORADO STATE
SOLAR ENERGY HOUSE I
Heating — Air Conditioning — Hot Water
Mechanical Equipment

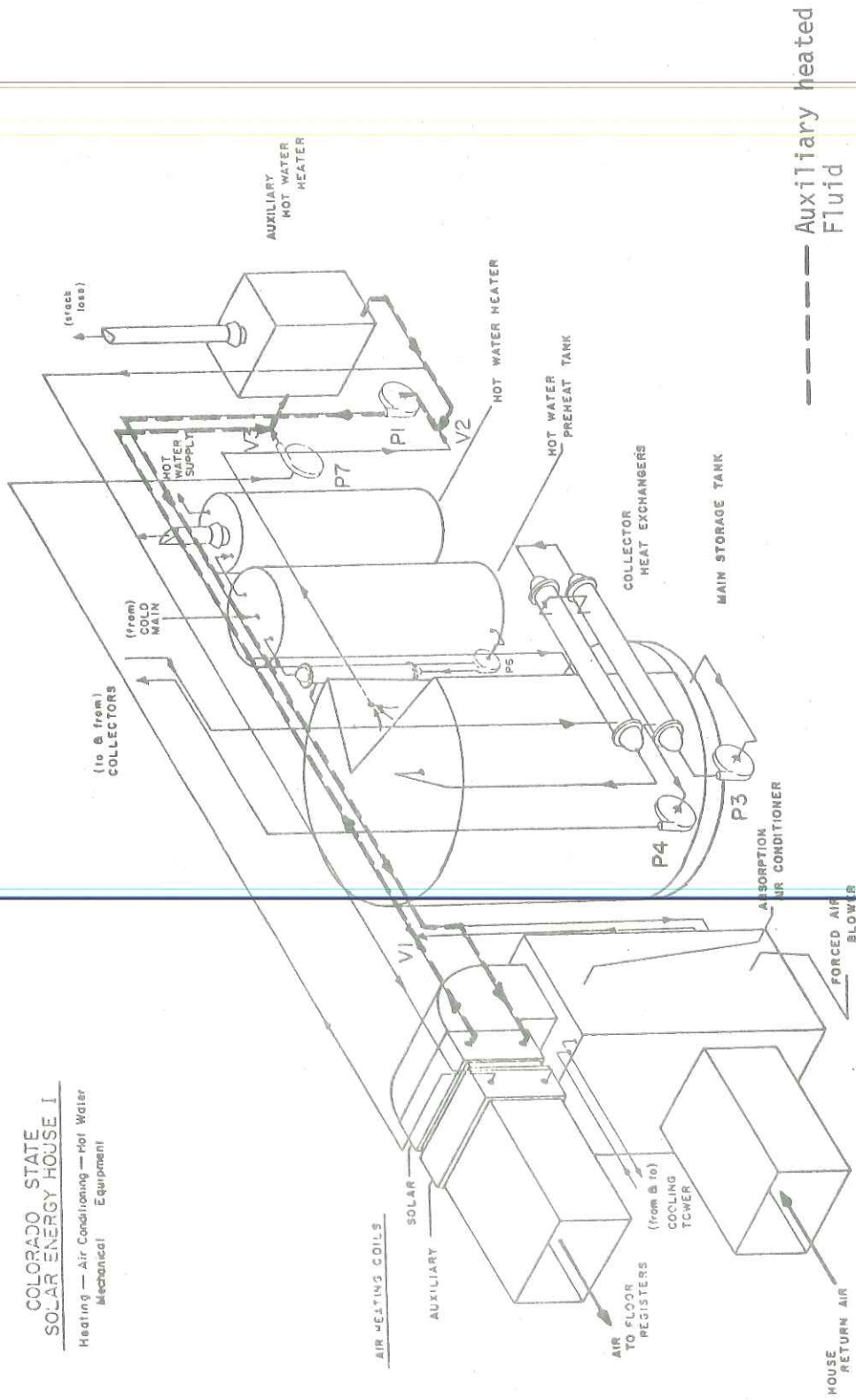


FIGURE 7.3.4. Mode 2 (Auxiliary) Heating.

7.3.3 Air Conditioning

Air conditioning operations are covered briefly here even though no simulations will be done for cooling seasons. The absorption air conditioner is run in two modes, similar to those for heating. If the room temperature rises 1°C above a set point and storage tank temperature is above 83°C , flow is started from the tank through V2 and P1. As shown in Figure 7.3.6, valve V1 closes directing flow to the generator of the air conditioner.

Should the room temperature continue to rise (indicating insufficient energy in storage to meet the load) or if tank temperature was below 83°C , V2 closes as shown in Figure 7.3.7 and energy to the generator is supplied exclusively by the auxiliary boiler.

No alternate mode is available for air conditioning.

7.3.4 Domestic (Service) Hot Water Operation

Figure 7.3.8 is an illustration of how the domestic hot water system operates. Operation is the same for all modes (heating and cooling). Flow is initiated on both sides of the heat exchanger whenever the hot water pre-heat tank temperature is below 41°C and the main tank temperature is 11°C warmer than the pre-heat tank.

COLORADO STATE
SOLAR ENERGY HOUSE I
Heating — Air Conditioning — Hot Water
Mechanical Equipment

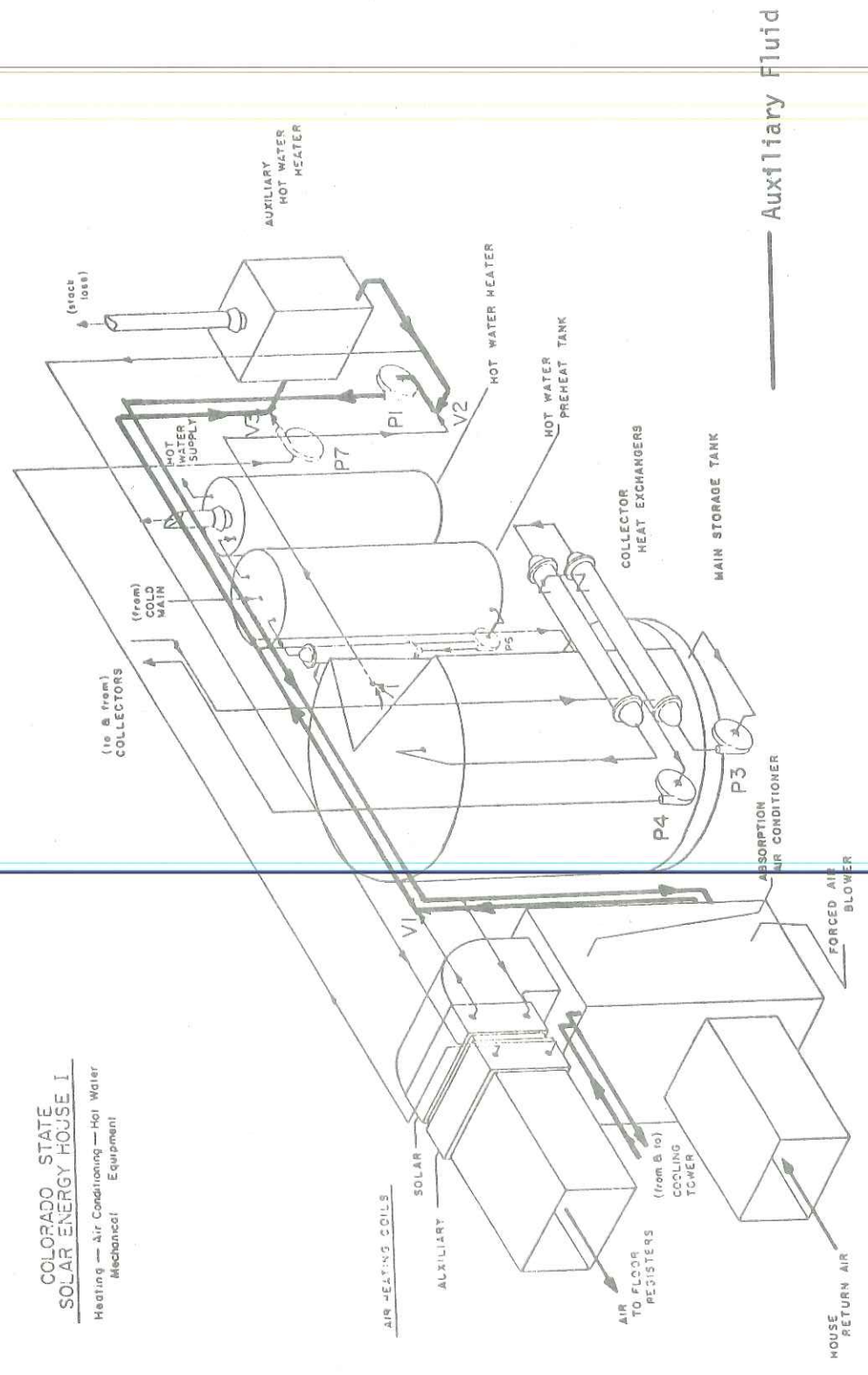


FIGURE 7.3.7. Mode 2 (Auxiliary) Air Conditioning.

8.0 COMPUTER MODELING OF CSU SYSTEM

8.1 Introduction

All of the computer modeling in this thesis was done with the simulation program, TRNSYS (3,4). TRNSYS is written in FORTRAN and solves for the transient performance of system components. Each component (collector, storage tank, wall, etc.) is a FORTRAN subroutine programmed to calculate performance from fixed parameters and time varying inputs. These inputs can come from meteorological data or outputs from other components.

The TRNSYS library of standard components contained many of the systems needed to simulate the CSU house. Basic system equations and parameters will be outlined for each model used. Further details on component models are available in the TRNSYS manual (4).

Several new components have been developed as a result of the CSU modeling effort. The transfer function wall and roof models have already been alluded to. Some other new models were developed and modifications were made on some existing components. These models are outlined in the sections following the standard component description.

Figure 8.1.1 is an overall schematic of the CSU model and is helpful in visualizing the interrelationships between components.

8.2 Standard TRNSYS Components

8.2.1 Collector Model

The flat plate solar collector is modeled using the Hottel and Whillier (28) equations for collector performance. The useful energy

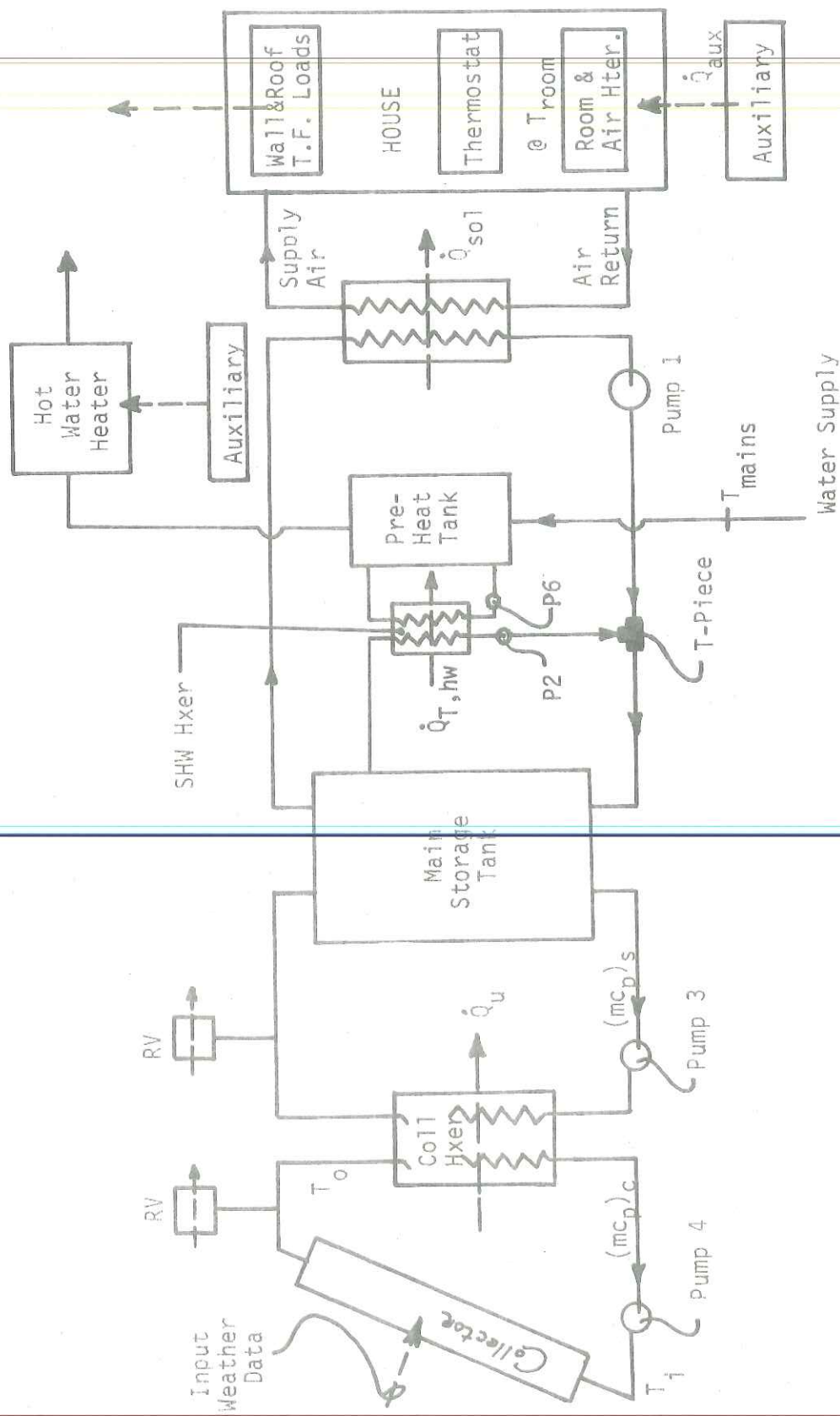


FIGURE 8.1.1. Overall Schematic of CSU TRNSYS Model.

Table 8.2.1 is a listing of parameters used for the main storage tank. The tank loss coefficient is from Oonk (10). All other values are taken from CSU publications (3,4).

| | | |
|--------------------------|-------|-------------------------|
| Volume, V | 4.284 | m ³ |
| Height, H | 1.83 | m |
| Specific Heat, c_p | 4.19 | KJ/kg-C |
| Fluid Density, ρ | 1000 | kg/m ³ |
| Tank Loss Coefficient, U | 1.535 | KJ/hr-m ² -C |

TABLE 8.2.1. Main Storage Tank Parameters.

8.2.3 Domestic Hot Water Tanks Models

The service hot water and hot water heater tanks are modeled similarly to the main storage tank. The service hot water system is schematically shown in Figure 8.2.2. There are slight changes from the main tank. The hot water source now comes from the hot water heat exchanger. In addition there is no return water from load, but instead cold water assumed to be at 9°C from the mains. The flow to the load goes to the hot water heater. An extra provision for the water heater allows auxiliary energy to be added when the tank temperature drops below a set value.

The main storage and pre-heat tanks were modeled using the standard TRNSYS tank model. A modification was made for the hot water heater to account for the combustion efficiency of the natural gas boiler. The hot water heater was modeled as having a 38,000 KJ/hr capacity even though this is less than the rated capacity. Observations of actual CSU performance data indicate that the heater supplies 9500 KJ when it comes

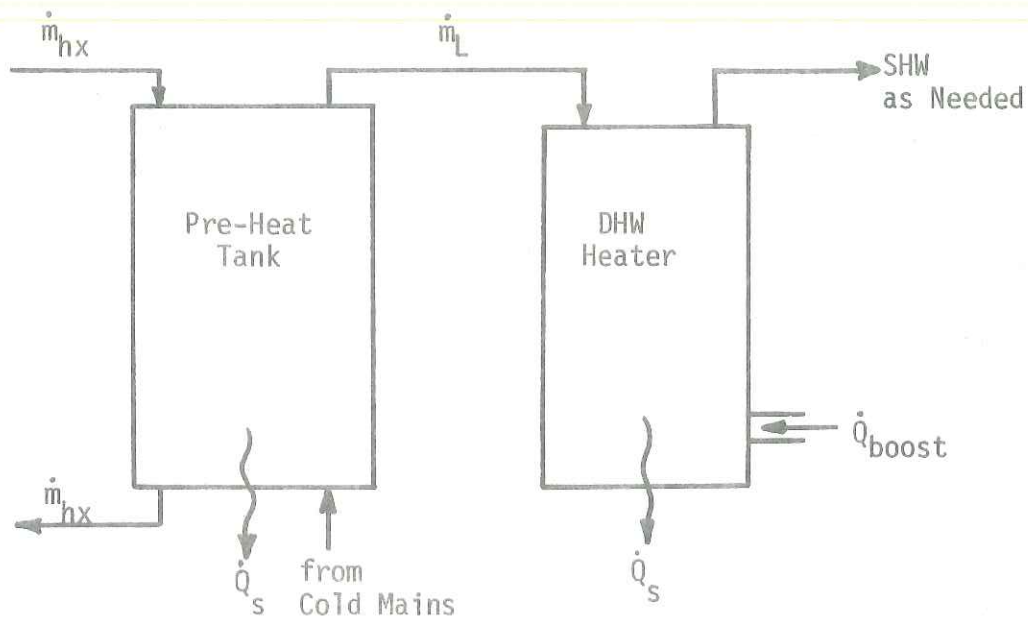


FIGURE 8.2.2. CSU Service Hot Water System Model.

| | Pre-Heat Tank | Hot Water Heater | |
|--------------------|---------------|------------------|--------------------------|
| V | 0.303 | 0.1515 | m ³ |
| H | 1.52 | 1.42 | m |
| c _p | 4.19 | 4.19 | KJ/kg-°C |
| ρ | 1000 | 1000 | kg/m ³ |
| U _L | 7.0 | 6.0 | KJ/hr-m ² -°C |
| Q _{boost} | | 19,000 | KJ/hr |
| T _{set} | | 51, 57 | °C |
| η | | 0.628 | |

TABLE 8.2.2. Domestic Hot Water Tanks Parameters.

$$T_o = (\dot{m}_1 T_1 + \dot{m}_2 T_2) / \dot{m}_o \quad (8.2.7)$$

where o denotes outlet state and 1,2 denote respective inlet conditions.

8.2.8 Air Heater Model

The air heating coils are diagramed in Figure 8.2.3. The heat transferred to the room air is

$$Q_{sol} = (\dot{m}c_p)_{air} \epsilon (T_{hi} - T_{room}) \quad (8.2.8)$$

The temperature of the water leaving the air heater is

$$T_{ho} = T_{hi} - Q_{sol} / (\dot{m}c_p)_{water} \quad (8.2.9)$$

The effectiveness of the air heater was found to be 0.668 using relations from Kays and London (31).

8.3 Additional Components Used With TRNSYS

This section describes modified or new components developed over the course of the CSU work. The wall and roof models have since been incorporated into TRNSYS and the time-load distributor is now a part of the TRNSYS room model.

8.3.1 Radiation Processor

The TRNSYS radiation processor converts radiation on a horizontal surface to radiation on a surface at any angle or orientation. Problems arose because the CSU weather data gives solar radiation data only for the 45° slope of the collector.

The following scheme was used to convert values at 45° to radiation on the horizontal surface. Radiation relationships are those of Liu and Jordan as presented by Duffie and Beckman (28).

Figure 8.3.1 is an illustration of the radiation sources that affect the measuring instrument (or collector) at angles. The total instantaneous radiation incident on the tilted surface per unit area, H_T , is:

$$H_T = H_b R_b + H_d \left(\frac{1 + \cos s}{2} \right) + (H_b + H_d) \rho \left(\frac{1 - \cos s}{2} \right) \quad (8.3.1)$$

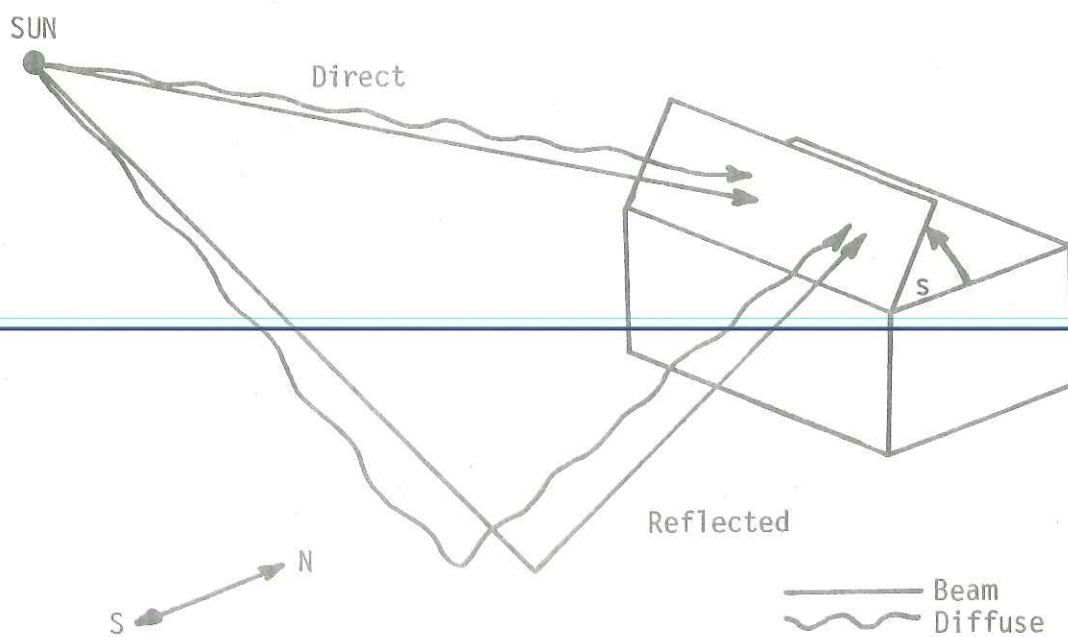


FIGURE 8.3.1. Sources of Radiation Incident on the Collector.

Equation 8.3.1. states that the radiation incident on a tilted surface is the sum of the beam and diffuse radiation that directly strike the surface plus the beam and diffuse radiation that strike the ground

The iteration procedure is illustrated in a flow diagram in Figure 8.3.2. A value of $|H^+ - H| = 50 \text{ KJ/hr-m}^2$ was necessary to restrict calculation costs. This is roughly 1 to 5% of the total radiation on the collector and although errors are inherent with this scheme, they occur not in the calculation of radiation incident on the collector, but instead for the solar contribution to building loads. In this way, the radiation for all surfaces can be obtained when available data is only for tilted surfaces.

8.3.2 Transfer Function Wall Model

The transfer function method of heat flow calculation was used for wall subroutine. The model used for the background and testing was presented in earlier portions of the thesis.

The wall can be used in one of two modes. Mode 1 provides for a single wall or flat roof model. Four (five with flat roof) of these are required to represent a rectangular house. Solar-air temperatures are calculated from methods described in Chapters 4 and 6. Mode 2 operation models all four walls simultaneously in a combined manner using an effective solar-air temperature as described in Section 5.8.

All previous heat fluxes are set equal to zero and all solar-air temperatures to 20°C to start a simulation. Transfer function coefficients are read in from parameter listings (b coefficients are converted internally from English to SI units, the d's are dimensionless). Figure 8.3.3 is a flow chart of the transfer function wall model operation. The $t_{sa,n}$ and q_n'' values must be indexed in the memory to maintain time series - coefficient alignment. The wall subroutine is

called only once for ambient weather is constant over the hour and a new q_0^0 is not calculated until the weather data changes.

Parameters for wall and window areas were obtained as closely as possible from blueprints (3). Table 8.3.1 lists wall and window dimensions used. The elevations in Figures 7.1.2 and 7.1.3 are helpful in understanding the tabulated values.

Figure 8.3.4 is an illustration of the CSU house as modeled. The east wall area includes the area of the cathedral ceiling in the living room. The garage is not modeled nor is the east entry way. The west wall is assumed to be a rectangle and a triangle (below ground level). Above room ceiling is treated as attic west wall area. The fraction of windows shaded were estimated and values are "yearly" averages. Southern window shading fractions were varied for different simulations.

8.3.3 Transfer Function Pitched Roof and Attic Model

The CSU roof and attic were regressionally modeled in Section 6.5.5 and all parameters used there were used in the simulations. The calculation scheme for the roof model is very similar to that diagramed in Figure 8.3.3 for the wall. Differences are that an equivalent solar-air temperature, $t_{sa,eq}$ is used as described in Chapter 6 and no window calculations are performed. Additional radiation terms along with collector temperature are needed for input.

8.3.4 Time Load Distributor

The nature (origin) of a heat gain or loss can be just as important to the total load as the magnitude of that gain (loss). The solar heat gain to a room has a much slower effect on the total load than a heat

SOUTH WALL

| | | | |
|-------------------|--------------------------------|----------------------------------|-----------------------------------|
| Length = 16.92 m | $A_{total} = 92.9 \text{ m}^2$ | $A_{wdw} = 22.2 \text{ m}^2$ | |
| Height = 5.49 m | $F_{wdw} = 0.24$ | $F_{wdw,shaded} = 0.53$ | |
| Windows- | F_{shaded}^* | $A_{total} \text{ (m}^2\text{)}$ | $A_{shaded} \text{ (m}^2\text{)}$ |
| Sliding Gl. Doors | 0.3 | 5.95 | 1.79 |
| Living Room | 0.8 | 10.30 | 8.24 |
| Bedrooms | 0.3 | 4.46 | 1.34 |
| Basement | 0.3 | 1.49 | 0.45 |
| | 0.53 | 22.20 | 11.82 |

EAST WALL

| | | |
|-----------------|--|-------------------------|
| Length = 7.87 m | $A_{total} = 27.5 \text{ m}^2$ (Includes Cathedral Living Rm.) | |
| Height = Varies | $A_{wdw} = 1.0 \text{ m}^2$ | |
| | $F_{wdw} = 0.036$ | $F_{wdw,shaded} = 0.25$ |

NORTH WALL

| | | |
|------------------|--------------------------------|------------------------------|
| Length = 12.95 m | $A_{total} = 31.6 \text{ m}^2$ | $A_{wdw} = 3.31 \text{ m}^2$ |
| Height = 2.44 m | $F_{wdw} = 0.10$ | $F_{wdw,shaded} = 0.0$ |

WEST WALL

| | | |
|-----------------|---------------------------------|------------------------------|
| Length = 7.87 m | $A_{total} = 21.08 \text{ m}^2$ | $A_{wdw} = 1.15 \text{ m}^2$ |
| Height = Varies | $F_{wdw} = 0.06$ | $F_{wdw,shaded} = 0.0$ |

* Indicates yearly average shading. Winter simulations assume all south windows are fully exposed to winter sun.

TABLE 8.3.1. Wall and Window Areas for CSU Walls.

gain (loss) through the walls or ceiling. The wall gain (loss) is mostly by convection although some radiation heat transfer occurs between walls and room air. The solar heat gain contributes to the total load by first heating the surface it is incident upon (floor, carpets, furniture, etc.) and that surface in turn heating the room air by convection. This occurs at a slower rate than the wall gain (loss). This is evidenced by a west facing room subject to solar insolation. The room will feel heating effects long after the sun has set, for room surfaces absorbed solar heat and transfer it at later times. The current load from solar gain, $Q_{\tau,shg}$, is related by ASHRAE (12) to the current gain $q_{\tau,shg}$ and the previous loads and gains by a transfer function in the following manner:

$$Q_{o,shg} = \sum_{i=0}^{\infty} v_i q_{i,shg} - \sum_{i=1}^{\infty} w_i Q_{i,shg} \quad (8.3.6)$$

Figure 8.3.5 is a plot of $Q_{o,shg}$ and $q_{o,shg}$ ($q_{o,shg} = H_T \tau$) for a west window for a May day in Madison, Wisconsin. The total load $Q_{o,shg}$, time lags $q_{o,shg}$ and affects the room long after the sun has set.

Equations similar to Equation 8.3.6 can be written for other sources of heat gain or loss. The time-distribution effects are dependent on the relative portion of the gain (loss) that is due to radiation and the portion due to convection. Wall or roof gains (losses) have a much more immediate effect on the total load. Figure 8.3.6 is a plot of $Q_{o,walls}$ and $q_{o,walls}$ for the same day in May as was used in Figure 8.3.5. The total load follows the hourly gain (loss) much more closely than for the solar gains. This is because more of the wall gain (loss)

is transferred by convection which is immediately transferred to room air than the radiation transfer of the solar gain.

ASHRAE (12) lists v_i and w_i coefficients for heat gains or losses from four sources - (1) solar heat gain, (2) wall, window and roof conduction gains, (3) lights and (4) energy generated by people and machinery and dissipated by radiation. Coefficients are available for light, medium or heavy construction. People and machinery generated heat gains that are dissipated by convection and infiltration and ventilation gains (losses) are like all convective gains or losses in that they are felt immediately. Any sources of constant generation need not be distributed for they would produce a constant load anyway after transient effects disappear.

The total area under the two curves in either Figure 8.3.5 or 8.3.6 is equal over long periods of time. This should be so for the time-distribution serves only to "weight" the gains (losses) not reduce them. ASHRAE (12) and Mitalas (32) suggest that a very small portion of room gains is conveyed out of the room before its effect is felt by the room. This can be explained by an electrical analogy as shown in Figure 8.3.7. A gain to the room (solar heat gain, lights, machinery, etc.) can be represented by a current input to room potential. Most of the input current is transferred to room air because it is the path of least resistance. A small portion, however, finds its way to outside air over the higher resistance path.

The fraction that gets to the room is F_c of the input gain. ASHRAE (12) suggests that F_c is a function of the total room conductance, K_T , where

duction losses from walls, windows and the roof are time-distributed using ASHRAE (12) coefficients for a light construction room.

8.3.5 Thermostat, Room and Air Heater Model

The basic three stage TRNSYS thermostat was used for the house model. The thermostat receives inputs of room and storage tank temperatures. The room temperature is compared with pre-set values as shown in Figure 8.3.8 to determine if heating or cooling is required. If T_{room} drops below 20°C and available storage is above 37.8°C , first stage (solar) heating is initiated as described in Mode 1 heating (section 7.3.2). Heating from solar storage will continue as long as $18.8^{\circ}\text{C} < T_{\text{room}} < 20^{\circ}\text{C}$ and $T_{\text{tank}} > 37.8^{\circ}\text{C}$. If the tank temperature is below 37.8°C or should T_{room} drop below 18.8°C , second stage (auxiliary) heating begins as described in Mode 2. When room temperature rises, the process is reversed and when T_{room} exceeds 20°C , the system remains idle until T_{room} again leaves the dead band. For cooling conditions an upper limit is placed on the dead band and cooling is begun when T_{room} exceeds this limit.

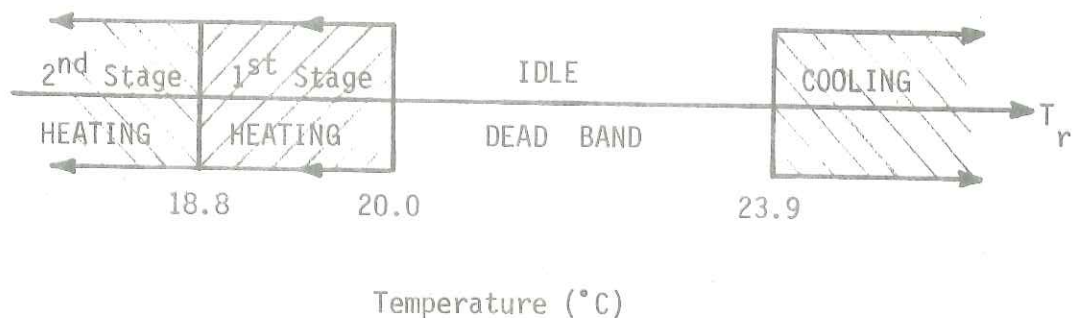


FIGURE 8.3.8. TRNSYS Thermostat Model.

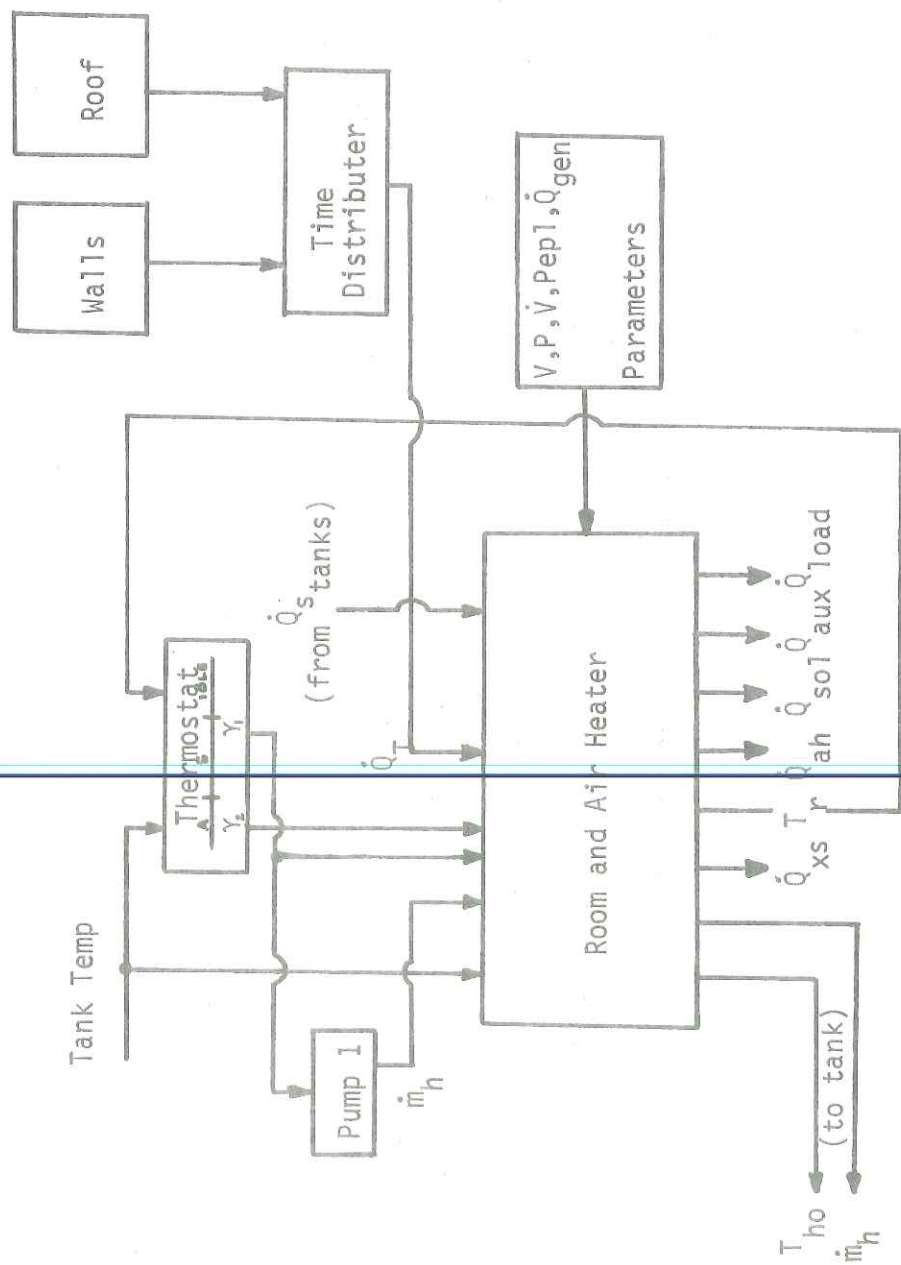


FIGURE 8.3.9. Information Flow Diagram for Room System.

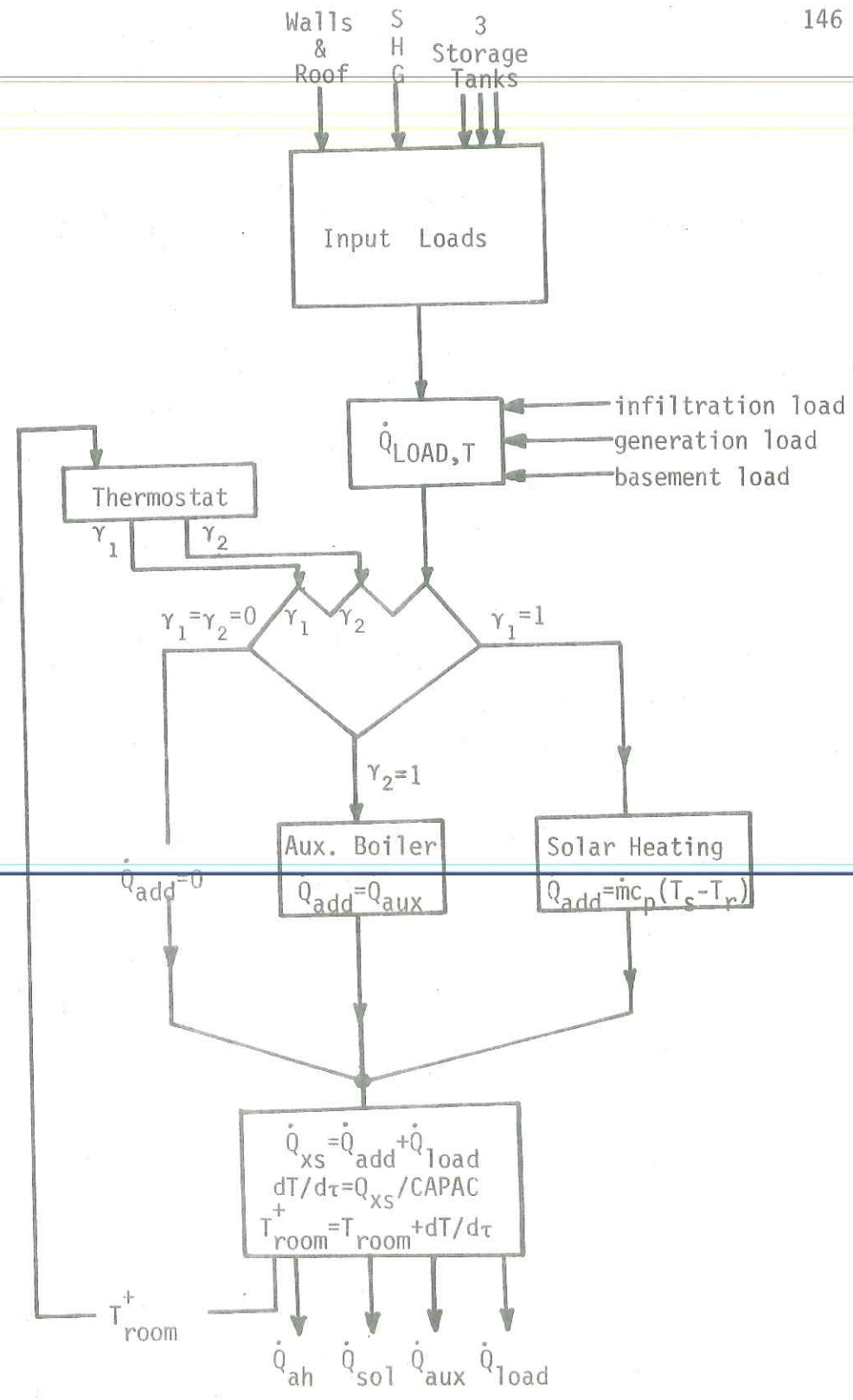


FIGURE 8.3.10. Flow Chart for Room Model in Mode 1 or 2 Heating.

9.0 SIMULATIONS OF CSU SOLAR HOUSE I

9.1 Introduction

One of the prime objectives of the CSU project was to make available weather and performance data from house operation. The hourly weather data, consisting of ambient temperature, solar radiation and windspeed (when available), was used to drive the TRNSYS CSU model. A constant value of 5.67 m/sec was used when wind recordings were not available. Performance data is then used to compare actual and simulated energy quantities and temperatures.

The load model described in Chapter 8 requires an internal rate of heat generation and a volumetric infiltration rate as constant parameters of the system. The internal generation was found by Oonk (10) to average 8800 KJ/hr. This value is higher than normal but an experimental house such as CSU has electrical instruments, pumps, etc., that dissipate energy and give off heat in addition to common items such as stoves and refrigerators. The infiltration rate was chosen so that the predicted heating load closely matched the actual heating load.

Weather and performance data was obtained from the Solar Energy Applications Lab at CSU for the heating season (November 1 - April 30) of 1974-75. This period of time started shortly after system startup at CSU and consequently some problems arose concerning this data. The first data of any value did not begin until November 22 and lasted only 272 hours until December 3. This is much of the same data used by Oonk (10) in his early studies. It is reexamined here and referred to as Simulation I. Faulty or inaccurate values were found in early December

ception. The house was locked up over the Thanksgiving, Christmas and New Year's holidays. The decrease in infiltration over these periods was modeled by reducing the number of air changes to 0.3 per hour.

Each of the three simulations is covered in a separate section of this chapter. Daily comparisons are made for simulated and actual quantities of useful energy gain, heating and energy transferred to the pre-heat tank. The main storage tank temperature is monitored with simulated and actual values plotted over the simulation. The main storage tank is the "guts" of the solar system so it is necessary that any representation of the house must closely match tank temperature and evidence temperature deviations and trends in time.

An additional simulation is run for the CSU house operating in Madison. A one month's simulation allows for examination of energy loss-ambient temperature relationships and the building's UA is also calculated.

9.2 Simulation I - November 22 to December 3

This simulation extends from 1:00 pm on November 22 to 7:00 pm, December 3. Even though this period was covered by Oonk (10) in his MS thesis, there is reason to re-examine this period. The first reason concerns the data itself. Oonk's data was released to him shortly after it was recorded and the data was not as complete or accurate as later information that was processed and released on the CSU weather and performance tape. Measured values of useful energy gain and energy delivered across the air heater differ slightly and totals for the same period are not equal. Conversations with CSU (30) reinforced beliefs that the current data is more likely to be correct.

TABLE 9.2.1

Measured Energy Quantities and Temperatures

11-22-13 hrs to 12-3-19 hrs

| | Tank 1 | Tank 2 | Tank 3 |
|----------------------|--------|--------|--------|
| $Q_{T,sol}$ | 2387.8 | 398.1 | 0.0 |
| Q_R | 2474.1 | 0.0 | 0.0 |
| T_s | 61.39 | 60.61 | 58.04 |
| T_r | 18.63 | 18.63 | 18.63 |
| Q_{loss} | 250.8 | 221.4 | 119.2 |
| T_i | 67.8 | 67.8 | 63.8 |
| T_f | 66.8 | 63.4 | 54.4 |
| ΔU_{tank} | -17.95 | -5.59 | -5.97 |
| ηQ_{aux} | --- | -- | 102.6 |
| % Closure Difference | 11.7 | 45.7 | 9.7 |

Energy quantities in MJ, Temperatures in C
 η for hot water tank is 0.628

If the gains to the tank are placed on the left side of Equation 9.2.2 and the losses on the right side, an energy balance on the main tank gives

$$2387.8 - (-17.95) \stackrel{?}{=} 2474.1 + 250.8 \quad (9.2.3)$$

$$2405.8 = 2724.9 \quad (9.2.4)$$

More energy is leaving the system than is being supplied as the balance fails to close by 11.7%. A possible error could be a ΔU term that is too

The simulated energy balances all closed within 1.4% or better. This is roughly the error tolerance value used in TRNSYS and is acceptable for it shows that all energy input to the system is accounted for by the program. It is interesting to note the large difference in ΔU_{tank} terms for the simulated and actual systems. This is largely due to the closure failure of the real system.

9.2.3 Comparison of Actual vs. Simulated Performance

Daily integrated values of Q_u , Q_{ah} and $Q_{T,shw}$ are compared for actual and simulated performance in Table 9.2.3. Note that the air heating loads differ by only 1.6% because of the careful selection of the volumetric infiltration rate. The simulated Q_u total is larger than the measured quantity and their 7% difference could be due to the errant collector flow measurements mentioned earlier.

The values for heat transferred to the pre-heat tank differ by 23%. Pre-heat tank losses are not totally accurate due to the assumed U_L value. Since the hot water system is dormant, the only means of energy removal is through tank losses. For this reason it is very difficult to predict energy transferred to the tank when one is uncertain of the amount of energy lost by the tank. Comparisons of auxiliary energy supplied to the hot water tank show only a 8.7% difference, indicating a better approximation of that tank's loss coefficient.

The daily values show fairly good comparisons. Some discrepancies occur but this is to be expected for system parameters are based on average values which may differ greatly in hourly comparisons but over many days even out to produce acceptable results.

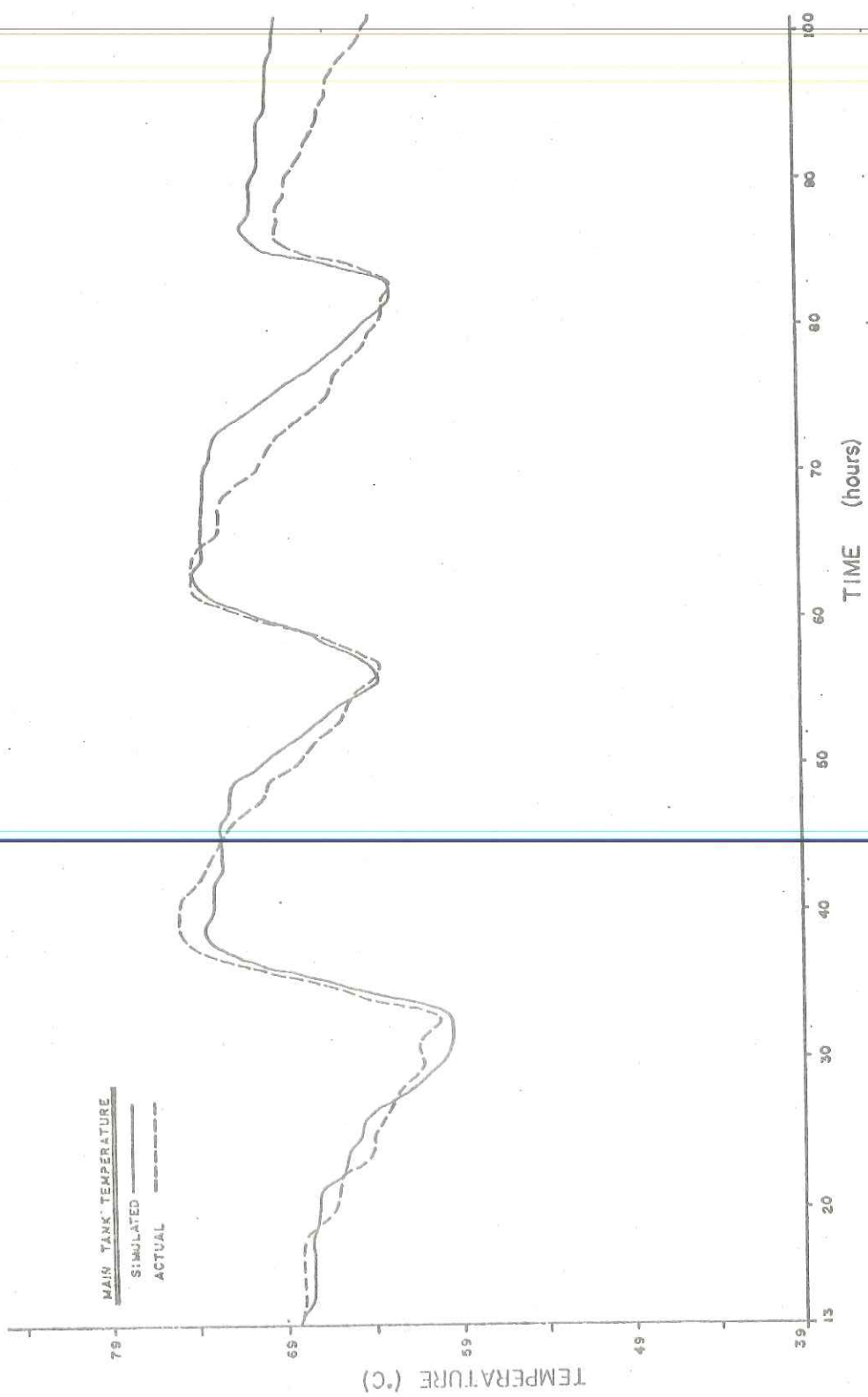


FIGURE 9.2.1.1. Storage Tank Temperature versus Time for Simulation I.

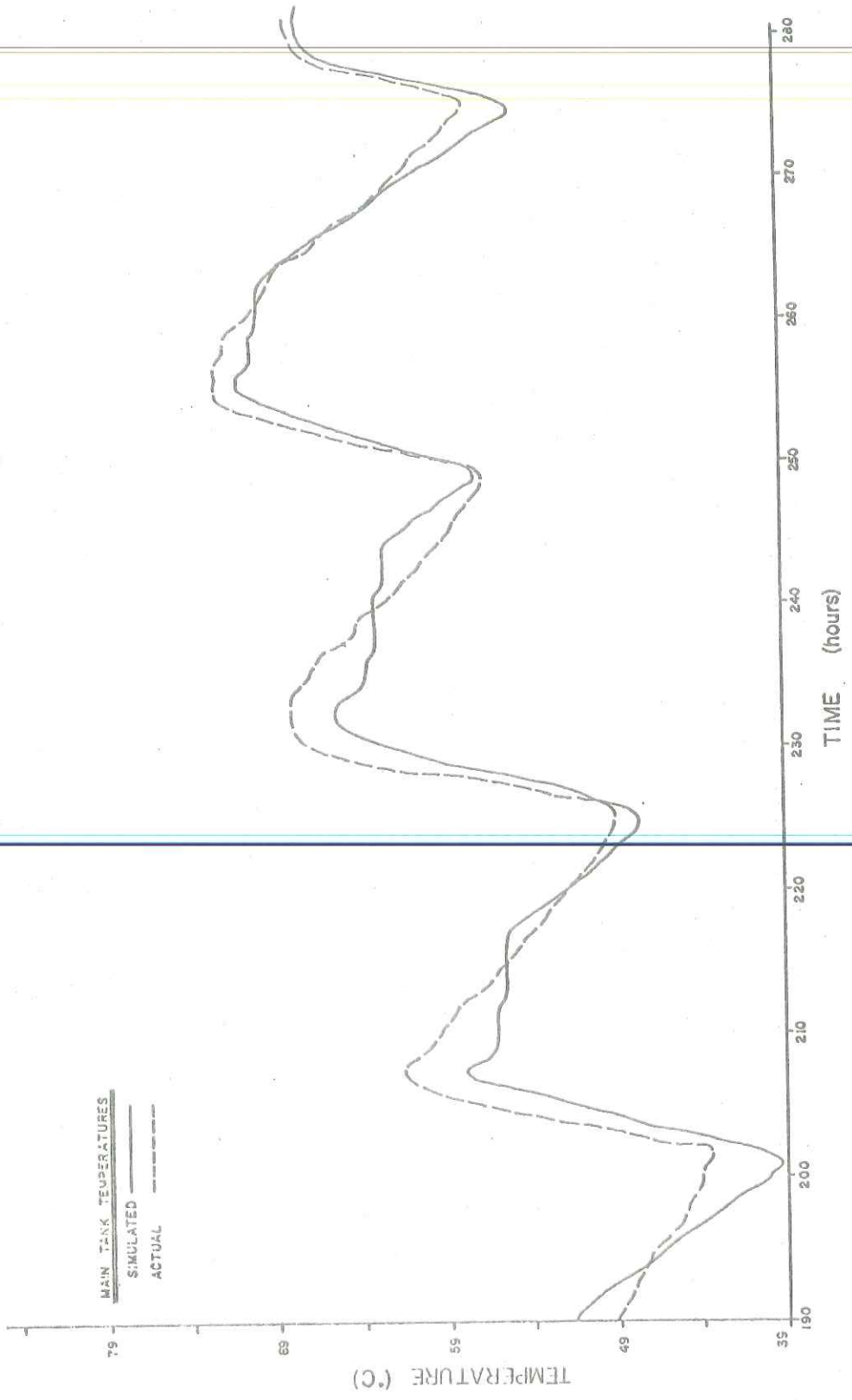


FIGURE 9.2.1 (con 'd)

exactly, within 0.1%. This is encouraging and indicates that the U_L value is fairly accurate for this period.

TABLE 9.3.1
Measured Energy Quantities and Temperatures
12-20-16 hrs to 12-30-10 hrs

| | Tank 1 | Tank 2 | Tank 3 |
|--------------------------|--------|--------|--------|
| $Q_{T, \text{sol}}$ | 2418.6 | 132.5 | 0.0 |
| Q_R | 2084.6 | 0.0 | 0.0 |
| T_s | 42.0 | 44.0 | 55.7 |
| T_r | 19.2 | 19.2 | 19.2 |
| Q_{loss} | 116.2 | 113.6 | 95.8 |
| T_i | 36.6 | 42.2 | 58.2 |
| T_f | 39.0 | 42.8 | 60.9 |
| ΔU_{tank} | 43.1 | 0.7 | 1.7 |
| ηQ_{aux} | ---- | --- | 98.1 |
| % Closure Difference | 7.2 | 13.7 | 0.1 |

Energy quantities in MJ, Temperatures in °C
 η for hot water tank is 0.628

9.3.2 Simulated Energy Balance

Energy balances on the simulated performance quantities listed in Table 9.3.2 all balance out and close to within 1.1% or better.

| Date | Q _u (MJ) | | Q _{ah} (MJ) | | Q _{sol} (MJ) | | Q _{aux} (MJ) | | Q _{T,hw} (MJ) | |
|--------------|---------------------|--------|----------------------|--------|-----------------------|--------|-----------------------|--------|------------------------|-------|
| | Sim | Act | Sim | Act | Sim | Act | Sim | Act | Sim | Act |
| 12-20 | 0.0 | 0.0 | 73.0 | 112.8 | 48.0 | 40.6 | 25.0 | 72.2 | 0.0 | 0.0 |
| 21 | 64.9 | 42.4 | 229.8 | 325.8 | 54.8 | 38.8 | 175.0 | 287.0 | 0.4 | 5.4 |
| 22 | 443.6 | 451.3 | 299.4 | 355.5 | 186.9 | 228.3 | 112.5 | 127.2 | 31.1 | 27.3 |
| 23 | 0.0 | 0.0 | 584.5 | 416.8 | 203.3 | 184.6 | 381.2 | 232.2 | 0.0 | 0.0 |
| 24 | 302.3 | 266.2 | 430.0 | 357.6 | 173.7 | 159.0 | 256.3 | 198.6 | 14.5 | 16.9 |
| 25 | 434.7 | 442.4 | 265.3 | 381.3 | 165.3 | 211.6 | 100.0 | 169.7 | 22.0 | 27.1 |
| 26 | 52.6 | 77.2 | 289.1 | 347.7 | 289.1 | 287.6 | 0.0 | 60.1 | 0.0 | 0.0 |
| 27 | 387.7 | 407.2 | 181.3 | 253.7 | 118.8 | 109.9 | 62.5 | 143.8 | 21.5 | 27.7 |
| 28 | 298.0 | 349.2 | 136.6 | 231.2 | 136.6 | 231.2 | 0.0 | 0.0 | 24.1 | 19.7 |
| 29 | 214.9 | 265.0 | 470.8 | 294.5 | 470.8 | 294.5 | 0.0 | 0.0 | 2.8 | 8.2 |
| 30 | 93.3 | 117.7 | 278.3 | 165.7 | 178.3 | 165.7 | 100.0 | 0.0 | 0.0 | 0.0 |
| TOTALS | 2292.0 | 2418.6 | 3238.0 | 3242.6 | 2025.0 | 1951.8 | 1213.0 | 1290.8 | 116.3 | 132.3 |
| % Difference | 5.2 | | 0.1 | | 3.6 | | 6.0 | | 12.0 | |

TABLE 9.3.3. Daily Values of Q_u, Q_{ah} and Q_{T,hw} for Simulation II.

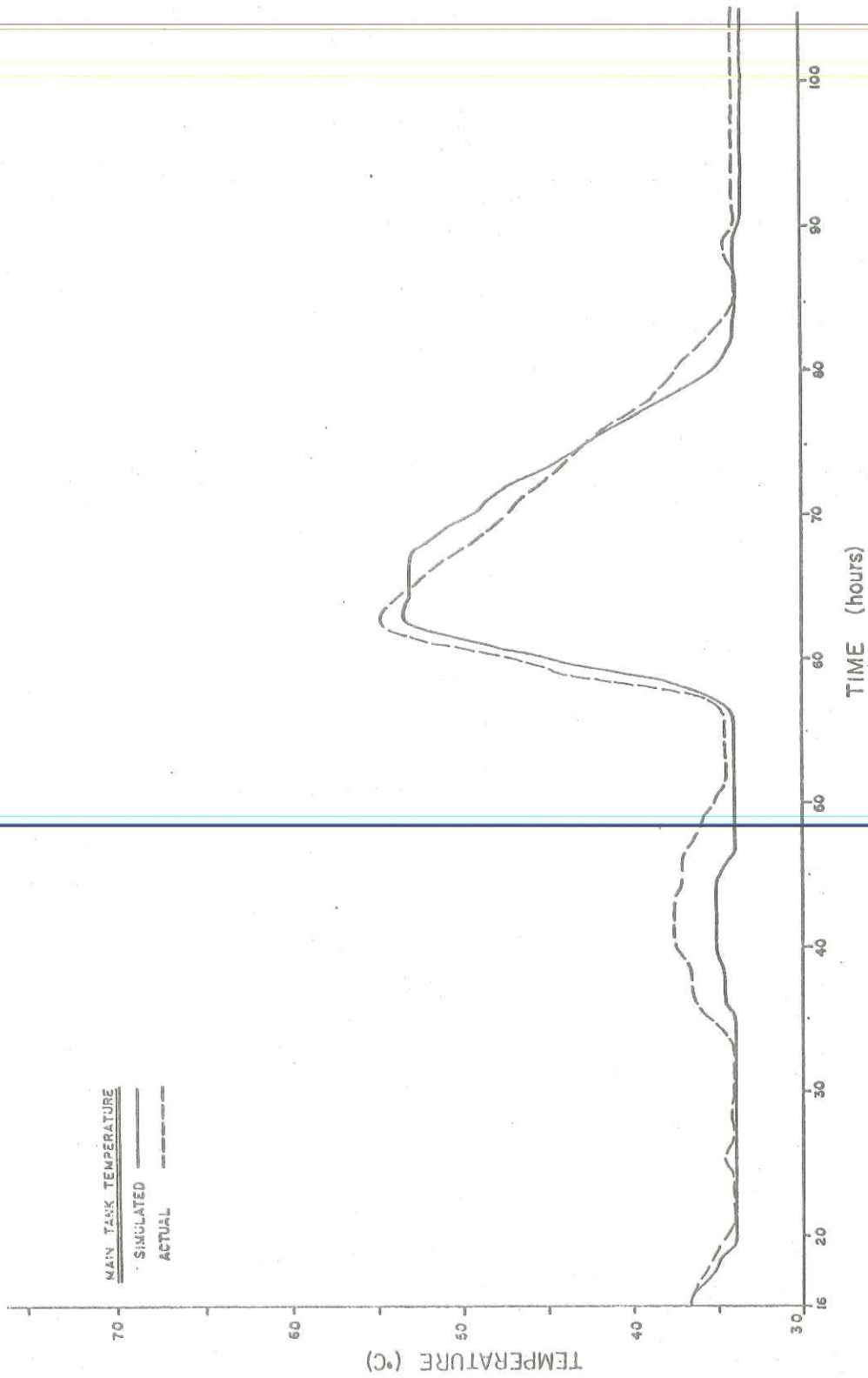


FIGURE 9.3.1.1. Storage Tank Temperature versus Time for Simulation II.

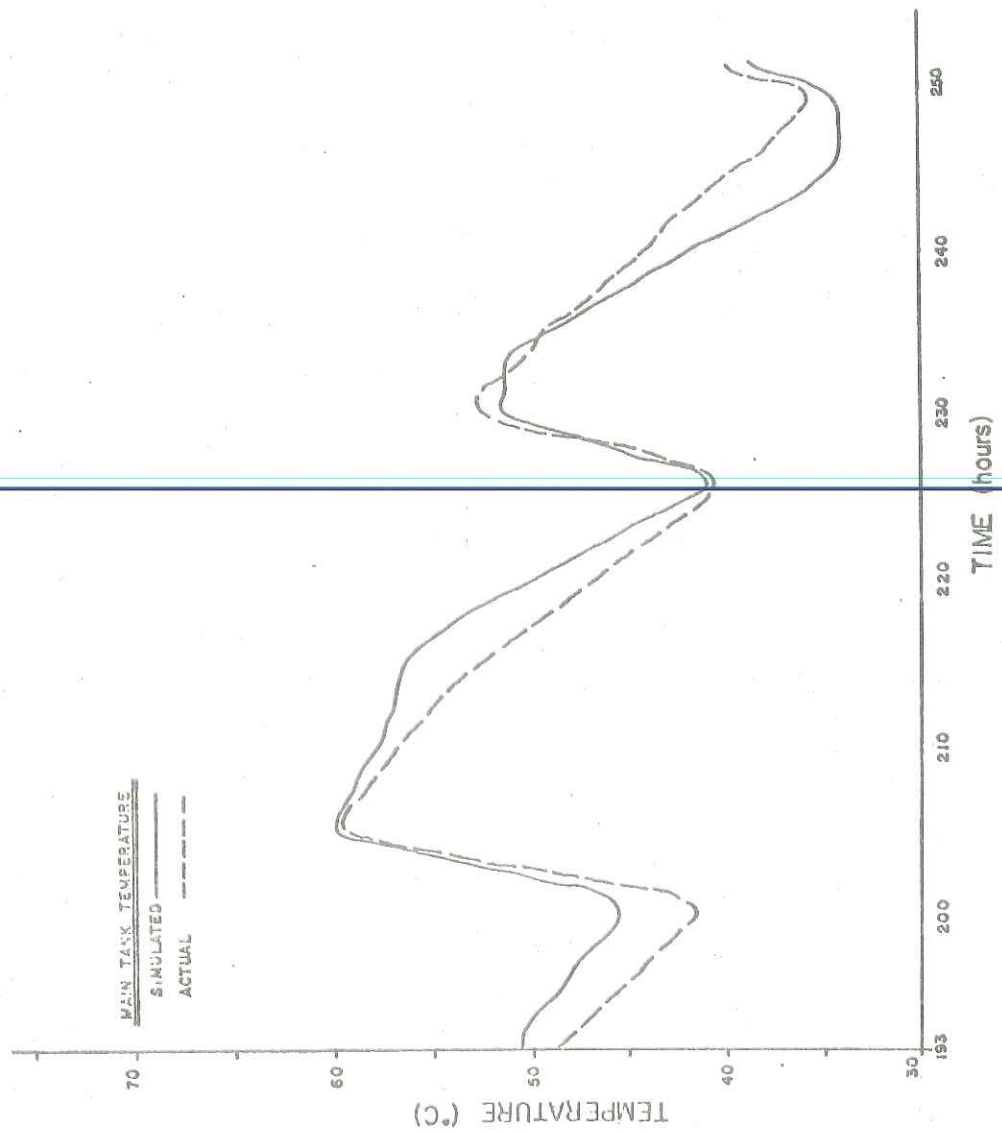


FIGURE 9.3.1 (con'd)

TABLE 9.4.2

Simulated Energy Quantities (MJ)

1-1-1 hrs to 1-7-23 hrs

| | TANK 1 | TANK 2 | TANK 3 |
|-------------------------|--------|--------|--------|
| $Q_{T,sol}$ | 2012.0 | 132.4 | 0.0 |
| Q_R | 1707.0 | 0.0 | 0.0 |
| Q_{loss} | 121.6 | 129.0 | 64.0 |
| ΔU_{tank} | 162.3 | 1.5 | 1.0 |
| ηQ_{aux} | --- | --- | 65.6 |
| % Closure Difference | 1.0 | 1.4 | 0.1 |

9.4.3 Comparison of Simulated and Actual Performance

Table 9.4.3 lists the daily integrated quantities of interest when comparing actual and simulated systems. Values of useful energy gain agree to within 3.5%, the best of any of the simulations. The heating performance is not quite as good as simulated values are 4% less than the actual requirements. The difference is primarily due to differences supplied since the values of solar heating delivered differ only slightly, by 0.1%. The service hot water system did not model very well, for actual heat transferred to the pre-heat tank exceeded simulated by 34%. Part of this is due to data from the evening of January 7, which is in error but was used to complete a full week's data. Auxiliary input to the hot water tank was predicted to be 104.5 MJ, which exceeds the actual value of 95.1 MJ by 9%.

| Date | Q _u (MJ) | | Q _{ah} (MJ) | | Q _{so1} (MJ) | | Q _{aux} (MJ) | | Q _{T,hw} (MJ) | |
|--------|---------------------|--------|----------------------|--------|-----------------------|--------|-----------------------|-------|------------------------|-------|
| | Sim | Act | Sim | Act | Sim | Act | Sim | Act | Sim | Act |
| 1-1 | 402.8 | 418.6 | 197.3 | 265.6 | 197.3 | 265.6 | 0.0 | 0.0 | 23.5 | 24.6 |
| 2 | 0.0 | 0.0 | 375.1 | 356.6 | 375.1 | 302.3 | 0.0 | 54.3 | 0.9 | 0.0 |
| 3 | 432.3 | 409.3 | 290.6 | 313.2 | 128.1 | 129.0 | 162.5 | 184.2 | 18.5 | 29.4 |
| 4 | 341.8 | 359.2 | 274.0 | 234.7 | 274.0 | 234.7 | 0.0 | 0.0 | 16.8 | 20.5 |
| 5 | 360.3 | 383.6 | 241.4 | 253.4 | 241.4 | 253.4 | 0.0 | 0.0 | 22.0 | 23.0 |
| 6 | 387.1 | 387.6 | 148.1 | 193.9 | 148.1 | 193.9 | 0.0 | 0.0 | 27.9 | 40.9 |
| 7 | 87.3 | 127.7 | 209.3 | 192.4 | 209.3 | 191.6 | 0.0 | 0.8 | 22.8 | 65.2 |
| TOTALS | 2012.0 | 2086.0 | 1736.0 | 1810.0 | 1573.0 | 1570.5 | 162.5 | 238.5 | 132.4 | 203.6 |

% Difference 3.5 4.0 0.1 32.0 34.0

TABLE 9.4.3. Daily Values of Q_u, Q_{ah} and Q_{T,hw} for Simulation III.

mean temperature and 18.33°C (65°F).

$$DD = 18.33 - T_a \quad (9.5.1)$$

Figure 9.5.1 depicts the energy exchanges for a house. An energy balance on this system yields:

$$Q_{\text{loss}} = Q_{\text{load}} + Q_{\text{shg}} + Q_{\text{gen}} \quad (9.5.2)$$

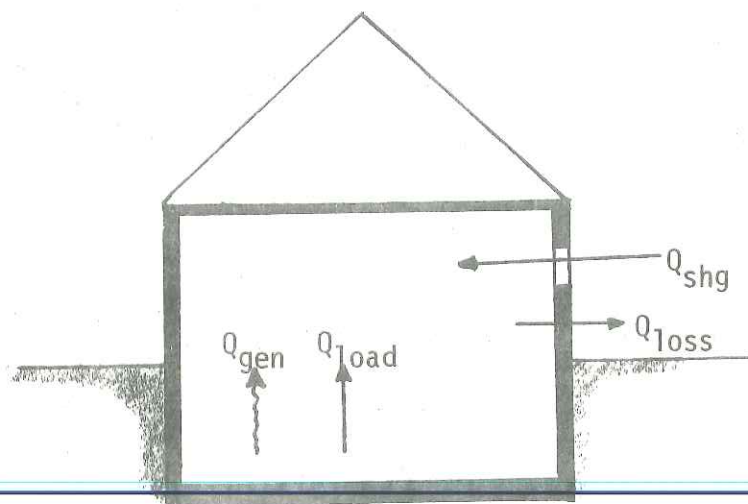


FIGURE 9.5.1. Energy Exchanges for House.

The heating load, Q_{load} , has customarily been calculated by

$$Q_{\text{load}} = (UA)(DD) \quad (9.5.3)$$

where UA is a heat transfer conductance usually expressed in KJ/degree-day and DD is the number of degree-days. This load was calculated using the 18.33°C (65°F) base in Equation 9.5.1. This was predicated on assumptions that room thermostats were set at 23.88°C (75°F) and that the non-furnace gains of Equation 9.5.2 (Q_{shg} and Q_{gen}) could produce

TABLE 9.5.1

Results of January Simulation of CSU House in Madison

| | |
|--|------------------------|
| Q_{loss} | |
| Total | 22,513.3 MJ |
| Daily Average | 804.1 MJ/day |
| Hourly Average | 33.5 MJ/hr |
| Q_{load} | |
| Total | 11,901.8 MJ |
| Daily Average | 425.1 MJ/day |
| Hourly Average | 17.7 MJ/hr |
| % $Q_{\text{load,T}}$ Met by Solar | 42.2% |
| % $Q_{\text{load,T}}$ Met by Auxiliary | 57.8% |
| UA (Q_{loss} Base) | |
| x | 31.4 MJ/deg C-day |
| s_x | ± 3.7 MJ/deg C-day |
| 95% Confidence Limit | ± 1.4 MJ/deg C-day |

A UA degree-day heating load model might be sufficient if one were faced with many repeated runs and cost restrictions. The total forecast load is almost identical as that calculated by the more exact transfer function method. Some accuracy in the solar contribution is lost however as the time of day nature of heating loads, which is not accurately UA modeled, might just be important enough to affect solar performance by a few percentage points.

duced over the holiday periods. This, in hindsight, is obvious, but was shown by a Simulation I without infiltration rate modification.

The simulated system provided nearly twice as much heating as actually occurred because it "saw" more of an infiltration load. This situation was improved by reducing simulated infiltration over the Thanksgiving, Christmas and New Year's holidays.

A second observation occurred over the Thanksgiving holiday when the thermostat was turned down. The actual system operated at reduced datum but the computer system continued to operate at the higher set point and consequently met a higher heating demand. This was remedied by a time varying thermostat model.

The third example was found in the Simulation III weather and performance data. Initially it appeared that more than 500 hours of data was available. Simulations proved, however, that the simulated system was meeting gigantic hot water loads. Careful examination of the data showed the errors mentioned in section 9.4. This resulted in a reduced simulation of only 168 hours.

10.2 Recommendations

The following recommendations are made for future computer simulation and solar experimental houses.

- (1) Statistical weather reduction should be examined to try and reduce the run time needed for studies of house systems. This has been done with some success by the Trane Air Conditioning Company with their TRACE (33) energy economic program.
- (2) An air conditioning model should be developed and incorporated into TRNSYS to simulate cooling season performance. Several are now under study at the University of Wisconsin and might be used to study the more critical time of day loads faced by cooling systems.
- (3) A means is necessary to more accurately predict the internal generation and rate of infiltration. The internal generation can be handled to a large extent by electrical and gas meter readings but the infiltration is not as easily gauged. An equation relating infiltration to wind speed, perimeter, window and wall area and quality of construction, etc. should approximate more accurately the rate of infiltration than estimating the air changes per hour.
- (4) A transfer function room model is outlined in ASHRAE (12). This looks worthwhile and should be incorporated into TRNSYS to eliminate the differential equation in the current room model. This should greatly simplify modeling and further reduce costs.

APPENDIX

Calculation of Capacitance Value for CSU House

A value of the internal capacitance was necessary in order to use the TRNSYS room model. The following is an approximation of the internal capacitance of some of the items in the CSU house.

Internal Walls -

non-insulated

$$C_{\text{int wall}} \approx 23.7 \text{ Btu/linear ft-F}$$

First Floor \approx 180 ft of wall

Basement \approx 70 ft of wall

Therefore the capacitance of the interior, non-insulated walls is

$$C_1 \approx 6000 \text{ Btu/F}$$

insulated (around mechanical room)

$$C_{\text{ins,int wall}} \approx 4.5 \text{ Btu/linear ft-F}$$

Mechanical Room \approx 45 ft of wall

Therefore

$$C_2 \approx 203 \text{ Btu/F}$$

Floor (1500 ft²) -

$$C_{\text{floor}} \approx 3.25 \text{ Btu/ft}^2\text{-F}$$

Therefore

$$C_3 \approx 4900 \text{ Btu/F}$$

BIBLIOGRAPHY

1. Klein, S.A., Ph.D. Thesis in Chemical Engineering, Madison, University of Wisconsin (1976). "A Design Procedure for Solar Heating Systems".
2. Solar Energy Laboratory of the University of Wisconsin, "TRNSYS-A Transient Simulation Program," Engineering Experiment Station Report 38 (September 1976).
3. Lof, G.O.G., and Ward, D.S., "Solar Heated and Cooled Building," annual progress report prepared for the National Science Foundation, February, 1974.
4. Lof, G.O.G., Ward, D.S., Ward, J.C., and Smith, C.C., "Design and Construction of a Residential Solar Heating and Cooling System," semi-annual progress report prepared for the National Science Foundation, August, 1974.
5. Ward, D.S. and Lof, G.O.G., "Design, Construction and Testing of a Residential Solar Heating and Cooling System," annual progress report prepared for the National Science Foundation and the Energy Research and Development Administration, June, 1975.
6. Lof, G.O.G. and Ward, D.S., "Design, Construction and Testing of a Residential Solar Heating and Cooling System," prepared for the Committee on the Challenges of Modern Society (CCMS), June, 1976.
7. Butz, L.W., M.S. Thesis in Mechanical Engineering, Madison, University of Wisconsin (1973). "Use of Solar Energy for Residential Heating and Cooling."
8. Butz, L.W., Beckman, W.A., and Duffie, J.A., "Simulation of a Solar Heating and Cooling System," Solar Energy, Vol. 16, No. 3/4, December, 1974.
9. Oonk, R.L., Beckman, W.A., and Duffie, J.A., "Modeling of the CSU Heating/Cooling System," paper presented at U.S. Section Meeting, Solar Energy Society, Fort Collins, Colorado, August 21-23, 1974.
10. Oonk, R.L., M.S. Thesis in Mechanical Engineering, Madison, University of Wisconsin (1975). "Modelling of the Colorado State University Solar House I".
11. Holman, J.P., Heat Transfer, McGraw-Hill, 1972.



